TBE-4617-3

TGAL-94-02

MAXIMUM-LIKELIHOOD NETWORK MAGNITUDE ESTIMATES OF LOW-YIELD UNDERGROUND NUCLEAR EXPLOSIONS

Rong-Song Jih and Richard R. Baumstark

Teledyne Brown Engineering
2111 Wilson Boulevard, Suite 900
Arlington, Virginia 22201-3058

31 March 1994

FINAL REPORT (PART 3): Task 3 (03 January 1994 - 31 March 1994)
PROJECT TITLE: Low-yield Regression Models and Their Transportability
CONTRACT NO.: F08606-91-C-0005, AFTAC PA T/0122

Prepared for / Monitored by:

AIR FORCE TECHNICAL APPLICATIONS CENTER
Directorate of Nuclear Treaty Monitoring (HQ AFTAC / TTR)
Patrick Air Force Base, Florida 32925-3002

REPORT DOCUMENTATION PAGE

Form Approved
OMB No 0704-0188

1. AGENCY USE ONLY (Leave Blank)	2. REPORT DATE	3. REPORT TYPE AND DATES COVERED
	31 March 1994	Final Report, 3 January 1994 - 31 March 1994

4. TITLE AND SUBTITLE

Maximum-likelihood Network Magnitude Estimates of Low-yield Underground Nuclear Explosions

5. FUNDING NUMBERS

Contract F08606-91-C-0005

AFTAC PA T / 0122

6. AUTHOR(S)

R.-S. Jih and R. R. Baumstark

7. PERFORMING ORGANIZATION NAME(S) AND ADDRESS(ES)

Teledyne Brown Engineering
2111 Wilson Boulevard, Suite 900
Arlington, Virginia 22201-3058

8. PERFORMING ORGANIZATION REPORT NUMBER

TBE-4617-3 / TGAL-94-02

9. SPONSORING / MONITORING AGENCY NAME(S) AND ADDRESS(ES)

Air Force Technical Applications Center
Directorate of Nuclear Treaty Monitoring
Patrick Air Force Base, Florida 32925-3002

10. SPONSORING / MONITORING AGENCY REPORT NUMBER

11. SUPPLEMENTARY NOTES

12a. DISTRIBUTION / AVAILABILITY STATEMENT

Approved for Public Release, Distribution Unlimited

12b. DISTRIBUTION CODE

13. ABSTRACT *(Maximum 200 words)*

This final report covers the analysis performed under Task 3 of this contract, using the raw station magnitudes collected under Task 1. 35,211 station m_b values from 6 major nuclear test sites have been fed into the GLM [General Linear Model] inversion to determine jointly the event sizes, the station corrections, and the specific path correction for each source-station pair. The simultaneously-inferred path and station corrections are related to known geological / geophysical features. Applying these path and station corrections to the raw station magnitudes of any individual explosion yields a systematic reduction in the fluctuational variation of station magnitudes across the whole network with a reduction factor ranging from 1.2 to 3 for all Soviet events in our data set. These station corrections have been used in estimating the event magnitudes of those isolated explosions which were not included in the GLM inversion. With these path-corrected / station-corrected $m_b(P_{max})$, the $m_b(P_{max})$ - $m_b(L_g)$ [NORSAR] bias between the southwest and northeast subregions of the Soviet's Balapan test site is assessed as 0.08 magnitude unit [m.u.]. Magnitude-magnitude regression were conducted with the standard errors in the event magnitudes fully counted for. We observed some inconsistency in the L_g scaling relationships. The systematic bias in the L_g scale can be removed by revising the absolute L_g excitation level for Novaya Zemlya explosions. That is, the L_g scale suitable for Iranian Plateau might be more appropriate for computing $m_b(L_g)$ of Novaya Zemlya explosions.

14. SUBJECT TERMS

m_b, $m_b(P_{max})$, $m_b(L_g)$, M_s, m_b-L_g Bias, General Linear Model, Maximum-likelihood, Regression Model, Uncertainty

15. NUMBER OF PAGES

16. PRICE CODE

17. SECURITY CLASSIFICATION OF REPORT	18. SECURITY CLASSIFICATION OF THIS PAGE	19. SECURITY CLASSIFICATION OF ABSTRACT	20. LIMITATION OF ABSTRACT
Unclassified	Unclassified	Unclassified	UL

(THIS PAGE INTENTIONALLY LEFT BLANK)

SUMMARY

Seismic yield estimation, which is based on the seismic magnitudes, is a function of source region elastic efficiency, near-source effects, path attenuation, and near-receiver effects. The interplay among these factors introduces uncertainties in the estimates of yields of underground nuclear explosions using the seismic technique. For explosions below 100 kt, the geophysical and geological conditions of the source region play a critical role.

Teledyne was awarded this contract in January 1991 to transcribe and measure the digital waveforms from six major nuclear test sites. The objectives of the project are to investigate seismic magnitude-yield regression models for various geophysical and geological regions and their associated errors, to study the transportation of these regression models between nuclear explosion test sites and estimation of associated errors, and to develop scaling laws that allow yield estimation of nuclear explosions emplaced in media with different geophysical and geological parameters. The project involves three major tasks:

[1] Collection and measurements of digital seismograms for waveforms from all six data sets. Due to the large amount of waveforms to be collected and measured, Task 1 was the most labor-intensive task throughout the whole contract period. There were 564 events in total measured / processed. The measurements and the station magnitudes of all 11 phases for all events are summarized in an accompanying final report, *TBE-4617-1 / TGAL-94-01* (Baumstark and Wagner, 1994).

[2] Construction of Geophysical and Geological [G&G] database. The results derived under this task are described in a separate volume of the final report.

[3] Data reduction and interpretation. This task would include
(a) the construction of magnitude-magnitude regression models (for all test sites) as well as magnitude-yield regression models (for NTS),
(b) investigate the scaling and transportability of the regression models.

This final report covers the unclassified work performed under Task 3 using the raw station magnitudes collected under Task 1. No attempt was made to utilize any G&G information obtained under Task 2, due to the classified nature of that task. This report also describes the inversion and regression algorithms used in this project.

Two magnitude determination schemes, GLM [General Linear Model] and EMILS [Expection-Maximization + Iterative Least Squares] were used for clustered and isolated nuclear tests, respectively. The GLM algorithm not only produces the network-averaged magnitudes, which are optimal in the maximum-likelihood sense, it also generates two types of by-products: the station corrections and the path corrections. This GLM routine has been applied to all time-domain magnitudes used in this study, although much attention was paid to m_b. Another non-standard algorithm we used in this study is a magnitude-magnitude regression routine which accounts for the uncertainties in the event magnitudes through Monte-Carlo resampling. A feature of automatic outlier rejection has been added to this routine.

The huge database of station m_b values based on short-period vertical-component (SPZ) recordings has been fed into the GLM inversion to determine simultaneously the event sizes, the station

corrections, and the specific path correction for each source-station pair. The linear system involves 35,211 equations and 3,306 unknowns. The simultaneously-inferred path and station corrections are related to known geological/geophysical features. Applying these path and station corrections to the raw station magnitudes of any individual explosion yields a systematic reduction in the fluctuational variation of station magnitudes across the whole network with a reduction factor ranging from 1.2 to 3 for all Soviet events in our data set. These station corrections have been used in computing the event magnitudes of those isolated explosions that were not included in the GLM inversion. With these path-corrected/station-corrected $m_b(P_{max})$, the $m_b(P_{max})-m_b(L_g)$ [NORSAR] bias between the southwest and northeast subregions of the Soviet's Balapan test site is assessed as 0.07 magnitude unit [m.u.], which is significantly smaller than that of previous studies.

The m_b results presented in this report are very consistent with those of our previous study (*cf.* Jih *et al.*, 1993) using essentially the same technologies and different explosion data set. In comparing m_b, M_S, and $m_b(L_g)$, we observe some inconsistency in the scaling relationships. The systematic bias in the L_g scale can be removed either by raising Nuttli's path attenuation coefficients (which were derived with the coda Q method), or by revising the absolute L_g excitation level for Novaya Zemlya explosions. Whichever approach adopted, there would be some question about whether the L_g scale is really as transportable as Nuttli suggested. The good results of applying his NTS L_g-yield formula to Semipalatinsk explosions may turn out to be a special case rather than a general rule. If the L_g scale suitable for Iranian Plateau were used in computing the $m_b(L_g)$ of Novaya Zemlya explosions, then all the magnitude-yield relationships for the three phases; m_b, M_S, and L_g would be consistent.

To fully digest the huge explosion dataset would require a significant amount of time and labor which are certainly beyond the level of efforts allocated to this Task 3. The results presented in this report should be regarded as preliminary in nature with many topics remain to be explored. This report is a pilot study which serves to illustrate how the carefully measured parameters (collected under Task 1) can be used in some magnitude-yield analysis utilizing the statistical software package developed at Teledyne.

Table of Contents

List of Figures

List of Figures (Continued)

List of Figures (Continued)

List of Tables

(THIS PAGE INTENTIONALLY LEFT BLANK)

I. INTRODUCTION

The scope of this project is to provide for seismological studies to investigate seismic yield scaling and transportation of magnitude-yield models for underground nuclear explosions below 100 kilotons (kt) between different test sites. The objectives of the project are to investigate seismic magnitude-yield regression models for distinct geophysical and geological regions and their associated errors, to study the transportation of these regression models between nuclear explosion test sites and estimation of associated errors, and to develop scaling laws that allow yield estimation of nuclear explosions emplaced in media with different geophysical and geological parameters.

Seismic yield estimation, which is based on the seismic magnitudes, is a function of source region elastic efficiency, near-source effects, path attenuation, and near-receiver effects. The interplay among these factors introduces uncertainties in the estimates of yields of underground nuclear explosions using the seismic technique. This project investigates yield estimation for explosions below 100 kt, for which the geophysical and geological conditions of the source region play a critical role. Path attenuation and near-receiver effects from previous studies or derived from this project are used. The emphasis of this project is the development of scaling laws that reflect source media with different geophysical and geological parameters.

To achieve these goals, AFTAC/TTR issued a contract to Teledyne Geotech Alexandria Laboratory [TGAL] in January 1991 to transcribe and measure the digital waveforms from six major data sets: Novaya Zemlya (NZ), Nevada Test Site (NTS), French Sahara (FS), Balapan (Shagan River, SR), Degelen Mountain (DM), and Peaceful Nuclear Experiments (PNEs). The project involves three major tasks:

[1] Collection and measurements of digital seismograms for waveforms from all six data sets.

[2] Construction of Geophysical and Geological [G&G] database (for all test sites except FS).

[3] Data reduction and interpretation. This task would include
(a) the construction of magnitude-magnitude regression models (for all test sites) as well as magnitude-yield regression models (for NTS),
(b) investigate the scaling and transportability of the regression models.

Due to the large amount of waveforms to be collected and measured, Task 1 was the most labor-intensive task throughout the whole contract period. There were 584 events in total measured / processed (Baumstark and Wagner, 1994):

US data set	246 events
Shagan River data set	97 events
Degelen Mountain data set	99 events
Novaya Zemelya data set	35 events
PNE data set	94 events
French Sahara data set	13 events

The processed digital waveforms (converted to CSS 3.0 format), instrument responses, as well as all the measurements made by the analysts using an interactive software package *"geotool"* developed

by Henson and Coyne (1993) were delivered to AFTAC/TTR in six 8-mm tapes in late 1993. The measurements and the station magnitudes of all 11 phases for all events are summarized in an accompanying final report *TBE-4617-1/TGAL-94-01* (Baumstark and Wagner, 1994). The results derived under Task 2 are described in a separate volume. This volume of the final report summarizes the results obtained under Task 3 using the data collected under Task 1. This report also describes the inversion and regression algorithms used in this project.

Two magnitude determination schemes, GLM [General Linear Model] and EMILS [Expection-Maximization + Iterative Least Squares] were used for clustered and isolated nuclear tests, respectively. A criterion was tested to reject those stations that recorded less than five events. As a result, the final number of events fed to the GLM inversion was slightly different than the number of events processed/measured under Task 1. The station corrections derived by the GLM inversions were applied to those recordings of isolated nuclear tests before the station magnitudes are fed into the single-event averaging scheme, EMILS. Those station recordings without GLM station corrections were not included in the EMILS computation. Therefore, the number of events used in the EMILS computation is also somewhat less than the total number of events actually measured.

Explosions Used in This Study	
Pahute Mesa, NTS	58
Rainier Mesa, NTS	22
Yucca Flat, NTS	148
Northeast Balapan (Shagan River)	30
Southwest Balapan (Shagan River)	48
Transition Zone, Balapan (Shagan River)	19
Degelen Mountain, E. Kazakh	98
Northern Novaya Zemlya	30
Ahaggar, French Sahara	9
(462 GLM events)	

Explosions Not Used in This Study	
Amchitka Island, Aleutians, U.S.A.	3
Outside Nevada Test Site, U.S.A.	6
Southern Novaya Zemlya	4
PNEs, U.S.S.R.	94
(107 EMILS events)	

This report contains three parts. Sections II and III describe the algorithms we used in computing the maximum-likelihood event magnitudes. The inversion results are summarized in Section IV. In Section V, we present some preliminary analysis and interpretation of the results.

II. STATION MAGNITUDE COMPUTATION

II.1 Formulae Used in Station Magnitude Computation

The measurements include the displacement amplitude in nm, the period in seconds, the phase name (*e.g.*, m_b, M_S, L_g, PS), the origin information which includes the epicenter and the event name. Each phase has a specific formula for determining the magnitude, and hence different parameters might be required. The formulae used in this study are described briefly in the following:

[1] m_b = log(A/T) + B(Δ) for 20° < Δ < 95°, where B(Δ) is the distance normalizer derived by Veith and Clawson (1972).

[2] m_b (P_n) = log(A) + 2.42 log(Δ) - 3.95 for Δ < 10° (*cf.* Vergino and Mensing, 1990).

[3] For M_S, two different formulae are used:
If Δ > 25°, M_S = log(A/T) + 1.66 log(Δ) + 3.30 (*cf.* Gutenberg, 1945).
If 10° < Δ < 25°, M_S = log(A/T) + 1.07 log(Δ) + 4.16 (*cf.* Nuttli and Kim, 1975).
All three long-period components were rotated using the unclassified location before an LQ was picked. If the rotated waveforms exhibit a station to event azimuth which is significantly different from the predicted azimuth, then the picked LR and/or LQ are treated as noisy recordings.

[4] For $m_b(L_g)$, Jih and Lynnes (1993) suggest the following formula:

$$m_b(L_g) = 4.0272 + \log A(\Delta) + \frac{1}{3}\log(\Delta(\text{km})) + \frac{1}{2}\log\left[\sin\left(\frac{\Delta(\text{km})}{111.1(\text{km/deg})}\right)\right] + \frac{\gamma(\Delta - 10\text{km})}{\ln(10)} . \qquad [1]$$

Although this $m_b(L_g)$ formula might appear to be different from most other formulae currently in use, this equation is actually equivalent to Nuttli's (1986ab, 1987). For instance, a seismic source in eastern U.S. with 1-sec L_g amplitude of 110 μm at 10 km epicentral distance would correspond to a $m_b(L_g)$ of 4.0272 + 2.0414 + 0.3333 - 1.4019 + 0.0000 = 5.000, the same value that Nuttli's original 2-step formulae would give. The Q_0 and η values used in this project are listed in Tables 1 through 3. L_g arrivals are picked between 0° and 40°. Two different velocity windows are used in picking the L_g arrivals:
(a) 4.0 km/sec to 2.5 km/sec (for Δ < 10°),
(b) 4.0 km/sec to 3.0 km/sec (for 10° < Δ < 40°).

II.2 Time-domain Determination of L_g Path Correction

There are several different approaches that have been proposed to determine the path Q_0/η:

[A] Apply the coda-Q method of Herrmann (1980), as did Nuttli (1986ab, 1987, 1988).

[B] Synthesize the path Q_0/η along the great-circle path between the source and the receiver using the 2-dimensional Q_0/η map of that region (Jih and Lynnes, 1993).

[C] Apply GLM [General Linear Model] or LSMF [Least square Matrix Factorization] inversion to infer the path corrections along with the source terms (Jih, 1992).

Approach [C] would perform very well when some extra reliable information about the events (*e.g.*, the average of m_b or $m_b(L_g)$ values) is available to constrain the joint inversion (Jih, 1992). Here we provide another approach which is very similar to [C] except that the stations are calibrated individually with those events for which Nuttli (1988) already determined the $m_b(L_g)$ values.

In processing the L_g data set assembled under this contract, the *"sustained maximum motion"* of L_g phase is measured in a manner identical to that which Nuttli (1986ab, 1987, 1988) proposed. That is, the amplitude equaled or exceeded by the three largest amplitude waves, of the vertical-component L_g waves with period around 1 second was picked. The station amplitude reading is first corrected for the effects of geometrical spreading and dispersion with the formula appropriate for the Airy phase; the residual (relative to Nuttli's $m_b(L_g)$) is then regarded as completely due to the anelastic attenuation along the path:

$$\gamma = \frac{\ln(10)}{(\Delta - 10\text{km})}\left[m_b(L_g) - 4.0272 - \log A(\Delta) - \frac{1}{3}\log(\Delta) - \frac{1}{2}\log\left[\sin\left(\frac{\Delta(\text{km})}{111.1(\text{km/deg})}\right)\right]\right], \qquad [2]$$

where Δ is the epicentral distance in km, $A(\Delta)$ is the observed L_g amplitude measured in the time domain in μm [microns] at the epicentral distance of Δ km. The corresponding $Q(f)$ can then be determined in a straightforward manner:

$$Q(f) = \frac{\pi \cdot f}{\gamma \cdot U}, \qquad [3]$$

where U is the group velocity. Once a suite of $Q(f)$ values is available for a station of interest, a linear regression is then conducted to find the maximum-likelihood estimate of the quality factor, Q_0, as well as the frequency-dependency, η, via the model:

$$Q(f) = Q_0 \cdot f^{\eta}, \text{ or}$$

$$\log[Q(f)] = \log[Q_0] + \eta \cdot f, \qquad [4]$$

The maximum-likelihood regression scheme for the censored case is described in Appendix B.

II.3 L_g Path Corrections for Novaya Zemlya, Semipalatinsk, and NTS

The resulting path corrections for Novaya Zemlya test site are listed in Table 1, along with those corrections of Nuttli's (1988). The match is fairly good. This simply suggests that Teledyne's L_g amplitude measurements furnished by Baumstark and Wagner (1994) are very consistent with Nuttli's. It is interesting to note that IST (Istanbul, Turkey) and TRI (Trieste, Italy) did record L_g phases from large historical Novaya Zemlya events. Along with the 7 WWSSN stations for which Nuttli (1988) already published the Q_0 values, now we have a total of 12 paths calibrated for L_g waves from Novaya Zemlya. Stations KON (Konsberg, Norway) and KBS (Kingsbay, Svalbard) are not well constrained due to the limited data size, and hence Nuttli's (1988) Q_0/η would have to be retained.

Table 1. Q_0/η for Novaya Zemlya L_g

Station	This Study		Nuttli (1988)	
Code	Q_0	η	Q_0	η
COP	668	0.41	633	0.4
DAG	270	0.69	—	—
ESK	463	0.63	—	—
IST	561	0.64	—	—
KBS	—	—	315	0.5
KEV	249	0.74	252	0.6
KON	—	—	496	0.5
NOR	223	0.43	—	—
NUR	433	0.42	420	0.5
STU	550	0.55	531	0.5
TRI	417	0.24	—	—
UME	397	0.82	391	0.5

Table 2. Q_0/η for Semipalatinsk L_g						
Station	This Study		Nuttli (1986b)		Bennett (1990)	
Code	Q_0	η	Q_0	η	Q_0	η
ARU	—	—	—	—	622	0.50
COP	—	—	700	0.40	—	—
GAR	—	—	—	—	428	0.50
HIA	—	—	—	—	568	0.50
KBL	—	—	360	0.60	—	—
KEV	—	—	580	0.40	—	—
KIV	—	—	—	—	580	0.50
KON	776	0.44	700	0.40	—	—
MHI	—	—	380	0.50	—	—
MSH	—	—	380	0.50	—	—
NDI	385	1.10	312	0.60	—	—
NIL	412	0.62	354	0.60	—	—
NUR	598	0.37	580	0.40	—	—
OBN	—	—	—	—	761	0.50
POO	364	0.14	—	—	—	—
QUE	—	—	300	0.60	—	—
SHL	—	—	340	0.60	—	—
UME	608	0.34	591	0.40	—	—
WMQ	—	—	—	—	452	0.50

Table 3. Q_0/η for NTS L_g

Station	This Study		Nuttli (1986a)		Patton (1988)	
Code	Q_0	η	Q_0	η	Q_0	η
AAM	463	0.4	—	—	—	—
ALQ	188	0.6	—	—	—	—
ATL	369	0.1	—	—	—	—
BKS	158	0.6	139	0.6	—	—
BLA	462	0.2	—	—	—	—
BOZ	145	0.4	—	—	—	—
COR	138	-0.7	—	—	—	—
DUG	207	-3.1	155	0.6	—	—
ELK	184	0.4	—	—	150	0.5
FLO	313	0.1	—	—	—	—
GEO	357	-0.3	—	—	—	—
GOL	181	0.5	—	—	—	—
JCT	316	0.2	—	—	—	—
KNB	218	-1.9	—	—	142	0.4
LAC	144	0.3	—	—	97	0.7
LON	168	0.4	—	—	—	—
MNV	—	—	—	—	93	0.6
OGD	474	0.1	—	—	—	—
OXF	412	0.2	—	—	—	—
RCD	185	-1.4	—	—	—	—
SCP	451	0.1	—	—	—	—
TUC	200	0.2	162	0.6	—	—
WES	515	0.2	—	—	—	—

III. MAXIMUM-LIKELIHOOD NETWORK MAGNITUDE ESTIMATORS

III.1 Single-event Maximum-likelihood Estimator

The problem of estimating body-wave magnitudes (m_b) using amplitudes read at a number of recording stations is frequently complicated by the fact that the data may be heavily censored. This arises either because of clipping, where all amplitudes can be determined only to exceed a given lower bound (*i.e.* the right-censored case in statistical terms), or because the signals are weaker than the ambient noise level and hence are not detected (*i.e.* the left-censored case). If one simply averages the magnitudes for those stations which detected an event, without regard for those that clipped or did not record, serious biases may result in the event magnitude estimated.

For single-event network m_b determination, at least three types of station magnitude ought to be considered:

[0] the station magnitude, X, is known as x_0,

[1] X is only known to be less than certain level, say, t_1,

[2] X is only known to be larger than certain level, say, t_2.

We assume that the observed station magnitude, X, can be represented as the sum of the unknown event magnitude, μ, and a perturbing random noise, v,

$$X = \mu + v \qquad [5]$$

where v is assumed to be a Gaussian random variable with mean zero and standard deviation σ. Elegant maximum-likelihood theory can be derived for this linear model. Suppose there are n_0, n_1, and n_2 station recordings for each type, respectively. The conditional likelihood function of the censored observations (X_0, t_1, t_2) given the network magnitude μ and σ is

$$L(X_0, t_1, t_2 \mid \mu, \sigma) = \prod_{j=1}^{n_0} P(X_j = x_{0j} \mid \mu, \sigma) \cdot \prod_{j=1}^{n_1} P(X_j < t_{1j} \mid \mu, \sigma) \cdot \prod_{j=1}^{n_2} P(X_j > t_{2j} \mid \mu, \sigma) \ , \qquad [6]$$

and the log-likelihood function is

$$\ln L(X_0, t_1, t_2 \mid \mu, \sigma) = -\frac{n_0}{2} \ln(2\pi\sigma^2) - \frac{1}{2\sigma^2} \sum_{j=1}^{n_0} (x_{0j} - \mu)^2 + \sum_{j=1}^{n_1} \ln \Phi(z_{1j}) + \sum_{j=1}^{n_2} \ln \Phi(-z_{2j}) \ , \qquad [7]$$

where $z_i = (t_i - \mu)/\sigma$; X_0, t_1, and t_2 are collections of the observed station magnitudes of each type, respectively, and

$$\phi(u) = \frac{1}{\sqrt{2\pi}} \exp(\frac{-u^2}{2}) \ , \ \Phi(u) = \int_{-\infty}^{u} \phi(x)dx \ . \qquad [8]$$

are the probability density function and probability distribution function, respectively, of the standard normal random variable.

Solving $\frac{\partial \ln L}{\partial \sigma} = 0$ implies that $\hat{\sigma}$, the optimal estimate of σ, must satisfy the following necessary condition:

$$\hat{\sigma}^2 = \frac{\sum_{j=1}^{n_0}(x_{0j} - \hat{\mu})^2}{n_0 + \sum_{j=1}^{n_1}\frac{\phi(z_{1j})}{\Phi(z_{1j})}z_{1j} - \sum_{j=1}^{n_2}\frac{\phi(z_{2j})}{\Phi(-z_{2j})}z_{2j}} \quad . \qquad [9]$$

Solving $\frac{\partial \ln L}{\partial \mu} = 0$ implies that $\hat{\mu}$, the optimal estimate of μ, must satisfy the following necessary condition:

$$n_0 \hat{\mu} = \sum_{j=1}^{n_0} x_{0j} - \hat{\sigma}\sum_{j=1}^{n_1}\frac{\phi(z_{1j})}{\Phi(z_{1j})} + \hat{\sigma}\sum_{j=1}^{n_2}\frac{\phi(z_{2j})}{\Phi(-z_{2j})} \quad . \qquad [10]$$

Adding $(n_1 + n_2)\,\hat{\mu}$ to both sides of [10], and then dividing both sides by $(n_0 + n_1 + n_2)$ yields

$$\hat{\mu} = \frac{1}{n_0 + n_1 + n_2}\left(\sum_{j=1}^{n_0} x_{0j} + \sum_{j=1}^{n_1}\left[\hat{\mu} - \hat{\sigma}\frac{\phi(z_{1j})}{\Phi(z_{1j})}\right] + \sum_{j=1}^{n_2}\left[\hat{\mu} + \hat{\sigma}\frac{\phi(z_{2j})}{\Phi(-z_{2j})}\right]\right) . \qquad [11]$$

The right-hand side of Equation [11] happens to be the sample mean of "all" data with the censored measurements replaced by their corresponding best fill-in (see Appendix A):

$$\frac{1}{n_0 + n_1 + n_2}\left(\sum_{j=1}^{n_0} E[\,X \mid X = x_{0j}\,] + \sum_{j=1}^{n_1} E[\,X \mid X < t_{1j}\,] + \sum_{j=1}^{n_2} E[\,X \mid X > t_{2j}\,]\right) . \qquad [12]$$

Consequently, within the context of Gaussian assumption, one can translate those seemingly not-that-precise statements of $X > t$ or $X < t$ into quantitative constraints which can couple with other measurements of type 0 easily. Thus Equations [11] and [12] provide the theoretical justification of an iteration procedure to be discussed below.

An iterative procedure called "EM algorithm" [Expectation-Maximization algorithm] (Dempster *et al.*, 1977) can be applied to solve for μ and σ in a very straightforward manner. To start the iteration, one needs an initial guess of σ and μ. A good initial value of μ is the sample mean of all type-0 station magnitudes. Since bulletin m_b typically exhibits a σ (of single observation) around 0.3 magnitude unit, this value can serve as the initial value of σ. The iteration procedure follows:

[1] Based on the current estimates of μ and σ, replace all the censored data with their corresponding conditional expectations (*cf.* the right-hand side of Equation [11]). This is the so-called "E step" of the EM algorithm.

[2] Compute $\hat{\mu}$ as the sample mean of these "refined observations."

[3] Update the estimate of σ using Equations [9].

[4] Repeat [1]-[3] until some convergence criterion is met.

Steps [2] and [3] constitute the "M step" of the EM algorithm. Note that in the non-censoring case, *i.e.*, $n_1 = n_2 = 0$, $\hat{\mu}$ and $\hat{\sigma}$ would reduce to the regular sample mean and the RMS residual, respectively:

$$\mu = \frac{\sum_{j=1}^{n_0} x_{0j}}{n_0}, \sigma^2 = \frac{\sum_{j=1}^{n_0} (x_{0j} - \mu)^2}{n_0}. \quad [10]$$

Example

The algorithm described above has been implemented as a utility program *"emlls"* which expects to read just two columns of data representing the data type ("=", "<", or ">") and the actual data. Take Novaya Zemlya event NZ661027 (October 27, 1966) as an example. Table 4 lists the station $m_b(L_g)$ values of this Novaya Zemlya event based on our $m_b(L_g)$ formula as well as the path corrections we installed.

Table 4. Station Recordings of Novaya Zemlya Explosion 661027

Station	Δ°	Amplitude [nm]	Period [sec]	Q_0	η	Velocity	$m_b(L_g)$
COP	24.57	870.5	1.21	668	0.41	3.5	6.341
KEV	9.48	<1833.6	0.88	249	0.74	3.7	<6.506
NUR	17.22	867.5	1.08	433	0.42	3.6	6.389
STU	31.67	234.3	1.50	550	0.55	3.5	6.514
UME	15.58	1168.2	1.20	397	0.82	3.5	6.525
ESK	29.23	155.7	1.68	463	0.63	3.6	6.423
IST	34.70	49.5	0.93	561	0.64	3.6	6.464
KON	21.91	789.3	1.22	496	0.50	3.6	6.518
TRI	33.38	163.1	2.09	417	0.24	3.6	6.221

There are 8 good signals and 1 noisy measurement:

"=" 6.341
"<" 6.506
"=" 6.389
"=" 6.514
"=" 6.525
"=" 6.423
"=" 6.464
"=" 6.518
"=" 6.221

If the censored recording of 6.506 at the station KEV is ignored, the event magnitude would be 6.424±0.037. The program *"emlls"* gives the maximum-likelihood estimate as 6.420±0.034, using all 9 observations. Basically, what the maximum-likelihood method does is to utilize the censored information of $m_b(L_g)$(KEV) < 6.506 as an extra constraint to refine the inferred parameter obtained with the standard least squares. For this event, Nuttli (1988) gave a $m_b(L_g)$ of 6.45. Our GLM $m_b(L_g)$ of this event is 6.42±0.03 (*cf.* Table 5).

III.2 Simultaneous Inversion of Event Magnitudes, Station Terms, and Path Terms

III.2.1 General Concepts of Joint Inversion Model

As described in Section II, the conventional definition of the station magnitude is computed as

$$m_b = \log_{10}(A/T) + B(\Delta) \quad , \qquad [14]$$

where A is the displacement amplitude (in nm) and T is the predominant period (in sec) of the *P* wave. The $B(\Delta)$ is the distance-correction term that compensates for the change of *P*-wave amplitudes with distance (*e.g.*, Gutenberg and Richter, 1956; Veith and Clawson, 1972). m_b in [14] is also denoted as m_1 in Marshall *et al.* (1979). The ISC [International Seismograph Centre] bulletin m_b is just the network average of these raw station m_b values without any further adjustment. Implicitly, the ISC bulletin assumes a linear model as the following:

$$m_b(j) = E + v(j) \quad , \qquad [15]$$

where $m_b(j)$ is the station magnitude recorded at the station j for the event of size E, and v is the random perturbing term.

Now consider N_E explosions detonated at N_F source regions that are recorded at some or all of N_S stations. In LSMF [Least squares Matrix Factorization] and the standard GLM [General Linear Model] schemes (*e.g.*, Douglas, 1966; Blandford and Shumway, 1982; Marshall *et al.*, 1984; Lilwall *et al.*, 1988; Jih and Shumway, 1989; Murphy *et al.*, 1989), it is assumed that the observed station $m_b(i,j)$ is the sum of the true source size of the i-th event, E(i), the receiver term of the j-th station, S(j), and the random noise, v(i,j):

$$m_b(i,j) = E(i) + S(j) + v(i,j) \quad , \qquad [16]$$

The receiver term, S(j), is constant with respect to all explosions from different test sites, and hence it would inherently reflect the "averaged" receiver effect — provided the paths reaching the station have broad azimuthal coverage. When world-wide explosions are used, the standard deviation (σ) of the noise v in [16] is typically around 0.3 m.u.

If LSMF or GLM is applied to events within a smaller area of source region, then the σ of v in [13] could reduce to 0.15–0.2 m.u. However, the result of such "single-test-site GLM" approach should be interpreted or utilized cautiously. The event m_b values (*i.e.*, the "E" term in [16]) so determined are excellent estimates of the "relative source size" for that test site only. If this "single-test-site GLM" inversion is applied to several test sites separately, it may not be easy or obvious to find a consistent baseline for estimating the "absolute yield," since the recording network is typically different from one test site to another, and hence the station terms are inevitably inconsistent. Furthermore, the station terms derived by the "single-test-site GLM" may not necessarily represent the attenuation underneath the receiver side alone. They could be "contaminated" or sometimes even overwhelmed by the path/near-source effects shared by the explosions confined in a narrow azimuthal range. This could explain the once puzzling and controversial phenomenon Butler and Ruff (1980) (also Butler, 1981; Burdick, 1981) reported, namely that using Soviet explosions from one test site alone may fail to discern the attenuation differential between the eastern and western U.S. There is no doubt, however, that the GLM or LSMF type of methodology can infer the station terms which are strongly correlated with the upper

mantle attenuation underneath the stations, provided the seismic sources have a broad spatial coverage as did those in North (1977), Douglas and Marshall (1983), Lilwall and Neary (1985), Ringdal (1986), Jih and Wagner (1991), and many others. The event magnitude derived with Equation [3] is hereby denoted as m_{22}. In Marshall *et al.* (1979), *a priori* information about the P_n velocity underneath each station is used to determine its associated "deterministic" receiver correction, S(j), and the network-averaged magnitude based on the station-corrected magnitudes is called m_2. The receiver corrections as derived in Equation [16], however, are inferred jointly from a suite of event-station pairs, and no *a priori* geophysical or geological condition is assumed (and hence the different notation m_{22}). The high correlation between the tectonic type and the GLM station terms suggests that the empirical station corrections do reflect the averaged upper mantle conditions underneath the receivers, if the azimuthal coverage at each station is broad enough.

Jih and Wagner (1992ab) and Jih *et al.* (1993) propose to reformulate the whole model [16] as

$$X(i,j) = E(i) + S(j) + F(k,j) + v(i,j) \quad , \qquad [17]$$

where F(k,j) is the correction term at the j-th station for the propagation effect or the near-source focusing/defocusing effect, which is constant for all events (including this ith event) in the k-th "geologically and geophysically uniform region." For each seismic station, this F can be regarded as its azimuthal variation around the mean station term S. However, as explained previously, it would be more appropriate to consider F the path or near-source term because the back azimuths at the station could be nearly identical for adjacent test sites (such as Degelen and Murzhik), and yet the "F" terms could be very different. By incorporating the F term into the model, the σ for world-wide explosions is reduced to about 0.2, roughly the same level that which a "single-test-site GLM" could achieve. Intuitively, the present scheme (Equation [17]) provides a more detailed (and hence better) model than that of Equation [16] in describing the whole propagation path from the source towards the receiver. Simply put, Equation [16] yields a stronger fluctuation in the source terms, E, as well as a larger standard deviation of v because each term in the right-hand side of Equation [16] would have to "absorb" part of the missing F term. The resulting new event magnitude (*viz.*, E(i) in [17]) is hereby called m_G to avoid confusion with the m_3 defined in Marshall *et al.* (1979) that corrects for the source-region attenuation and station terms solely based on published P_n velocity.

Roughly speaking, the model described in [17] has the following advantages:

- It provides more stable m_b measurements across the whole recording network, as compared to the conventional GLM or LSMF procedure which only corrects for the station terms. The reduction in the standard deviation of network m_b from m_1 to m_G could reach a factor of nearly 3. As a result, the scatter in m_G versus log(yield) is smaller than that for other m_b.
- The separation of the path effect from the station effect is a crucial step to investigate the various propagation phenomena, which in turn would improve our understanding of the seismic source as well.

We have applied this model to 462 worldwide explosions, and the resulting m_G values of these explosions are listed in Table 5. The 194 stations are selected such that each station records 5 or more good explosion signals. Most of the earlier magnitude-yield study at Teledyne has been relying primarily on WWSSN as the core recording network (Blandford *et al.*, 1983; *e.g.*, Jih *et al.*, 1993; and many

others), this data set contains significant fraction of data contributed by USAEDS [United States Atomic Energy Detection System] seismic network (Baumstark and Wagner, 1994). In this data set, there are 25,890 signals, 1,169 noise measurements, and 7,152 clipped measurements from 10 test sites that are used to invert for the 3306 unknown parameters with the maximum-likelihood approach. The standard deviation of v(i,j) in [14] is 0.168, as compared to that of 0.240 if the conventional GLM (Equation [13]) is applied to the same data set. The algorithm and sample input files are described in the next section.

III.2.2 GLM Iteration Procedure

Equation [17] is a special case of the general linear models [GLM]. An iterative procedure based on the EM algorithm is presented below. The basic ideas are very similar to those underlying the single-event network averaging presented in Section III.1.

Step 0

Set up initial conditions as follows:

[1] σ = 0.3 magnitude unit,

[2] S(j) = 0 for j = 1, 2,..., N_S,

[3] F(k,j) = 0 for j = 1, 2,..., N_S, and k = 1, 2,..., N_E.

Step 1

Compute event magnitudes, E(i), for i = 1,..., N_E as

$$E(i) = \frac{1}{\#(j)} \sum_j [X(i,j) - S(j) - F(k,j)] ,$$

where #(j) is the number of stations that "recorded" the event i.

Step 2

Compute station corrections, S(j), for j = 1,..., N_S as

$$S(j) = \frac{1}{\#(i)} \sum_i [X(i,j) - E(i) - F(k,j)] ,$$

where #(i) is the number of events "recorded" at station j.

Step 3

Compute path corrections, F(k,j), for j = 1,..., N_S; k = 1,..., N_E as

$$F(k,j) = \frac{1}{\#((k,j))} \sum_i [X(i,j) - E(i) - S(j)] ,$$

where #((k,j)) is the number of paths from the test site k (where the event i is located) to the station j. This step is skipped if options 0 through 2 are chosen. Consequently, F(k, j) will remain 0 for all k and j when $m_{2.2}$ is the desired event magnitude.

Step 4

Remove the mean of S(j) from each station term so that $\sum_j S(j) = 0$.

Step 5

For each source-station pair, (i, j), compute $\mu(i,j) = E(i) + S(j) + F(k,j)$.

Step 6

For maximum-likelihood estimators, compute σ(MLE) via

$$\sigma^2 = \frac{\sum_{j=1}^{n_0}(x_{0j} - \mu_0)^2}{n_0 + \sum_{j=1}^{n_1}\frac{\phi(z_{1j})}{\Phi(z_{1j})}z_{1j} - \sum_{j=1}^{n_2}\frac{\phi(z_{2j})}{\Phi(-z_{2j})}z_{2j}} \quad . \qquad [18]$$

For iterative least-squares estimators, compute σ(ILS) via

$$\sigma^2 = \frac{\sum_{j=1}^{n_0}(x_{0j} - \mu_0)^2}{n_0 + n_1 + n_2 - \sum_{j=1}^{n_1}\left[\frac{\phi(z_{1j})}{\Phi(z_{1j})}\right]^2 - \sum_{j=1}^{n_2}\left[\frac{\phi(z_{2j})}{\Phi(-z_{2j})}\right]^2} \quad . \qquad [19]$$

where $z_i = (t_i - \mu)/\sigma$; X_0, t_1, and t_2 are collections of the observed station magnitudes of each type, respectively, and

$$\phi(u) = \frac{1}{\sqrt{2\pi}}\exp(\frac{-u^2}{2}) \; , \; \Phi(u) = \int_{-\infty}^{u}\phi(x)dx \; .$$

are the probability density function and probability distribution function, respectively, of the standard normal random variable.

If no censored recording is involved, [18] and [19] would be equally applicable since $n_1 = n_2 = 0$.

Step 7

Replace censored and missing observations X(I,J) with the corresponding conditional expectations:

$$\text{For type–1 paths: } E[\, X \mid X < t_{1_j} \,] = \mu - \sigma\frac{\phi(z_{1j})}{\Phi(z_{1j})} \quad .$$

$$\text{For type–2 paths: } E[\, X \mid X > t_{2_j} \,] = \mu + \sigma\frac{\phi(z_{2j})}{\Phi(-z_{2j})} \quad .$$

$$\text{For type–3 paths: } E[\, X \mid X \text{ is missing} \,] = \mu(I,J) = E(I) + S(J) + F(K,J) \quad .$$

These conditional expectations are then used as X(I,J) in steps 1 through 3.

Step 8

Repeat steps [1]-[7] to update E, S, F, and σ until convergence.

In the first iteration, only type 0 data are used in steps 1 through 3. Starting from the second loop, however, all types of observations are used with censored data replaced by their corresponding "refined pseudo-observations" as described in step 6. In other words, the symbol X(I,J) in steps 1-3 actually represents the conditional expectation of X given the censoring or non-censoring assumption. For type-0 data, $E[\, X \mid X = x_{0_j} \,] = x_{0_j}$, and hence the actually observed magnitude is utilized in each iteration without change. For other types of data, however, the "expected" observation will be varying as the iterations proceeds, since the optimal estimate of σ and all other parameters will change at each step.

Once the "E step" (viz., steps 5 and 7) is executed, the "M step" (viz., steps 1 through 4) in each iteration loop can be replaced with standard matrix inversion techniques such as *Singular Value Decomposition*, [SVD] or *Gaussian elimination* method. To do so, type-3 paths should be excluded from step 7. Numerical algorithms like SVD and Gaussian elimination are called *direct methods*. However, direct methods can be impractical if the design matrix is large and sparse. In our case, the linear system

involves 3,306 unknown parameters and 35,211 station magnitudes. For these types of problems, iterative methods are superior to Gaussian elimination and matrix factorization. The largest area for the application of iterative methods is that of the linear systems arising in the numerical solution of partial differential equations. Systems of orders 10,000 to 100,000 are not unusual in aerospace sciences, although the majority of the coefficients of the systems are typically zeros.

IV. GLM INVERSION RESULTS

IV.1 GLM Event Magnitudes

Table 5 gives the listing of event magnitudes based on six time-domain measurements: $m_b(P_{max})$, $m_b(P_b)$, $m_b(P_a)$, $m_b(P_n)$, $m_b(L_g)$, and M_S (LR) of clustered explosions. This covers the major tests including NTS, DM, SR, NNZ, and FS. Four hundred sixty two events were used in the GLM inversion. For the L_g phase, since the path attenuation has been accounted for in computing the raw station magnitude, Equation [16] was used to determine the event $m_b(L_g)$ and the station terms. All the remaining magnitudes are m_G. That is, the resulting event magnitudes are the maximum-likelihood network average of the station magnitudes that have been corrected for the path and receiver effects. The event magnitudes based on these 6 phases have been used in the magnitude-magnitude regressions, and the regression results are summarized in a later section.

As mentioned in Section 1, there are actually many other events for which the station m_b (or other magnitudes) were measured under Task 1, and yet they were not used in this particular GLM inversion. The model described in Equation [17] works best when there exists a suite of events clustered in the same geological / geophysical region. That is, the redundancy of events in each source region is the key to constrain the unknowns, particularly the path terms. PNEs and explosions in Amchitka, South Novaya Zemlya, Colorado, and Mississippi were not fed into the same GLM inversion. The magnitudes of these 107 events were computed with another algorithm, and the results are listed in Appendix C. These event magnitudes are called the EMILS magnitudes, *i.e.*, the single-event network averages, with the station terms inferred from the GLM inversion removed. They are furnished by Baumstark and Wagner (1994), and listed in this report merely for reference.

To illustrate the robustness of the proposed m_b determination scheme, Figures 1 through 6 show the raw and corrected m_b of 6 typical explosions from Eastern Kazakhstan and Novaya Zemlya. Figure 1 shows the scatter plot of 3 different types of station m_b s for Soviet Joint Verification Experiment [JVE] explosion SH880914. The 26 good recordings and 1 clipped signal are shown with filled circles and upward arrow, respectively. The raw station m_b s (top) have a standard deviation of 0.30 m.u. Applying the "primary" station corrections (*i.e.*, the "Rcv" column in Table 6 or the "S" term in Equation [17]) and the "secondary" corrections (*i.e.*, the "Path" column in Table 6 or "F" term in Equation [17]) reduces the scatter down to 0.14 m.u. The dashed lines of 1 σ range around the network-averaged m_b clearly illustrate the remarkable reduction of fluctuation across the recording stations. The mean event m_b itself is not significantly changed, however.

Among these six explosions, the Novaya Zemlya event NZ691014 (Figure 5) has the smallest scatter in the resulting m_G values. The dramatic reduction of variation from m_1 to m_G shows a factor of nearly 3. Note that the path correction proposed in this study not only reduces the m_b scatter for large events, it also improves the data consistency for the small events, as illustrated by Figures 4 and 6.

Table 5. GLM Event Magnitudes							
Event	Site	P_{max}	P_b	P_a	P_n	L_g	M_S
US660224	PMA	4.91±0.06	4.48±0.06	4.33±0.06	4.78±0.09	5.23±0.10	±___
US660414	PMA	5.06±0.04	4.77±0.04	4.50±0.05	5.00±0.09	5.51±0.10	±___
US660506	PMA	5.33±0.04	5.02±0.04	4.71±0.04	5.28±0.09	5.61±0.08	4.87±0.17
US660630	PMA	6.14±0.04	5.73±0.04	5.47±0.04	___±___	___±___	5.28±0.06
US670523	PMA	5.63±0.03	5.42±0.03	5.12±0.03	5.39±0.25	5.72±0.12	4.95±0.10
US670526	PMA	5.26±0.04	4.92±0.04	4.74±0.04	5.20±0.11	5.74±0.21	4.67±0.06
US680322	PMA	5.70±0.03	5.26±0.03	4.98±0.03	5.62±0.14	5.78±0.08	±___
US680615	PMA	5.92±0.04	5.61±0.04	5.25±0.04	5.97±0.25	___±___	4.75±0.07
US680628	PMA	5.34±0.05	4.94±0.05	4.48±0.05	5.44±0.25	___±___	4.56±0.05
US680829	PMA	5.92±0.03	5.65±0.03	5.39±0.03	___±___	6.00±0.08	5.24±0.17
US681208	PMA	4.69±0.07	4.28±0.07	3.92±0.08	4.56±0.09	5.16±0.15	±___
US690507	PMA	5.79±0.03	5.49±0.03	5.24±0.03	5.75±0.25	6.11±0.09	4.94±0.12
US691008	PMA	5.57±0.03	5.30±0.03	5.04±0.04	___±___	___±___	___±___
US730606	PMA	6.21±0.03	5.98±0.03	5.67±0.03	6.07±0.14	___±___	5.20±0.05
US750514	PMA	5.99±0.03	5.77±0.03	5.52±0.03	5.96±0.14	6.23±0.07	5.15±0.05
US750603	PMA	5.81±0.03	5.53±0.03	5.23±0.03	5.92±0.12	6.01±0.07	4.71±0.07
US750619	PMA	6.05±0.03	5.77±0.03	5.47±0.03	6.00±0.12	6.21±0.11	5.33±0.07
US751120	PMA	5.92±0.03	5.75±0.04	5.44±0.04	5.72±0.12	6.06±0.07	5.14±0.10
US760214	PMA	5.88±0.04	5.72±0.04	5.48±0.04	5.83±0.12	6.33±0.15	5.36±0.07
US760309	PMA	5.94±0.04	5.69±0.04	5.40±0.04	5.91±0.12	6.13±0.15	5.32±0.06
US760317	PMA	6.05±0.04	5.74±0.04	5.53±0.04	5.90±0.12	6.06±0.11	4.99±0.05
US780411	PMA	5.46±0.03	5.05±0.03	4.85±0.03	5.38±0.10	5.65±0.10	4.20±0.05
US780411	PMA	5.52±0.03	5.23±0.03	4.96±0.03	5.57±0.14	___±___	4.57±0.05
US780831	PMA	5.67±0.06	5.39±0.06	5.18±0.06	5.57±0.14	5.63±0.12	4.47±0.05
US781216	PMA	5.62±0.06	5.34±0.06	4.98±0.06	5.61±0.12	5.63±0.12	4.46±0.05
US790611	PMA	5.56±0.04	5.32±0.04	5.11±0.04	5.60±0.12	5.92±0.15	4.68±0.03
US790926	PMA	5.57±0.05	5.30±0.05	4.99±0.05	5.53±0.18	___±___	4.60±0.04
US800426	PMA	5.54±0.04	5.25±0.04	4.94±0.04	5.55±0.11	5.69±0.11	4.64±0.04
US800612	PMA	5.58±0.04	5.26±0.04	4.95±0.04	5.56±0.11	5.98±0.12	4.62±0.04
US800725	PMA	5.55±0.04	5.31±0.04	5.03±0.04	5.63±0.10	5.73±0.11	4.64±0.04
US801217	PMA	5.13±0.07	4.72±0.07	4.28±0.07	4.99±0.09	5.22±0.10	4.28±0.06
US810606	PMA	5.51±0.04	5.22±0.04	4.84±0.04	5.42±0.10	5.68±0.09	4.39±0.06
US820212	PMA	5.38±0.05	5.04±0.05	4.75±0.06	5.31±0.09	5.62±0.08	4.67±0.05
US820212	PMA	5.47±0.07	5.22±0.07	5.04±0.07	5.48±0.09	5.79±0.10	4.53±0.04
US820425	PMA	5.36±0.06	5.10±0.06	4.87±0.07	5.23±0.09	5.46±0.10	4.52±0.04
US820624	PMA	5.57±0.04	5.32±0.04	5.05±0.04	5.37±0.09	5.74±0.07	4.52±0.04
US830326	PMA	5.26±0.06	4.99±0.06	4.58±0.06	5.00±0.10	5.07±0.12	4.11±0.04
US830901	PMA	5.30±0.04	5.10±0.04	4.84±0.04	5.30±0.09	5.62±0.10	4.27±0.04
US840725	PMA	5.30±0.04	5.05±0.04	4.79±0.06	5.40±0.09	5.65±0.12	4.17±0.04
US841209	PMA	5.45±0.04	5.11±0.04	4.82±0.05	5.41±0.12	5.46±0.15	4.30±0.04

Table 5. GLM Event Magnitudes (Cont)							
Event	Site	P_{max}	P_b	P_a	P_n	L_g	M_S
US841215	PMA	5.38±0.04	5.10±0.04	4.79±0.04	5.29±0.11	5.60±0.21	4.23±0.04
US850502	PMA	5.69±0.05	5.37±0.04	5.03±0.05	5.52±0.12	6.07±0.15	4.30±0.05
US850612	PMA	5.39±0.04	5.19±0.04	4.99±0.04	5.44±0.11	5.67±0.21	4.51±0.04
US850725	PMA	5.24±0.05	5.03±0.05	4.82±0.05	5.14±0.18	5.42±0.21	4.28±0.04
US851228	PMA	5.25±0.05	4.87±0.06	4.80±0.06	5.27±0.11	5.45±0.21	4.28±0.04
US860422	PMA	5.29±0.05	4.97±0.05	4.75±0.05	5.34±0.12	5.66±0.15	4.33±0.04
US860625	PMA	5.44±0.04	5.13±0.04	4.78±0.04	5.35±0.10	5.62±0.15	4.30±0.03
US860717	PMA	5.57±0.03	5.30±0.03	4.99±0.04	5.45±0.14	5.84±0.10	4.45±0.04
US860930	PMA	5.42±0.04	5.16±0.04	4.90±0.04	5.39±0.12	5.67±0.21	4.50±0.04
US861016	PMA	5.52±0.04	5.14±0.04	4.78±0.04	5.39±0.11	5.85±0.21	4.53±0.04
US861213	PMA	5.55±0.05	5.10±0.05	4.61±0.05	5.41±0.12	5.72±0.21	4.60±0.05
US870418	PMA	5.49±0.04	5.14±0.04	4.87±0.04	5.38±0.09	5.74±0.15	4.37±0.04
US870430	PMA	5.43±0.04	5.14±0.04	4.84±0.04	5.34±0.12	5.69±0.15	4.51±0.04
US870924	PMA	5.57±0.04	5.27±0.04	5.00±0.04	5.41±0.12	5.70±0.21	4.45±0.03
US880215	PMA	5.31±0.05	5.01±0.06	4.84±0.06	5.28±0.12	±___	4.27±0.04
US880817	PMA	5.49±0.04	5.18±0.04	4.91±0.04	5.40±0.12	5.61±0.12	4.39±0.04
US890622	PMA	5.10±0.12	5.06±0.12	4.90±0.12	5.23±0.25	±___	4.12±0.10
US891208	PMA	5.39±0.08	5.37±0.08	5.11±0.10	±___	±___	4.22±0.09
US631016	RNA	5.35±0.06	5.03±0.06	5.08±0.06	4.94±0.10	5.51±0.09	±___
US670626	RNA	5.01±0.08	4.65±0.08	±___	4.45±0.10	5.16±0.11	±___
US670831	RNA	4.99±0.10	4.74±0.10	4.63±0.10	4.38±0.09	4.98±0.09	±___
US680229	RNA	5.14±0.07	±___	±___	4.69±0.09	5.18±0.10	±___
US680924	RNA	5.33±0.08	4.77±0.10	4.69±0.08	4.60±0.11	5.29±0.10	±___
US690115	RNA	5.36±0.04	5.15±0.04	4.84±0.04	4.94±0.12	5.59±0.09	±___
US690212	RNA	5.05±0.17	±___	±___	4.31±0.12	4.95±0.11	±___
US691205	RNA	5.19±0.10	4.67±0.10	4.48±0.10	4.48±0.10	5.05±0.10	±___
US700505	RNA	5.16±0.07	4.79±0.08	4.46±0.08	4.63±0.14	4.92±0.15	±___
US700526	RNA	4.81±0.08	4.44±0.08	4.23±0.10	4.23±0.12	4.55±0.12	±___
US710629	RNA	5.02±0.10	4.58±0.10	4.50±0.10	4.50±0.11	4.85±0.12	±___
US720502	RNA	5.06±0.12	4.55±0.12	4.26±0.12	4.49±0.12	5.11±0.11	±___
US720720	RNA	5.06±0.08	4.80±0.08	4.77±0.10	4.58±0.12	5.12±0.12	±___
US730605	RNA	5.00±0.07	4.68±0.07	4.51±0.07	4.30±0.12	5.26±0.10	±___
US731012	RNA	4.80±0.12	±___	±___	4.15±0.12	4.82±0.11	±___
US740619	RNA	4.92±0.10	4.50±0.10	4.19±0.10	4.57±0.12	4.97±0.12	±___
US750405	RNA	5.06±0.12	4.71±0.12	±___	4.57±0.12	4.96±0.15	±___
US751024	RNA	4.95±0.12	4.69±0.12	4.14±0.12	4.54±0.11	5.08±0.15	±___
US760512	RNA	4.88±0.12	4.53±0.12	±___	4.43±0.12	4.98±0.15	3.61±0.12
US780913	RNA	4.69±0.17	±___	±___	4.57±0.14	4.83±0.15	±___
US820923	RNA	5.30±0.07	4.94±0.07	4.55±0.10	4.70±0.10	5.23±0.15	3.76±0.06
US840215	RNA	5.23±0.07	4.87±0.07	4.55±0.07	4.82±0.11	5.13±0.21	3.63±0.06

Table 5. GLM Event Magnitudes (Cont)							
Event	Site	P_{max}	P_b	P_e	P_n	L_g	M_S
US620512	YFT	4.96±0.12	4.89±0.12	4.72±0.12	4.92±0.25	___±___	___±___
US620627	YFT	4.69±0.10	4.57±0.10	4.30±0.10	4.80±0.18	5.42±0.21	___±___
US620706	YFT	4.73±0.17	4.42±0.17	3.90±0.17	4.39±0.18	4.86±0.21	4.26±0.09
US620713	YFT	6.74±0.17	6.16±0.17	5.59±0.17	3.97±0.25	4.78±0.21	___±___
US621005	YFT	5.13±0.07	4.81±0.07	4.75±0.07	4.88±0.14	___±___	4.12±0.12
US630522	YFT	4.85±0.10	4.76±0.10	4.49±0.10	4.46±0.11	5.17±0.21	___±___
US630913	YFT	5.81±0.03	5.57±0.03	5.38±0.03	5.74±0.18	6.10±0.10	5.12±0.06
US631122	YFT	5.02±0.12	___±___	___±___	4.54±0.14	4.79±0.21	___±___
US640116	YFT	5.25±0.07	4.80±0.07	4.68±0.07	4.92±0.14	___±___	3.95±0.17
US640220	YFT	5.11±0.08	4.64±0.08	4.32±0.08	4.83±0.10	5.32±0.21	___±___
US640424	YFT	4.99±0.05	4.55±0.05	4.18±0.06	4.91±0.12	5.64±0.21	4.08±0.10
US640716	YFT	4.50±0.12	4.10±0.12	4.33±0.12	4.25±0.10	4.96±0.15	___±___
US641009	YFT	4.76±0.07	4.51±0.07	4.52±0.10	4.57±0.10	5.13±0.21	___±___
US641205	YFT	4.81±0.06	4.31±0.06	4.20±0.07	4.67±0.11	5.14±0.21	3.44±0.17
US650218	YFT	4.47±0.12	4.27±0.12	4.42±0.12	4.14±0.10	4.95±0.15	___±___
US650303	YFT	5.31±0.04	4.96±0.04	4.72±0.04	5.03±0.11	5.67±0.10	___±___
US650326	YFT	5.15±0.05	4.94±0.06	4.86±0.06	5.18±0.11	___±___	4.07±0.17
US650514	YFT	4.73±0.17	3.97±0.17	___±___	4.44±0.10	4.71±0.15	___±___
US650521	YFT	4.69±0.08	4.01±0.08	4.11±0.10	4.44±0.09	5.14±0.15	___±___
US650723	YFT	5.43±0.04	5.04±0.04	4.80±0.04	5.29±0.11	5.70±0.21	4.39±0.06
US650910	YFT	5.05±0.06	4.78±0.06	4.49±0.06	4.90±0.14	___±___	3.79±0.09
US651203	YFT	5.63±0.04	5.31±0.04	5.06±0.04	5.53±0.14	5.96±0.07	4.82±0.17
US651216	YFT	5.22±0.04	4.85±0.04	4.67±0.05	5.00±0.09	___±___	___±___
US660118	YFT	5.13±0.06	4.81±0.06	4.54±0.06	4.95±0.10	5.64±0.09	___±___
US660513	YFT	5.56±0.07	5.08±0.10	4.95±0.08	5.42±0.14	5.83±0.09	4.35±0.17
US660519	YFT	5.76±0.03	5.46±0.03	5.17±0.03	5.40±0.12	6.06±0.08	4.54±0.17
US660527	YFT	4.96±0.06	4.71±0.06	4.16±0.07	4.90±0.14	5.44±0.21	3.52±0.07
US660602	YFT	5.55±0.03	5.30±0.03	4.97±0.03	5.61±0.14	5.79±0.10	4.63±0.05
US660603	YFT	5.66±0.03	5.24±0.03	4.99±0.03	5.53±0.18	5.95±0.07	4.46±0.12
US660615	YFT	5.07±0.06	4.76±0.06	4.42±0.06	4.95±0.14	5.32±0.21	3.65±0.06
US660625	YFT	4.61±0.07	4.07±0.08	3.83±0.10	4.34±0.11	5.04±0.21	___±___
US670119	YFT	5.31±0.06	4.98±0.06	4.66±0.06	5.18±0.11	___±___	4.20±0.17
US670120	YFT	5.12±0.07	4.70±0.07	4.50±0.07	4.98±0.14	___±___	___±___
US670223	YFT	5.70±0.03	5.30±0.03	5.08±0.04	5.63±0.18	6.10±0.12	___±___
US670510	YFT	4.98±0.07	4.37±0.07	4.12±0.08	4.60±0.11	5.57±0.15	3.39±0.17
US670520	YFT	5.91±0.03	5.60±0.03	5.37±0.03	5.96±0.25	6.17±0.12	___±___
US670727	YFT	4.78±0.10	4.19±0.10	4.47±0.10	4.36±0.12	4.79±0.15	___±___
US670907	YFT	4.99±0.06	4.78±0.06	4.40±0.06	4.87±0.09	___±___	3.87±0.07
US670927	YFT	5.80±0.03	5.48±0.03	5.21±0.04	5.77±0.14	6.06±0.11	4.71±0.10
US671018	YFT	5.68±0.03	5.43±0.03	5.17±0.03	5.64±0.11	6.00±0.10	___±___

Table 5. GLM Event Magnitudes (Cont)							
Event	Site	P_{max}	P_b	P_a	P_n	L_g	M_S
US671108	YFT	4.84±0.08	___±___	___±___	4.74±0.09	5.16±0.11	___±___
US680119	YFT	4.68±0.17	4.48±0.17	4.40±0.17	4.53±0.18	___±___	___±___
US680221	YFT	5.66±0.07	5.52±0.07	5.31±0.07	5.60±0.14	6.11±0.10	___±___
US680325	YFT	4.45±0.12	___±___	___±___	4.21±0.12	4.73±0.15	___±___
US680410	YFT	4.78±0.12	3.96±0.12	4.01±0.12	4.37±0.10	___±___	___±___
US680418	YFT	5.08±0.05	4.74±0.05	4.47±0.05	4.89±0.18	5.33±0.21	3.57±0.07
US680517	YFT	4.89±0.05	4.32±0.05	4.32±0.05	4.75±0.09	5.03±0.15	___±___
US680906	YFT	5.55±0.03	5.25±0.03	5.02±0.04	5.54±0.18	6.04±0.11	4.87±0.12
US680917	YFT	4.81±0.07	4.49±0.07	4.18±0.08	4.56±0.09	5.41±0.15	3.86±0.17
US690130	YFT	4.91±0.10	4.25±0.10	4.07±0.10	4.69±0.10	4.91±0.15	___±___
US690321	YFT	4.94±0.08	4.29±0.12	4.26±0.12	4.65±0.11	___±___	___±___
US690430	YFT	5.33±0.04	4.94±0.04	4.62±0.04	5.04±0.14	5.56±0.10	4.21±0.17
US690527	YFT	4.91±0.05	4.63±0.05	4.23±0.06	4.81±0.11	5.33±0.21	___±___
US690716	YFT	4.40±0.12	___±___	___±___	4.29±0.14	___±___	___±___
US690716	YFT	5.45±0.04	5.10±0.04	4.89±0.04	5.37±0.14	5.71±0.21	___±___
US691029	YFT	5.67±0.03	5.27±0.03	4.92±0.03	5.41±0.11	5.85±0.11	___±___
US691121	YFT	4.79±0.08	4.46±0.10	4.42±0.10	4.77±0.12	5.30±0.21	___±___
US691217	YFT	5.45±0.04	5.15±0.04	4.94±0.04	5.22±0.18	___±___	___±___
US691217	YFT	5.61±0.12	4.81±0.12	4.61±0.12	4.46±0.14	___±___	___±___
US700204	YFT	5.67±0.04	5.33±0.04	5.03±0.04	5.47±0.14	___±___	4.27±0.08
US700205	YFT	4.72±0.08	4.33±0.08	4.02±0.10	4.40±0.09	4.98±0.15	___±___
US700225	YFT	5.05±0.04	4.67±0.04	4.51±0.05	4.83±0.09	5.49±0.21	___±___
US700323	YFT	5.48±0.07	5.05±0.08	4.61±0.08	5.33±0.14	5.78±0.08	___±___
US700521	YFT	4.99±0.06	4.53±0.06	4.21±0.07	4.65±0.10	4.91±0.15	___±___
US701014	YFT	5.57±0.04	5.29±0.03	5.02±0.04	5.45±0.18	5.69±0.15	4.61±0.12
US701105	YFT	4.83±0.10	4.42±0.10	4.45±0.10	4.66±0.11	5.08±0.21	___±___
US701216	YFT	5.18±0.04	4.75±0.04	4.40±0.05	5.04±0.14	___±___	___±___
US701217	YFT	5.87±0.03	5.58±0.03	5.19±0.03	5.78±0.25	5.95±0.12	4.91±0.17
US710624	YFT	5.13±0.06	4.47±0.06	4.36±0.07	4.74±0.08	5.21±0.21	___±___
US710708	YFT	5.51±0.03	5.16±0.03	4.92±0.03	5.45±0.14	5.83±0.07	___±___
US710818	YFT	5.26±0.04	4.82±0.04	4.49±0.04	4.97±0.11	5.83±0.09	3.78±0.06
US720519	YFT	4.65±0.10	___±___	___±___	4.44±0.25	5.06±0.15	___±___
US720921	YFT	5.68±0.03	5.26±0.03	4.99±0.03	5.55±0.18	6.07±0.12	4.48±0.06
US721221	YFT	5.05±0.06	4.62±0.06	4.45±0.07	4.71±0.10	___±___	___±___
US730308	YFT	5.38±0.04	5.04±0.04	4.70±0.05	5.08±0.12	5.62±0.07	4.02±0.17
US730426	YFT	5.54±0.03	5.13±0.03	5.00±0.03	5.30±0.12	5.86±0.08	4.25±0.08
US730628	YFT	4.93±0.05	4.46±0.05	4.21±0.06	4.76±0.09	5.18±0.11	___±___
US740227	YFT	5.65±0.04	5.38±0.04	5.17±0.04	5.65±0.12	6.00±0.10	4.48±0.10
US740523	YFT	4.84±0.06	4.28±0.07	4.11±0.07	4.38±0.09	5.12±0.21	___±___
US740710	YFT	5.74±0.03	5.29±0.03	5.03±0.03	5.45±0.14	5.66±0.12	4.53±0.05

Table 5. GLM Event Magnitudes (Cont)							
Event	Site	P_{max}	P_b	P_a	P_n	L_g	M_S
US740830	YFT	5.71±0.05	5.48±0.05	5.33±0.05	5.56±0.25	5.86±0.12	4.56±0.09
US740926	YFT	5.54±0.04	5.10±0.04	4.84±0.04	5.43±0.14	5.64±0.10	±___
US750228	YFT	5.76±0.03	5.43±0.03	5.23±0.03	5.63±0.12	±___	4.62±0.10
US750307	YFT	5.61±0.03	5.27±0.03	4.93±0.03	5.55±0.14	5.84±0.09	±___
US750424	YFT	4.57±0.10	3.96±0.10	3.69±0.10	4.51±0.10	4.83±0.15	±___
US750430	YFT	5.12±0.05	4.83±0.05	4.70±0.05	4.85±0.12	5.58±0.10	±___
US750603	YFT	5.70±0.03	5.42±0.03	5.19±0.03	5.44±0.14	5.78±0.15	4.54±0.10
US751220	YFT	5.79±0.03	5.48±0.03	5.25±0.03	5.83±0.11	5.92±0.11	±___
US760204	YFT	5.69±0.03	5.36±0.03	5.15±0.04	5.30±0.12	5.86±0.09	4.58±0.07
US760204	YFT	5.73±0.03	5.49±0.03	5.29±0.03	5.32±0.18	±___	4.68±0.10
US760317	YFT	5.91±0.04	5.71±0.04	5.44±0.04	5.50±0.25	±___	4.74±0.06
US760727	YFT	5.21±0.08	5.02±0.08	4.74±0.08	4.91±0.18	±___	±___
US760826	YFT	5.26±0.05	4.89±0.05	4.45±0.06	5.15±0.12	5.67±0.15	4.08±0.07
US761228	YFT	5.59±0.04	5.25±0.04	5.05±0.04	5.27±0.14	5.84±0.10	4.38±0.09
US770405	YFT	5.71±0.04	5.46±0.04	5.08±0.04	5.60±0.14	±___	4.32±0.10
US770427	YFT	5.42±0.04	5.17±0.04	4.92±0.04	5.24±0.10	5.78±0.07	4.34±0.07
US770525	YFT	5.43±0.05	5.05±0.05	4.81±0.05	5.29±0.11	5.55±0.10	±___
US770804	YFT	5.21±0.04	4.85±0.04	4.52±0.04	5.06±0.08	5.59±0.10	4.06±0.06
US770819	YFT	5.66±0.04	5.46±0.04	5.07±0.04	5.37±0.25	6.23±0.21	4.59±0.12
US770927	YFT	4.97±0.05	4.54±0.06	4.34±0.06	4.91±0.11	5.46±0.15	±___
US771109	YFT	5.81±0.03	5.52±0.03	5.28±0.04	±___	±___	4.87±0.06
US771214	YFT	5.81±0.04	5.56±0.04	5.29±0.04	5.64±0.18	±___	4.82±0.07
US780223	YFT	5.67±0.03	5.38±0.04	5.05±0.04	5.61±0.14	5.58±0.21	4.36±0.06
US780323	YFT	5.66±0.03	5.31±0.03	5.05±0.03	5.64±0.11	±___	4.66±0.07
US780712	YFT	5.68±0.03	5.31±0.03	5.00±0.03	5.27±0.12	5.88±0.10	4.37±0.04
US780927	YFT	5.23±0.04	4.85±0.04	4.55±0.04	5.01±0.11	5.47±0.21	±___
US780927	YFT	5.92±0.04	5.62±0.04	5.37±0.04	5.62±0.25	±___	4.72±0.03
US781118	YFT	5.36±0.05	5.06±0.05	4.82±0.05	5.19±0.11	5.54±0.15	4.36±0.06
US790208	YFT	5.66±0.04	5.38±0.04	5.05±0.04	5.45±0.12	6.15±0.10	4.53±0.05
US790215	YFT	5.06±0.07	4.69±0.07	4.38±0.07	4.87±0.10	5.33±0.15	±___
US790628	YFT	5.18±0.05	4.89±0.05	4.46±0.05	5.05±0.10	5.66±0.11	4.22±0.06
US790803	YFT	4.74±0.06	4.40±0.06	4.21±0.08	4.70±0.11	5.23±0.12	±___
US790808	YFT	4.76±0.06	4.41±0.07	4.40±0.06	4.59±0.09	5.29±0.11	±___
US790829	YFT	5.06±0.08	4.64±0.08	4.57±0.08	4.83±0.12	5.51±0.15	±___
US790906	YFT	5.96±0.03	5.63±0.03	5.37±0.03	5.65±0.11	6.09±0.08	4.77±0.04
US800403	YFT	4.99±0.07	4.59±0.07	4.50±0.08	4.63±0.14	5.30±0.21	±___
US800416	YFT	5.45±0.08	5.26±0.08	4.97±0.08	5.21±0.11	5.89±0.11	4.47±0.05
US810115	YFT	5.70±0.04	5.29±0.04	5.00±0.04	5.30±0.11	5.86±0.07	4.73±0.04
US811001	YFT	5.04±0.06	4.52±0.07	4.38±0.07	4.93±0.08	5.41±0.08	4.11±0.17
US811111	YFT	4.96±0.07	4.47±0.07	4.31±0.07	4.71±0.09	5.31±0.10	3.57±0.17

Table 5. GLM Event Magnitudes (Cont)							
Event	Site	P_{max}	P_b	P_a	P_n	L_g	M_S
US811112	YFT	5.43±0.04	5.11±0.04	4.78±0.04	5.20±0.09	5.67±0.09	4.35±0.04
US811203	YFT	4.94±0.17	___±___	___±___	4.58±0.08	5.17±0.08	___±___
US820128	YFT	5.91±0.04	5.58±0.04	5.33±0.04	5.54±0.09	5.92±0.07	4.77±0.04
US820507	YFT	5.64±0.04	5.32±0.04	5.07±0.04	5.45±0.09	5.88±0.07	4.37±0.04
US820729	YFT	4.54±0.10	3.87±0.12	4.03±0.12	4.44±0.07	4.90±0.09	3.32±0.07
US820805	YFT	5.77±0.04	5.51±0.04	5.26±0.04	5.46±0.09	5.76±0.08	4.84±0.04
US821210	YFT	4.72±0.07	4.27±0.07	3.80±0.08	4.45±0.08	4.76±0.11	3.10±0.07
US830414	YFT	5.65±0.04	5.26±0.04	5.08±0.04	5.38±0.09	5.84±0.07	4.35±0.04
US831216	YFT	5.49±0.07	4.84±0.10	4.04±0.17	4.67±0.11	5.36±0.15	4.04±0.04
US840131	YFT	4.44±0.12	4.08±0.12	4.37±0.17	4.24±0.08	4.93±0.11	___±___
US840301	YFT	5.83±0.04	5.46±0.04	5.25±0.04	5.64±0.12	5.18±0.12	4.59±0.04
US840501	YFT	5.48±0.04	5.18±0.04	4.88±0.04	5.22±0.11	5.80±0.11	4.60±0.04
US840531	YFT	5.75±0.05	5.47±0.05	5.16±0.05	5.47±0.09	6.11±0.15	4.63±0.04
US840620	YFT	4.74±0.07	4.28±0.07	4.23±0.07	4.38±0.11	___±___	3.45±0.05
US840913	YFT	5.10±0.07	4.74±0.07	4.51±0.07	4.66±0.11	5.42±0.15	3.91±0.05
US850315	YFT	4.84±0.06	4.51±0.06	4.31±0.07	4.49±0.10	___±___	3.39±0.06
US850323	YFT	5.34±0.04	5.04±0.04	4.75±0.04	4.99±0.12	___±___	4.19±0.04
US850402	YFT	5.74±0.04	5.42±0.04	5.23±0.04	5.38±0.12	5.97±0.15	4.81±0.04
US851205	YFT	5.55±0.04	5.26±0.04	4.95±0.04	5.55±0.12	___±___	4.39±0.04
US860322	YFT	5.29±0.05	4.77±0.05	4.51±0.06	5.21±0.11	___±___	3.97±0.07
US860605	YFT	5.33±0.05	4.98±0.05	4.76±0.05	5.09±0.11	5.59±0.15	4.41±0.04
US861114	YFT	5.69±0.04	5.40±0.04	5.00±0.04	5.38±0.11	5.91±0.21	4.59±0.04
US870716	YFT	4.94±0.07	4.56±0.07	4.31±0.07	4.69±0.18	5.50±0.21	3.83±0.05
US870813	YFT	5.86±0.04	5.58±0.04	5.27±0.04	5.52±0.14	6.16±0.21	4.62±0.04
US871023	YFT	5.46±0.06	4.81±0.06	4.50±0.06	5.12±0.11	5.40±0.15	3.90±0.06
US881013	YFT	5.88±0.06	5.36±0.06	4.89±0.06	___±___	___±___	4.77±0.06
US890210	YFT	5.26±0.12	4.95±0.12	4.78±0.12	___±___	___±___	4.35±0.12
US890309	YFT	5.19±0.17	4.82±0.17	4.71±0.17	5.47±0.25	___±___	___±___
SH680619	BNE	5.39±0.03	5.13±0.03	4.89±0.03	___±___	5.57±0.12	___±___
SH720210	BNE	5.44±0.03	5.19±0.03	4.97±0.03	___±___	5.29±0.11	___±___
SH721210	BNE	6.10±0.03	5.89±0.03	5.69±0.03	___±___	5.99±0.10	4.72±0.04
SH731214	BNE	5.88±0.04	5.70±0.04	5.44±0.04	___±___	5.78±0.11	4.59±0.06
SH741016	BNE	5.53±0.03	5.30±0.03	5.06±0.03	___±___	5.42±0.21	___±___
SH741227	BNE	5.66±0.03	5.43±0.03	5.21±0.03	___±___	5.57±0.12	3.61±0.08
SH751225	BNE	5.80±0.03	5.50±0.03	5.24±0.03	4.97±0.25	___±___	3.94±0.08
SH760609	BNE	5.25±0.03	5.03±0.03	4.75±0.03	4.86±0.25	___±___	3.29±0.12
SH760828	BNE	5.76±0.03	5.54±0.03	5.23±0.03	5.57±0.25	5.45±0.11	3.96±0.05
SH761123	BNE	5.85±0.03	5.67±0.03	5.40±0.03	4.94±0.25	___±___	3.98±0.05
SH770629	BNE	5.31±0.03	4.98±0.03	4.77±0.03	4.25±0.25	___±___	___±___
SH770905	BNE	5.87±0.03	5.62±0.03	5.32±0.03	6.20±0.18	5.83±0.12	4.08±0.05

Table 5. GLM Event Magnitudes (Cont)							
Event	Site	P_{max}	P_b	P_a	P_n	L_g	M_S
SH771029	BNE	5.80±0.04	5.48±0.04	5.40±0.05	4.81±0.25	5.64±0.15	4.15±0.06
SH780829	BNE	5.94±0.04	5.84±0.04	5.62±0.04	4.95±0.18	5.92±0.21	4.11±0.05
SH781104	BNE	5.64±0.03	5.47±0.03	5.23±0.03	___±___	___±___	4.03±0.04
SH790201	BNE	5.42±0.03	5.13±0.03	4.87±0.03	5.01±0.25	___±___	3.38±0.05
SH790707	BNE	5.96±0.04	5.78±0.04	5.50±0.03	5.97±0.18	5.69±0.11	4.46±0.05
SH791028	BNE	6.09±0.03	5.86±0.03	5.59±0.03	___±___	5.77±0.12	4.46±0.03
SH800612	BNE	5.66±0.03	5.47±0.03	5.16±0.03	5.75±0.25	5.53±0.12	3.70±0.04
SH801012	BNE	5.96±0.03	5.74±0.03	5.49±0.03	5.63±0.14	5.58±0.12	4.47±0.04
SH801227	BNE	5.91±0.03	5.74±0.03	5.47±0.03	5.55±0.14	5.71±0.12	4.09±0.04
SH810329	BNE	5.59±0.03	5.37±0.03	5.06±0.03	5.25±0.25	5.60±0.21	3.85±0.03
SH810527	BNE	5.40±0.04	5.16±0.04	4.89±0.04	___±___	5.35±0.09	3.56±0.04
SH821226	BNE	5.74±0.03	5.50±0.03	5.21±0.03	5.75±0.25	___±___	3.82±0.04
SH831120	BNE	5.52±0.03	5.27±0.03	4.98±0.03	___±___	___±___	3.70±0.05
SH840307	BNE	5.75±0.03	5.50±0.03	5.22±0.03	4.64±0.25	5.88±0.21	4.04±0.04
SH840526	BNE	6.12±0.03	5.96±0.03	5.66±0.03	6.31±0.25	5.83±0.12	4.50±0.06
SH841202	BNE	5.94±0.03	5.74±0.03	5.43±0.03	5.99±0.18	5.82±0.15	4.12±0.03
SH881112	BNE	5.36±0.04	5.16±0.04	4.96±0.05	5.81±0.14	___±___	3.29±0.05
SH890902	BNE	5.01±0.06	4.81±0.06	4.62±0.06	5.67±0.18	___±___	3.66±0.05
SH721102	BSW	6.30±0.03	6.10±0.03	5.80±0.03	___±___	6.02±0.10	4.48±0.05
SH760421	BSW	5.13±0.12	4.97±0.12	4.72±0.12	___±___	___±___	2.93±0.17
SH761207	BSW	5.85±0.03	5.63±0.03	5.35±0.03	___±___	5.93±0.21	4.11±0.05
SH770529	BSW	5.83±0.03	5.58±0.03	5.27±0.03	___±___	5.47±0.11	3.82±0.06
SH780611	BSW	5.93±0.03	5.71±0.03	5.38±0.03	6.12±0.18	5.65±0.12	4.46±0.04
SH780705	BSW	5.84±0.03	5.66±0.03	5.30±0.03	___±___	5.70±0.15	3.89±0.04
SH780915	BSW	5.96±0.04	5.79±0.04	5.49±0.04	5.76±0.18	5.79±0.12	4.26±0.04
SH781129	BSW	6.04±0.04	5.82±0.04	5.55±0.04	___±___	5.67±0.11	4.28±0.04
SH790623	BSW	6.13±0.03	5.98±0.03	5.73±0.03	6.06±0.25	5.87±0.15	4.42±0.04
SH790804	BSW	6.21±0.03	6.02±0.03	5.75±0.03	5.90±0.18	6.00±0.12	4.50±0.03
SH791202	BSW	6.04±0.03	5.83±0.03	5.56±0.03	5.89±0.25	5.88±0.21	4.52±0.04
SH791223	BSW	6.21±0.03	6.00±0.03	5.71±0.03	5.95±0.18	___±___	4.29±0.03
SH800629	BSW	5.83±0.03	5.64±0.03	5.37±0.04	___±___	5.74±0.11	3.83±0.04
SH800914	BSW	6.26±0.03	6.09±0.03	5.81±0.03	6.01±0.25	6.00±0.12	4.36±0.03
SH810422	BSW	6.00±0.03	5.79±0.03	5.51±0.03	7.31±0.25	___±___	4.40±0.04
SH811018	BSW	6.05±0.03	5.85±0.03	5.58±0.03	6.19±0.25	5.87±0.15	4.39±0.04
SH811129	BSW	5.63±0.03	5.45±0.03	5.14±0.03	5.23±0.25	___±___	4.25±0.04
SH811227	BSW	6.22±0.03	6.04±0.03	5.75±0.03	6.63±0.25	___±___	4.44±0.03
SH820704	BSW	6.25±0.03	6.03±0.03	5.73±0.03	___±___	___±___	___±___
SH820831	BSW	5.27±0.04	5.03±0.04	4.71±0.04	___±___	___±___	3.89±0.04
SH821205	BSW	6.17±0.03	5.96±0.03	5.69±0.03	5.74±0.25	___±___	4.43±0.03
SH831006	BSW	6.03±0.03	5.80±0.03	5.51±0.03	5.55±0.25	5.78±0.15	4.47±0.03

Table 5. GLM Event Magnitudes (Cont)							
Event	Site	P_{max}	P_b	P_a	P_n	L_g	M_S
SH831026	BSW	6.16±0.03	5.95±0.03	5.65±0.03	5.93±0.25	5.88±0.15	4.50±0.03
SH840219	BSW	5.85±0.03	5.63±0.03	5.34±0.03	___±___	___±___	4.38±0.03
SH840425	BSW	5.93±0.03	5.72±0.03	5.49±0.03	5.80±0.18	5.66±0.21	4.54±0.03
SH840714	BSW	6.15±0.03	5.93±0.03	5.65±0.03	6.15±0.25	___±___	4.57±0.03
SH841027	BSW	6.29±0.03	6.10±0.03	5.81±0.03	___±___	5.92±0.21	4.46±0.03
SH841216	BSW	6.17±0.03	5.98±0.03	5.68±0.03	5.81±0.18	5.97±0.21	4.59±0.03
SH841228	BSW	6.01±0.03	5.86±0.03	5.54±0.03	6.77±0.25	5.87±0.21	4.37±0.03
SH850210	BSW	5.93±0.03	5.73±0.03	5.42±0.03	5.76±0.25	5.93±0.21	4.51±0.03
SH850615	BSW	6.10±0.03	5.92±0.03	5.60±0.03	___±___	5.81±0.15	4.23±0.03
SH850630	BSW	5.99±0.03	5.83±0.03	5.49±0.03	___±___	6.00±0.15	4.33±0.03
SH850720	BSW	5.98±0.03	5.79±0.03	5.48±0.03	___±___	5.73±0.21	4.22±0.03
SH870312	BSW	5.42±0.03	5.18±0.03	4.90±0.03	5.42±0.25	___±___	4.09±0.04
SH870403	BSW	6.31±0.06	6.08±0.05	5.84±0.05	___±___	___±___	4.72±0.09
SH870417	BSW	6.05±0.03	5.85±0.03	5.58±0.03	___±___	___±___	4.26±0.04
SH870620	BSW	6.11±0.03	5.92±0.03	5.66±0.03	5.90±0.25	___±___	4.25±0.04
SH870802	BSW	5.88±0.04	5.68±0.04	5.42±0.04	5.80±0.25	___±___	4.02±0.04
SH871115	BSW	6.08±0.03	5.90±0.03	5.61±0.03	6.19±0.25	5.89±0.21	4.64±0.03
SH871213	BSW	6.13±0.04	5.94±0.04	5.72±0.04	6.15±0.14	___±___	4.50±0.04
SH871227	BSW	6.18±0.04	5.95±0.04	5.75±0.04	5.94±0.14	___±___	4.31±0.04
SH880213	BSW	6.10±0.04	5.88±0.03	5.61±0.04	6.13±0.14	5.97±0.21	4.49±0.03
SH880504	BSW	6.19±0.04	5.98±0.03	5.74±0.03	6.00±0.14	5.90±0.21	4.40±0.05
SH880914	BSW	6.12±0.03	5.96±0.03	5.66±0.03	5.99±0.18	___±___	4.55±0.03
SH881217	BSW	5.83±0.04	5.66±0.04	5.39±0.04	6.15±0.18	___±___	4.40±0.04
SH890122	BSW	6.07±0.04	5.88±0.04	5.60±0.04	6.22±0.25	___±___	4.49±0.04
SH890212	BSW	5.85±0.04	5.63±0.04	5.42±0.04	5.85±0.18	5.85±0.21	4.56±0.04
SH890708	BSW	5.60±0.03	5.38±0.03	5.10±0.03	5.76±0.14	___±___	4.08±0.03
SH650115	BTZ	5.93±0.04	5.81±0.04	5.57±0.04	___±___	5.90±0.12	4.59±0.10
SH691130	BTZ	6.09±0.03	5.82±0.03	5.55±0.03	___±___	5.90±0.12	4.32±0.03
SH710630	BTZ	5.21±0.04	5.00±0.04	4.76±0.05	5.68±0.25	5.35±0.12	3.32±0.12
SH730723	BTZ	6.33±0.04	6.11±0.04	5.82±0.04	___±___	5.95±0.08	4.33±0.05
SH740531	BTZ	5.88±0.03	5.64±0.03	5.38±0.03	___±___	5.79±0.11	___±___
SH750427	BTZ	5.60±0.03	5.33±0.03	4.99±0.03	___±___	5.45±0.15	3.86±0.07
SH751029	BTZ	5.64±0.03	5.38±0.03	5.10±0.03	___±___	5.60±0.15	3.56±0.17
SH760704	BTZ	5.94±0.03	5.72±0.03	5.45±0.03	___±___	5.58±0.09	4.29±0.04
SH771130	BTZ	5.85±0.03	5.62±0.03	5.30±0.03	5.72±0.18	5.88±0.12	3.95±0.05
SH790818	BTZ	6.13±0.03	5.93±0.03	5.69±0.03	5.90±0.18	5.86±0.12	4.14±0.04
SH800425	BTZ	5.46±0.03	5.29±0.03	5.03±0.03	___±___	5.32±0.15	3.34±0.06
SH801214	BTZ	5.91±0.03	5.75±0.03	5.49±0.03	6.04±0.14	5.84±0.11	4.27±0.03
SH810913	BTZ	6.12±0.03	5.91±0.03	5.61±0.03	___±___	___±___	4.52±0.04
SH820425	BTZ	6.08±0.03	5.87±0.03	5.55±0.03	___±___	___±___	4.43±0.03

Table 5. GLM Event Magnitudes (Cont)							
Event	Site	P_{max}	P_b	P_a	P_n	L_g	M_S
SH830612	BTZ	6.07±0.03	5.87±0.03	5.56±0.03	±___	5.79±0.12	4.62±0.03
SH840329	BTZ	5.88±0.03	5.70±0.03	5.43±0.03	±___	±___	4.32±0.03
SH850425	BTZ	5.93±0.03	5.68±0.03	5.37±0.03	±___	±___	4.33±0.03
SH880403	BTZ	6.09±0.03	5.93±0.03	5.64±0.03	6.19±0.14	5.95±0.15	4.52±0.03
SH891019	BTZ	5.89±0.03	5.62±0.03	5.34±0.03	6.08±0.18	5.71±0.21	4.59±0.03
DM620202	Deg	5.47±0.08	5.20±0.08	4.78±0.08	±___	±___	±___
DM640315	Deg	5.51±0.04	5.20±0.04	4.92±0.04	±___	±___	±___
DM640516	Deg	5.50±0.04	5.25±0.04	4.97±0.04	±___	±___	4.05±0.10
DM640719	Deg	5.30±0.03	5.10±0.03	4.91±0.03	±___	±___	4.35±0.10
DM641116	Deg	5.55±0.04	5.23±0.04	5.13±0.04	±___	±___	4.37±0.12
DM650303	Deg	5.46±0.04	5.17±0.04	4.89±0.04	±___	±___	4.59±0.17
DM650617	Deg	5.17±0.04	5.00±0.04	4.75±0.04	±___	±___	±___
DM650917	Deg	5.05±0.05	4.80±0.05	4.58±0.05	±___	±___	±___
DM651008	Deg	5.36±0.04	5.10±0.03	4.87±0.04	±___	±___	±___
DM651121	Deg	5.55±0.03	5.32±0.03	5.12±0.03	±___	±___	3.95±0.17
DM660213	Deg	6.18±0.04	6.03±0.04	5.86±0.04	6.62±0.25	5.89±0.12	4.65±0.05
DM660320	Deg	5.95±0.04	5.74±0.04	5.44±0.03	±___	5.91±0.11	4.82±0.17
DM660421	Deg	5.31±0.03	5.08±0.03	4.81±0.03	±___	±___	3.47±0.12
DM660629	Deg	5.43±0.04	5.16±0.04	4.93±0.04	±___	±___	±___
DM660721	Deg	5.29±0.03	5.10±0.03	4.83±0.03	5.48±0.25	±___	±___
DM660805	Deg	5.34±0.03	5.16±0.03	4.88±0.03	±___	±___	3.90±0.12
DM661019	Deg	5.65±0.03	5.44±0.03	5.24±0.03	±___	5.37±0.15	4.04±0.12
DM670226	Deg	5.97±0.03	5.81±0.03	5.57±0.03	5.87±0.25	±___	4.42±0.04
DM670325	Deg	5.24±0.03	5.02±0.03	4.77±0.03	±___	±___	±___
DM670420	Deg	5.48±0.03	5.30±0.03	5.06±0.03	±___	±___	3.84±0.12
DM670528	Deg	5.38±0.03	5.13±0.03	4.87±0.03	5.30±0.25	5.17±0.12	3.90±0.09
DM670629	Deg	5.20±0.03	4.96±0.03	4.72±0.03	±___	±___	±___
DM670715	Deg	5.33±0.03	5.13±0.03	4.82±0.03	±___	±___	3.81±0.09
DM670804	Deg	5.26±0.03	5.03±0.03	4.72±0.03	±___	±___	4.24±0.12
DM671017	Deg	5.57±0.03	5.29±0.04	5.01±0.04	±___	±___	4.20±0.12
DM671030	Deg	5.30±0.03	5.10±0.03	4.88±0.03	±___	±___	3.71±0.12
DM671208	Deg	5.20±0.03	4.95±0.03	4.75±0.04	±___	±___	±___
DM680611	Deg	5.12±0.04	4.83±0.04	4.60±0.04	5.21±0.25	±___	±___
DM680712	Deg	5.25±0.05	5.06±0.05	4.73±0.05	±___	±___	3.66±0.17
DM680905	Deg	5.41±0.04	5.18±0.04	4.93±0.04	±___	±___	±___
DM680929	Deg	5.76±0.03	5.60±0.03	5.35±0.03	5.41±0.25	5.53±0.11	4.04±0.09
DM681218	Deg	4.99±0.05	4.79±0.05	4.47±0.05	±___	±___	±___
DM690307	Deg	5.53±0.03	5.36±0.03	5.08±0.03	5.25±0.25	±___	3.91±0.07
DM690516	Deg	5.16±0.03	4.95±0.03	4.78±0.03	±___	±___	±___
DM690704	Deg	5.17±0.03	4.98±0.03	4.76±0.03	±___	±___	3.55±0.10

Table 5. GLM Event Magnitudes (Cont)							
Event	Site	P_{max}	P_b	P_e	P_n	L_g	M_S
DM690723	Deg	5.40±0.03	5.20±0.03	5.00±0.03	___±___	5.40±0.12	___±___
DM691001	Deg	5.16±0.03	4.94±0.03	4.62±0.03	5.00±0.25	___±___	3.36±0.12
DM700129	Deg	5.45±0.03	5.30±0.03	5.07±0.03	___±___	___±___	4.07±0.06
DM700628	Deg	5.72±0.03	5.51±0.03	5.24±0.03	5.50±0.25	___±___	___±___
DM700724	Deg	5.25±0.03	5.00±0.03	4.73±0.03	5.45±0.25	___±___	___±___
DM700906	Deg	5.50±0.03	5.30±0.03	5.06±0.03	5.29±0.25	___±___	3.67±0.08
DM701217	Deg	5.37±0.03	5.19±0.03	4.97±0.03	___±___	___±___	3.65±0.09
DM710322	Deg	5.66±0.03	5.46±0.03	5.21±0.03	4.87±0.25	5.40±0.12	4.21±0.05
DM710425	Deg	5.90±0.03	5.72±0.03	5.53±0.03	5.42±0.18	5.82±0.08	4.34±0.04
DM711129	Deg	5.30±0.03	5.16±0.03	4.90±0.03	___±___	___±___	___±___
DM711230	Deg	5.70±0.03	5.50±0.03	5.23±0.03	___±___	___±___	3.89±0.06
DM720310	Deg	5.40±0.03	5.23±0.03	4.97±0.03	5.20±0.25	___±___	3.86±0.07
DM720328	Deg	5.13±0.03	4.96±0.03	4.73±0.03	4.94±0.14	___±___	___±___
DM720607	Deg	5.35±0.03	5.01±0.03	4.74±0.03	5.07±0.18	___±___	3.85±0.08
DM720816	Deg	5.07±0.03	4.90±0.03	4.63±0.03	5.08±0.18	___±___	3.89±0.10
DM721210	Deg	5.69±0.03	5.47±0.03	5.23±0.03	5.57±0.25	___±___	4.98±0.04
DM730216	Deg	5.35±0.03	5.21±0.03	5.04±0.03	5.09±0.25	___±___	___±___
DM730710	Deg	5.21±0.03	5.05±0.03	4.74±0.04	5.57±0.25	___±___	3.51±0.17
DM731026	Deg	5.12±0.03	4.98±0.04	4.72±0.04	5.61±0.25	___±___	3.82±0.09
DM740130	Deg	5.35±0.03	5.17±0.03	4.96±0.03	4.36±0.25	___±___	3.58±0.12
DM740516	Deg	5.17±0.03	4.96±0.03	4.69±0.03	___±___	___±___	___±___
DM740710	Deg	5.07±0.03	4.87±0.03	4.63±0.03	5.08±0.18	___±___	3.53±0.09
DM740913	Deg	5.06±0.03	4.88±0.03	4.57±0.03	5.10±0.18	___±___	___±___
DM750220	Deg	5.68±0.03	5.46±0.03	5.13±0.03	5.38±0.25	___±___	4.01±0.09
DM750311	Deg	5.34±0.03	5.21±0.03	4.86±0.03	5.53±0.25	___±___	___±___
DM750608	Deg	5.42±0.03	5.18±0.03	5.00±0.03	5.27±0.14	___±___	3.96±0.10
DM750807	Deg	5.14±0.03	4.87±0.03	4.64±0.04	___±___	___±___	___±___
DM751213	Deg	4.95±0.04	4.68±0.04	4.45±0.04	5.03±0.18	___±___	___±___
DM760115	Deg	5.06±0.04	4.86±0.03	4.62±0.04	4.95±0.14	___±___	___±___
DM760723	Deg	4.93±0.03	4.76±0.03	4.49±0.04	4.72±0.25	___±___	3.88±0.09
DM761230	Deg	4.88±0.04	4.63±0.04	4.47±0.04	4.38±0.18	___±___	___±___
DM770329	Deg	5.18±0.03	4.87±0.03	4.69±0.03	4.40±0.25	___±___	3.35±0.08
DM770425	Deg	4.85±0.03	4.67±0.03	4.42±0.03	4.66±0.18	___±___	2.71±0.10
DM770730	Deg	5.00±0.03	4.81±0.03	4.49±0.03	4.66±0.12	___±___	2.85±0.10
DM770817	Deg	4.83±0.03	4.64±0.03	4.39±0.04	5.46±0.25	___±___	___±___
DM771029	Deg	5.36±0.03	5.14±0.03	5.02±0.03	5.66±0.25	___±___	4.05±0.05
DM780326	Deg	5.60±0.04	5.37±0.04	5.17±0.04	5.61±0.14	___±___	4.16±0.05
DM780422	Deg	5.20±0.03	5.03±0.03	4.81±0.03	4.99±0.18	___±___	3.60±0.04
DM780728	Deg	5.63±0.03	5.49±0.03	5.20±0.03	5.74±0.18	5.39±0.12	3.84±0.04
DM781015	Deg	5.00±0.03	4.86±0.03	4.70±0.03	4.70±0.25	___±___	3.61±0.06

Table 5. GLM Event Magnitudes (Cont)							
Event	Site	P_{max}	P_b	P_a	P_n	L_g	M_S
DM781031	Deg	5.05±0.03	4.90±0.03	4.71±0.04	___±___	___±___	3.25±0.06
DM781129	Deg	4.99±0.04	4.87±0.04	4.66±0.04	___±___	___±___	4.35±0.04
DM790506	Deg	5.05±0.04	4.91±0.04	4.67±0.04	4.88±0.25	___±___	3.14±0.09
DM790531	Deg	5.06±0.04	4.93±0.04	4.73±0.04	5.01±0.25	___±___	3.25±0.07
DM791018	Deg	4.98±0.03	4.86±0.03	4.58±0.03	___±___	___±___	___±___
DM800410	Deg	4.85±0.04	4.69±0.04	4.41±0.04	4.63±0.25	___±___	2.83±0.08
DM800522	Deg	5.25±0.04	5.06±0.04	4.82±0.04	5.10±0.18	___±___	3.45±0.05
DM800731	Deg	5.16±0.03	4.97±0.03	4.70±0.03	5.19±0.25	5.15±0.15	4.00±0.04
DM810630	Deg	4.91±0.04	4.73±0.04	4.53±0.04	4.84±0.25	___±___	3.35±0.05
DM810717	Deg	4.88±0.04	4.71±0.04	4.52±0.04	___±___	___±___	___±___
DM820219	Deg	5.12±0.03	4.93±0.03	4.67±0.03	5.22±0.18	___±___	3.29±0.06
DM820921	Deg	4.99±0.03	4.83±0.03	4.52±0.03	___±___	___±___	___±___
DM830530	Deg	5.32±0.03	5.13±0.03	4.92±0.03	___±___	___±___	3.55±0.04
DM831129	Deg	5.22±0.03	5.08±0.03	4.79±0.03	___±___	___±___	3.56±0.04
DM831226	Deg	5.28±0.03	5.13±0.03	4.90±0.03	5.41±0.25	___±___	3.43±0.06
DM840415	Deg	5.61±0.03	5.46±0.03	5.24±0.03	5.54±0.14	5.53±0.21	3.99±0.03
DM870226	Deg	5.13±0.04	4.97±0.04	4.72±0.04	4.93±0.14	___±___	___±___
DM870506	Deg	5.49±0.04	5.27±0.04	5.04±0.04	5.32±0.18	___±___	___±___
DM870606	Deg	5.16±0.03	4.99±0.03	4.76±0.03	5.19±0.14	___±___	3.16±0.07
DM870717	Deg	5.76±0.03	5.62±0.03	5.36±0.03	___±___	5.49±0.15	4.34±0.05
DM881123	Deg	5.09±0.04	4.92±0.04	4.67±0.04	5.36±0.18	___±___	3.57±0.06
DM890217	Deg	4.77±0.17	4.63±0.12	4.01±0.10	5.13±0.14	___±___	___±___
DM891004	Deg	5.58±0.17	5.45±0.17	5.37±0.17	4.75±0.25	___±___	___±___
NZ641025	NNZ	4.67±0.04	4.47±0.04	4.28±0.04	5.19±0.11	5.34±0.11	___±___
NZ661027	NNZ	6.42±0.03	6.29±0.03	6.09±0.03	___±___	6.44±0.07	5.31±0.04
NZ671021	NNZ	5.76±0.03	5.62±0.03	5.42±0.03	6.04±0.14	6.12±0.10	4.50±0.04
NZ681107	NNZ	5.99±0.02	5.81±0.02	5.55±0.02	6.12±0.18	6.25±0.11	4.79±0.04
NZ691014	NNZ	6.08±0.03	5.93±0.03	5.72±0.03	6.39±0.25	6.33±0.11	4.87±0.04
NZ701014	NNZ	6.80±0.04	6.61±0.04	6.34±0.03	___±___	6.83±0.10	5.41±0.02
NZ710927	NNZ	6.57±0.03	6.47±0.03	6.20±0.03	___±___	6.48±0.11	5.53±0.03
NZ720828	NNZ	6.32±0.03	6.18±0.03	5.93±0.03	___±___	6.52±0.10	5.30±0.02
NZ730912	NNZ	6.98±0.06	6.86±0.06	6.64±0.06	___±___	6.95±0.21	5.71±0.02
NZ740829	NNZ	6.51±0.03	6.34±0.03	6.06±0.03	___±___	6.56±0.15	5.35±0.03
NZ750823	NNZ	6.41±0.03	6.32±0.03	6.11±0.03	___±___	6.47±0.12	5.20±0.03
NZ751021	NNZ	6.43±0.03	6.28±0.03	6.11±0.03	___±___	6.51±0.10	5.31±0.03
NZ760929	NNZ	5.58±0.02	5.44±0.02	5.27±0.03	5.89±0.25	5.99±0.11	4.15±0.06
NZ761020	NNZ	4.83±0.03	4.57±0.03	4.40±0.03	5.18±0.09	5.29±0.12	3.57±0.07
NZ770901	NNZ	5.62±0.02	5.45±0.02	5.20±0.02	6.49±0.14	5.89±0.12	4.04±0.05
NZ771009	NNZ	4.53±0.03	4.26±0.04	4.04±0.03	5.10±0.12	___±___	3.82±0.10
NZ780810	NNZ	5.80±0.04	5.56±0.04	5.29±0.04	6.16±0.12	___±___	4.32±0.04

Table 5. GLM Event Magnitudes (Cont)							
Event	Site	P_{max}	P_b	P_e	P_n	L_g	M_S
NZ780927	NNZ	5.54±0.04	5.31±0.04	5.07±0.04	6.34±0.14	±___	4.40±0.04
NZ790924	NNZ	5.64±0.03	5.45±0.03	5.27±0.03	6.78±0.18	5.79±0.21	4.34±0.04
NZ791018	NNZ	5.65±0.03	5.44±0.03	5.18±0.03	6.11±0.18	±___	4.01±0.05
NZ801011	NNZ	5.61±0.03	5.40±0.03	5.17±0.03	6.18±0.14	5.76±0.15	4.18±0.04
NZ811001	NNZ	5.73±0.03	5.51±0.03	5.24±0.03	6.50±0.18	±___	4.42±0.04
NZ821011	NNZ	5.40±0.03	5.22±0.03	5.02±0.03	6.00±0.11	5.99±0.21	4.07±0.04
NZ830818	NNZ	5.68±0.03	5.50±0.03	5.26±0.03	5.93±0.12	5.86±0.21	4.34±0.03
NZ830925	NNZ	5.57±0.03	5.43±0.03	5.21±0.03	±___	5.68±0.15	4.04±0.05
NZ841025	NNZ	5.67±0.02	5.46±0.02	5.22±0.02	6.03±0.11	6.10±0.21	4.40±0.04
NZ870802	NNZ	5.60±0.03	5.43±0.03	5.19±0.03	6.23±0.12	5.97±0.12	4.33±0.04
NZ880507	NNZ	5.43±0.03	5.27±0.03	5.11±0.03	6.07±0.12	5.86±0.12	4.23±0.04
NZ881204	NNZ	5.62±0.04	5.43±0.03	5.21±0.03	6.19±0.12	5.92±0.12	4.45±0.04
NZ901024	NNZ	5.60±0.05	5.28±0.05	5.01±0.05	±___	±___	4.33±0.06
FS620501	Sahara	5.32±0.07	5.03±0.07	4.90±0.07	±___	±___	±___
FS630318	Sahara	4.96±0.05	4.62±0.05	4.57±0.05	±___	±___	±___
FS631020	Sahara	5.65±0.03	5.41±0.03	5.07±0.03	±___	±___	±___
FS640214	Sahara	4.42±0.17	±___	±___	±___	±___	±___
FS641128	Sahara	4.66±0.12	4.43±0.12	4.45±0.12	±___	±___	±___
FS650227	Sahara	5.84±0.03	5.60±0.03	5.35±0.03	±___	±___	5.02±0.12
FS651001	Sahara	4.51±0.17	±___	±___	±___	±___	±___
FS651201	Sahara	5.31±0.05	4.80±0.05	4.80±0.05	±___	±___	±___
FS660216	Sahara	5.02±0.05	4.80±0.05	4.67±0.05	±___	±___	±___

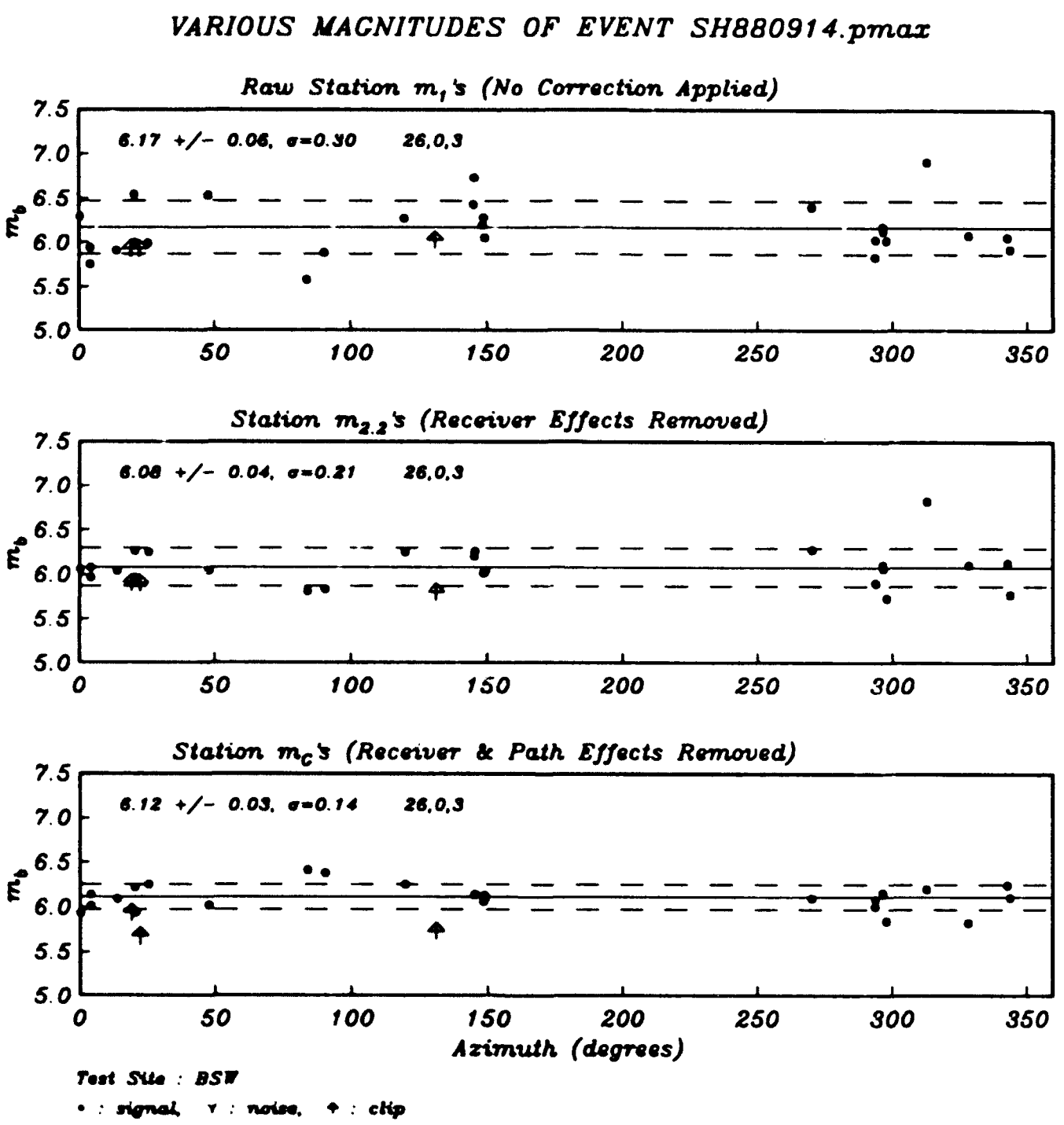

Figure 1. Scatter plot of 3 different types of station m_b s for Balapan event 880914 (JVE). The 26 good recordings and 1 clip are shown with filled circles and upward arrow, respectively. The raw station m_b s (top) have a standard deviation of 0.30 m.u. Applying the "primary" station corrections reduces the scatter to 0.21 m.u. Applying the proposed "secondary" corrections to count for the path effects reduces the scatter further down to 0.14 m.u.

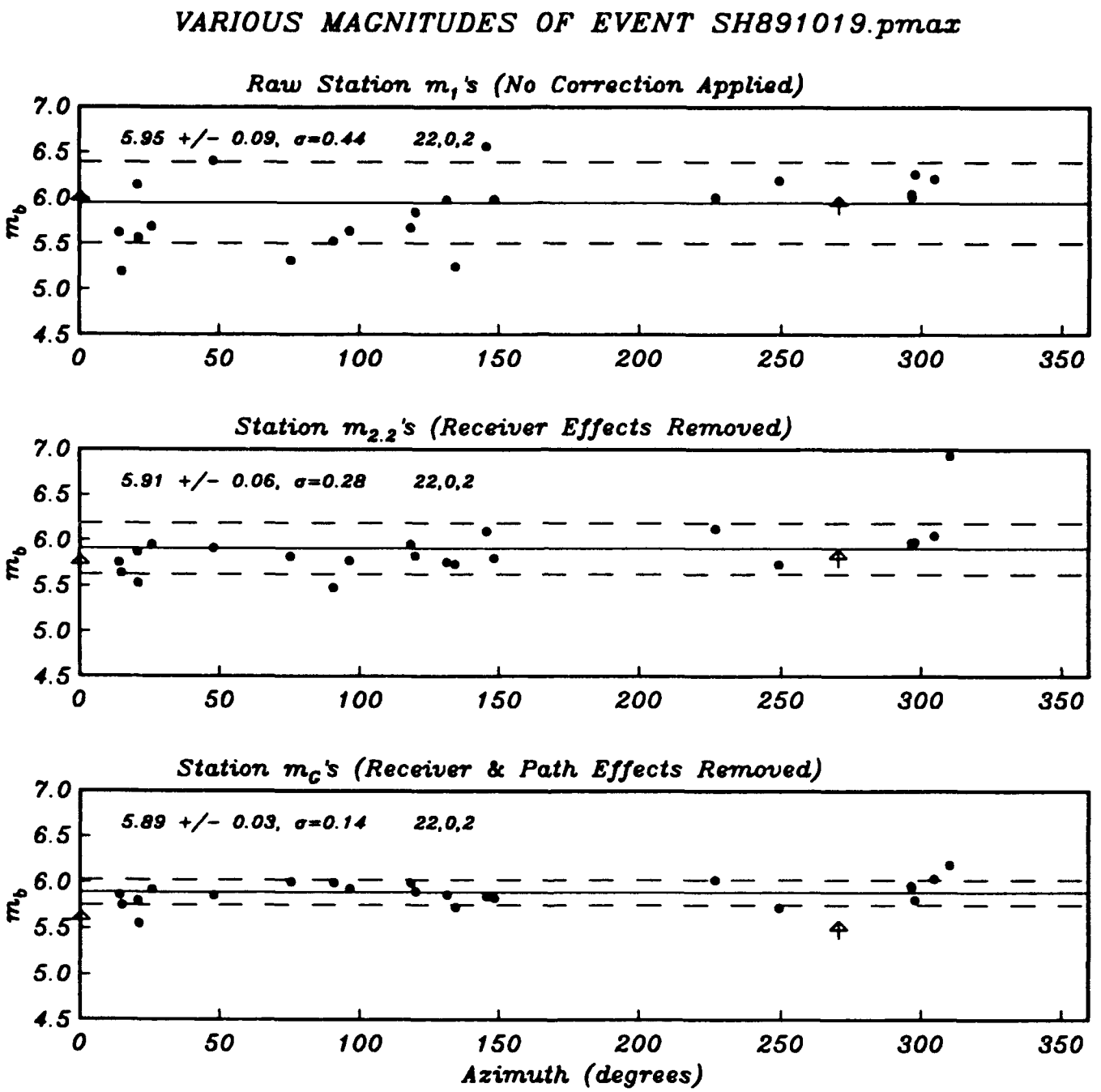

Figure 2. Scatter plot of 3 different types of station m_b s for Balapan event 891019.

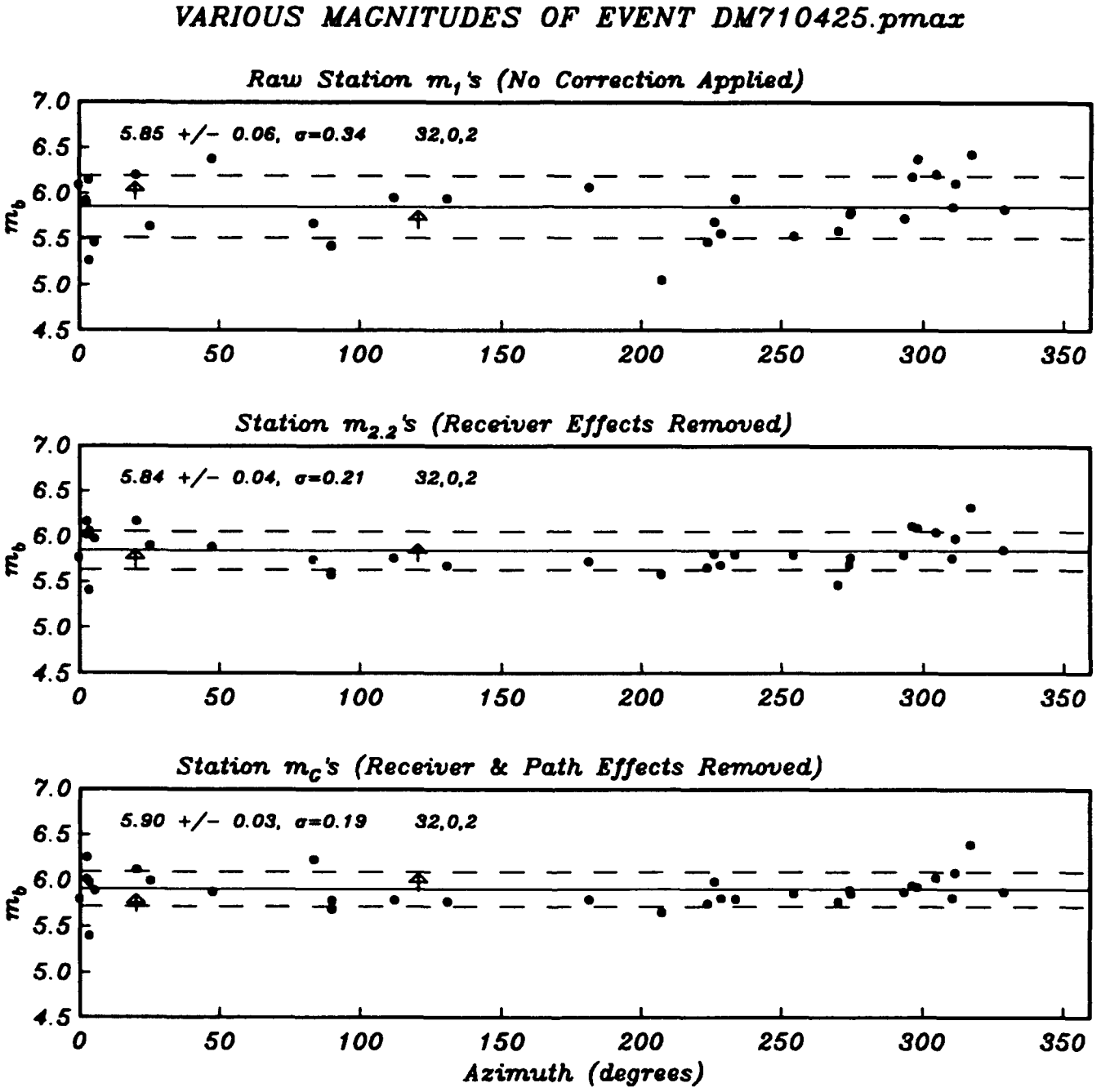

Figure 3. Scatter plot of 3 different types of station m_b s for Degelen event 710425.

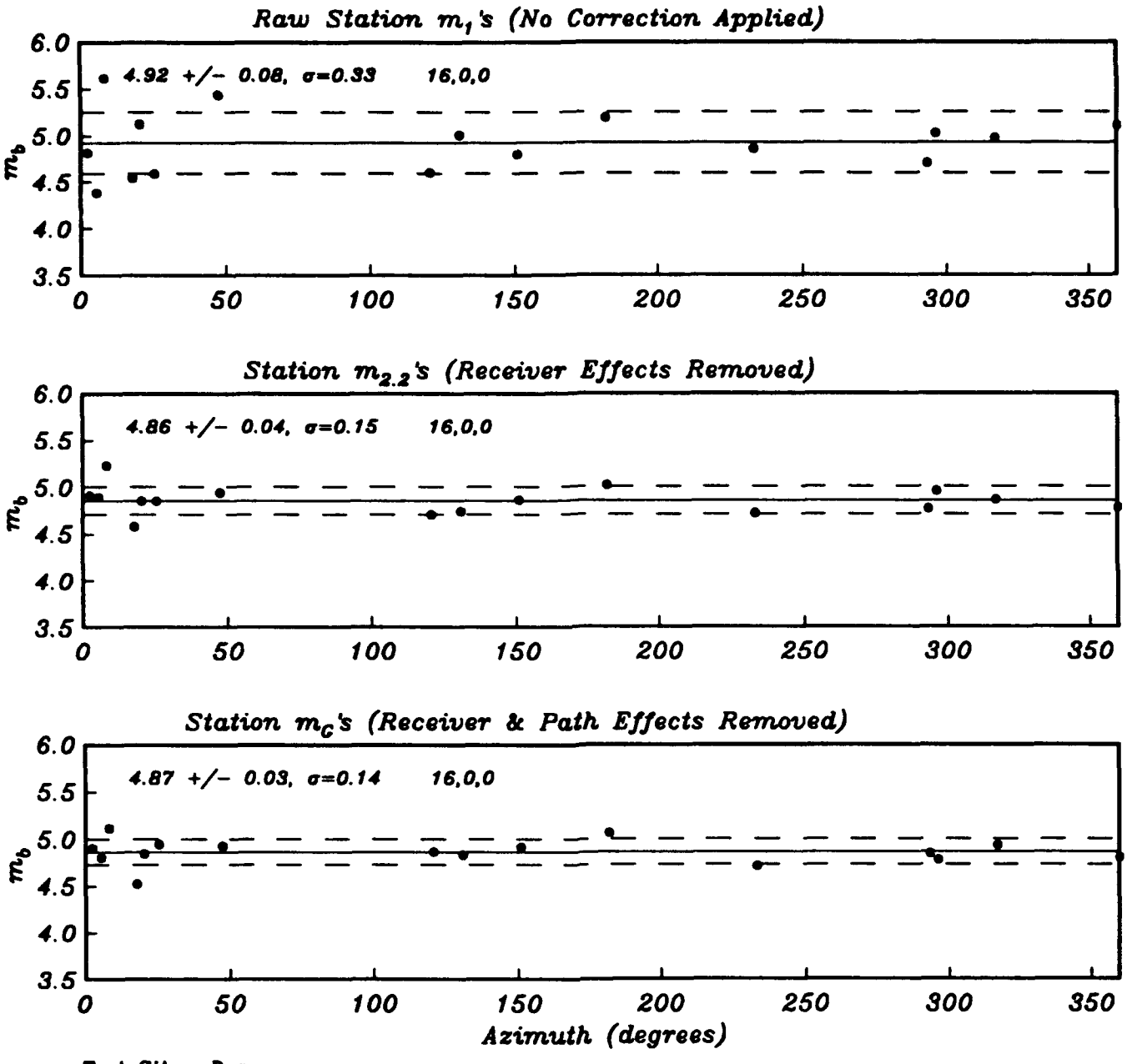

Figure 4. Scatter plot of 3 different types of station m_b s for Degelen event 761230.

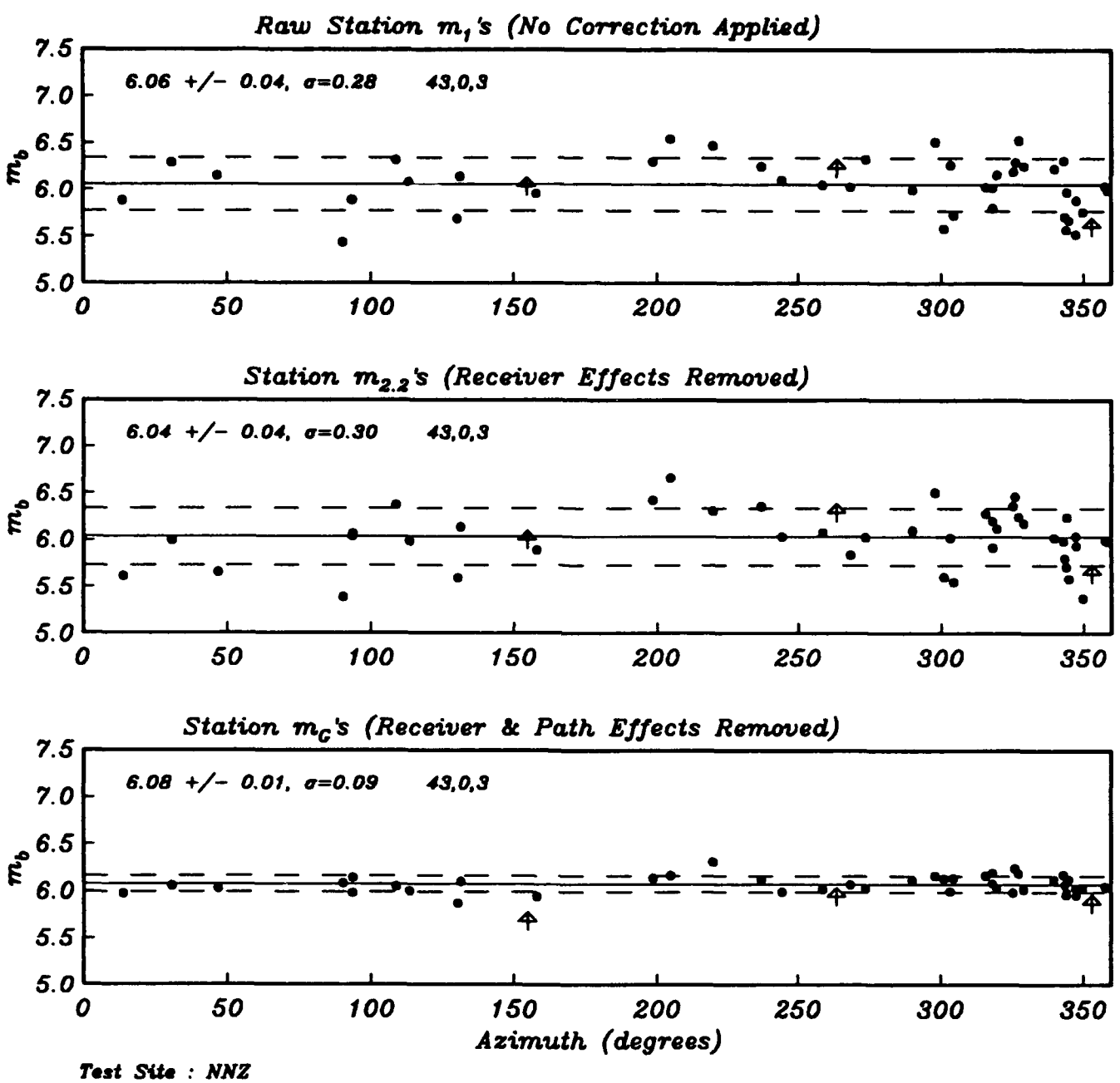

Figure 5. Scatter plot of 3 different types of station m_b s for Novaya Zemlya event 691014.

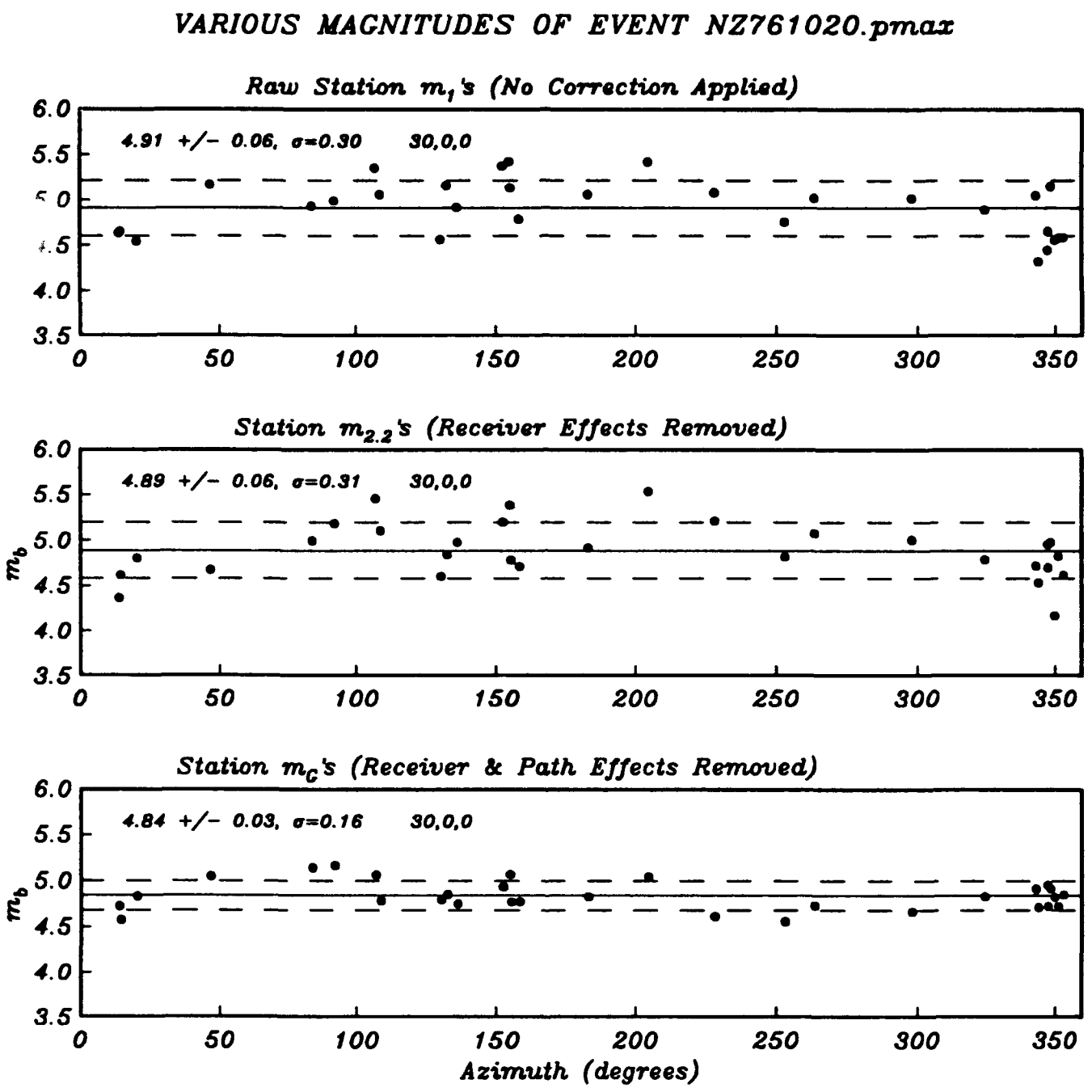

Figure 6. Scatter plot of 3 different types of station m_b s for Novaya Zemlya event 761020.

IV.2 Receiver and Path Effects on Seismic Waves

Along with the event m_b values, the station terms and the path terms are generated by *"mlglm"* at one single inversion. Table 6 lists the station corrections and path corrections for explosions in nine nuclear test sites. Note that the station terms are applicable to other source regions of the world as well. Applying these path and station corrections to any individual explosions would yield a reduction in the fluctuational variation of station magnitudes with a factor ranging from 1.2 to 3. Most Novaya Zemlya events have a typical reduction factor of 2, as noted by Jih and Wagner (1992a).

Figure 7 shows our receiver terms which are inferred jointly along with the source-size estimates and path terms from the worldwide explosions. The receiver corrections derived with our approach match the average tectonic structure underneath each station very well, mainly due to the broad coverage of azimuths at each station. Generally speaking, the station terms are positive in shield regions such as Australia, Canada, India, and Scandinavia, and they are negative in the east Africa rift valleys, mid-ocean ridges (*e.g.*, Iceland and Azores Islands), island arcs (*e.g.*, Indonesia, Japan, and Taiwan), and Himalaya Mountain Ranges (Chaman Fault, northern India, Nepal, and Burman Arc). Solomon and Toksoz (1970) and many other studies (*e.g.*, Evernden and Clark, 1970; Booth *et al.*, 1974) found that for stations in the U.S., the attenuation is higher between the Rockies and Cascades, and in the northeastern U.S. This pattern is also observable in Figure 7 (see also North, 1977). As North (1977) put it, it is gratifying that a simple parameter such as m_b can be utilized to reveal the tectonics. It should be noted, however, that our empirical station terms also include the effect due to the crustal amplification if such local site effect is shared by all ray paths from different test sites to a particular station. This could be the reason of a few outliers such as HNR (Honiara, Solomon Islands), PMG (Port Moresby, East Papua New Guinea), and RAB (Rabaul, New Britain), which do not show negative station terms as would be expected from the strong seismicity in that region (*cf.* Figure 7). Another possible reason is that these stations have relatively poorer azimuthal sampling in our data set, and hence the station bias at these three stations is not well constrained. The minor discrepancy between the deterministic corrections by Marshall *et al.* (1979) and our empirical corrections could be due to the same reason. Note that HNR, PMG, and RAB also show positive station terms in another m_b study using a different data set (Jih *et al.*, 1993).

Figures 8 through 16 show the map of the "pure path effect" (top) and the combined station amplification (bottom) (defined as the sum of the receiver term and the path effect) for all 9 test sites used in the GLM inversion. The Semipalatinsk test range is divided into four test sites including Degelen Mountain [Deg] and three subregions as defined in Ringdal *et al.* (1992): southwestern Balapan [BSW], northeastern Balapan [BNE], and the transition zone [BTZ] between BSW and BNE. The path term at each station can be regarded as the azimuthal variation (towards the various source regions) relative to the averaged station amplification. An important observation is that all these five test sites exhibit very different azimuthal and radial amplitude variations. Events from Degelen and BTZ are systematically enhanced in the western U.S. and reduced in the eastern U.S., whereas events from BSW and BNE are enhanced in essentially the whole of U.S. Such highly direction-dependent, distance-dependent, and site-dependent patterns of the amplitude fluctuation could be a diagnostic for the path effects in the proximity of the test sites. Back projections (*e.g.*, Lynnes and Lay, 1990) of the m_b residuals onto the upper mantle and the lower crust reveal that similar m_b residuals come into

alignment in several regions partitioned by known geological features (Jih and Wagner, 1991). Degelen events in the western U.S., and SW Balapan events at western European stations must pass through the area between Chinrau fault and Chingiz-Kalba shear zone. All these paths show positive m_b residuals. The area north of Chinrau fault might have some complex features that result in negative mean m_b residuals. Paths from NE Balapan to North America and many continental European stations must cross this area or even travel along the Chinrau fault before entering the deeper mantle, and hence the complexity in the waveforms is inevitable. It seems that the mean $m_b - L_g$ separation of 0.07–0.17 m.u. (*e.g.*, Ringdal and Hokland, 1987; Ringdal *et al.*, 1992; Richards *et al.*, 1990; Section V.2 of this report) between the NE and SW subregions of Balapan could be due in part to the path effects, in addition to the difference of source medium postulated previously by Marshall *et al.* (1984). A detailed discussion on the seismic variability within Balapan test site is given in a later section. Path effects can also explain why the SW Balapan waveforms tend to be more complex at YKA than those recorded at WRA, EKA, and GBA arrays.

The initial *P* waves from the three adjacent test sites have virtually the same incident angle at each teleseismic station, and anything in common across all events (such as the crustal amplification as well as the upper mantle attenuation underneath the receiver) would have been lumped into the constant station term. Thus the station residuals averaged over all events from the same test site would correlate very little with the receiver. Instead, they should reveal more site-dependent information about the focusing/defocusing pattern underneath E. Kazakhstan.

The largest and most prominent fault in the region is the southeast-trending Chingiz right-lateral strike-slip fault that passes about 10 km southwest of Degelen Mountain and right across the Murzhik test area (Rodean, 1979; Bonham *et al.*, 1980; Leith, 1987b). Soviets reported that this fault has a very steep dip, which is consistent with its linear expression over large distance as seen on Landsat imagery (Bonham *et al.*, 1980). A distinct fault-line scarp is developed along much of the oldest metamorphic rocks. Chingiz Fault extends for a total length of about 700 km. Soviet reports postulate that this fault extends down to the boundary of the granite layer of the crust and possibly into the upper mantle.

The inferred path terms for Novaya Zemlya explosions are very consistent with those in Jih and Wagner (1992a). Jih and Wagner (1992a) also compared the path terms with the travel-time residuals. Their results indicate that paths from the northern test site in Novaya Zemlya to stations in North America have systematically faster arrivals and smaller amplitudes, suggesting a profound defocusing effect on the first arrivals; while stations in Ireland, Scotland, Spain, Bangladesh, northern India, Pakistan, Korea, and Kenya report slow arrivals and large amplitudes, suggesting a focusing effect. Amplitudes for paths to Greenland, Iceland, Alaska, Turkey, Germany, Luzon, Zimbabwe, Italy, Pueto Rico, Ethiopia, and Hawaii, however, seem to be controlled by the anelastic attenuation with slow rays also associated with small amplitudes, and fast rays associated with large amplitudes.

Table 6. m_b Receiver and Path Terms for Eurasian Nuclear Test Sites										
Station Term [S]		Path Terms [F]								
Code	Rcv[1]	BNE	BSW	BTZ	Deg	NNZ	PMA	RNA	Sahara	YFT
AAE	-.122	-.399			-.439	.310			-.007	
AAM	.193	.005	.380	.107		.206	-.023	.307	-.569	-.084
AFI	.053						-.103			-.051
AKU	-.101	.003	.191	.185		-.020	-.294		.364	-.134
ALE	-.164				-.491		-.057			.098
ALQ	-.140	-.049	-.059	-.049	.014	-.249			.326	
ANMO	-.212	-.100	-.049	-.082	.102	-.177				
ANP	-.465					-.129				
ANTO	.125						-.058			-.009
AQU	-.231	-.092		-.233		.729	-.286			-.047
ARE	.316						-.002	-.117	-.403	.017
ARU	.384						.030			.169
AS023	.268	-.014	.127	-.037	-.094					
AS1027	.224	.114	.072	-.108	-.081					
ATL	.098	-.066				-.040	.067	-.433	.372	-.007
ATU	.091	.008	.091	.069	-.205	.241			-.299	
AZ043	-.176	.116		.230	-.171	-.077				
BAG	-.051	-.166	-.244	-.220	-.329	.321				
BC045	.026	.042	-.034	.006	.050	-.282				
BCAO	.456	-.103	-.063	.009	.001	.184				
BDF	-.068						-.008			-.048
BE051	.124	.318	.179	.316	-.299	.069				
BEC	-.057					-.260	.124			-.087
BER	.003		.046	.094		-.176				-.155
BHP	-.221					-.030	-.043		.453	-.133
BJI	-.135	.176	-.060	-.156	.136	-.127	.010			
BKS	.042	-.012	-.049	-.041		-.057				
BLA	.151	-.350	-.331	-.337		.126	.238	-.336	-.061	-.005
BLC	-.062									-.043
BM068	-.037	.030	-.001	.029	.055	-.190				
BOCO	-.034						-.013			-.082
BOD	-.196				-.313	.018				
BOG	.251					.272	-.253			-.300
BUL	-.118	-.011	-.100	.100	-.176	.493			-.100	
CAR	.243					.021	-.014	-.175	-.707	-.013
CHG	-.041	.376			-.033	-.191			-.388	
CHS	-.271					-.063				
CHTO	.226	.159	.072	.120	-.291	-.375				

1) the station bias which needs to be corrected (in addition to the path effect).

2) BSW = SW subsite, Balapan; BNE = NE subsite, Balapan; BTZ = transition zone, Balapan; Deg = Degelen Mountain; NNZ = northern island, Novaya Zemlya; PMA = Pahute Mesa, NTS; YFT = Yucca Flat, NTS; RNA = Rainier Mesa, NTS; Sahara = Ahaggar, French Sahara.

Table 6. m_b Receiver and Path Terms for Eurasian Nuclear Test Sites (cont)										
Station Term [S]		Path Terms [F]								
Code	Rcv[1]	BNE	BSW	BTZ	Deg	NNZ	PMA	RNA	Sahara	YFT
CM074	.468	.337	.120	.249	-.099	-.576				
CMB	-.444		-.042	-.115		-.045				
CMC	-.428						-.032		.092	-.059
COL	.036	.016	.019	-.022	.050	.041	-.126	-.071		-.085
COP	.163	.066	-.156	.010	.018	.784	-.136		-.263	-.346
COR	.006					-.057				
CTAO	.020	-.004	.001	-.076	-.082					
DAG	-.101	-.081		.063			-.076			.002
DAV	-.161					-.127				
DUG	.385	-.138	-.105	-.088	.113	-.653			-.679	
EIL	-.259				-.062					
EKAB4	-.058	-.202	-.056	-.023	.292	.343	-.172			-.187
EPT	-.211					-.005				
ESK	.126	-.260	-.098	-.095		.478	-.442		.115	-.379
FCC	-.297						.067			-.090
FFC	-.137				.436		.164			-.136
FL099	.238	.090	.124	.149	.038	-.178				
FLO	-.064					.191	-.039		.389	-.098
FRA0	-.083		-.002				-.175			
FRB	.214						.135			-.060
FVM	-.215	.102	.190	.154		.098	.066	-.262		-.110
FX118	.493	.043	.016	.053	.012	-.373				
GBAB1	.034	-.061	-.057	.097	-.054	.320				
GDH	-.115	.046	.261	.094	.016	-.278	-.113		.369	-.141
GEO	.039	-.059				.081	.017		-.040	-.167
GIE	.124						.174			-.105
GOL	-.094	-.149	-.114	-.149	.004	-.266			-.401	
GRFO	.065	-.167	-.074	-.001	.097	.213	-.023	-.046		-.033
GSC	-.008	-.036				-.022				
GUA	.313					-.618	.245			.094
GUMO	.087						.477			.170
GWC	.063									-.048
HA122	.088	-.160		-.189	.087	-.542				
HIA	-.504	-.121	-.260	-.184		.441	.340			.028
HKC	.091	-.105	-.091	-.161		-.016				
HLW	-.130				-.283	1.090				
HNR	.416						-.028			-.034
IB132	.327	.011	.137	.061	-.029	-.192				
IL1154	.273	.048	.045	.068	.004	-.361				

1) the station bias which needs to be corrected (in addition to the path effect).

2) BSW = SW subsite, Balapan; BNE = NE subsite, Balapan; BTZ = transition zone, Balapan; Deg = Degelen Mountain; NNZ = northern island, Novaya Zemlya; PMA = Pahute Mesa, NTS; YFT = Yucca Flat, NTS; RNA = Rainier Mesa, NTS; Sahara = Ahaggar, French Sahara.

Table 6. m_b Receiver and Path Terms for Eurasian Nuclear Test Sites (cont)										
Station Term [S]		Path Terms [F]								
Code	Rcv[1]	BNE	BSW	BTZ	Deg	NNZ	PMA	RNA	Sahara	YFT
IM182	.027	.002	.226	.165	.027	-.474				
INK	-.269						.135			-.136
IST	.029	.182		.253	-.086	.716				.430
JAS	-.166		-.013	-.047		-.092				
JCT	.037					.005				
JER	-.046	-.005			-.174	.308			-.320	
JO191	.170	.024	-.009	-.039	-.128	.062				
KAAO	.233					-.012				
KBS	-.098	-.370		-.334	.027		-.097			.029
KEV	-.022	.007	.280	.186	-.027		-.478		.290	-.256
KIP	.297					-.066	-.180	.166		.039
KMI	-.488	.426	-.086	.007		-.060				
KOD	.347	-.015	.262	.118	-.067	.014			-.683	
KON	.134	-.034	.168	.184	-.105	-.196	-.081		-.229	-.021
KRK	.111						-.598			.068
KS213	-.150	.048	-.054	-.035	-.109	.058				
KTG	-.018	-.357				-.532	-.019	.040	-.454	.058
KU238	-.107	-.268	-.373	-.419	-.158	.395				
LA251	-.084					-.064				
LEM	-.360		-.141	-.408		-.012				
LHC	-.223									-.031
LON	-.132	-.083	-.050	-.109	.113	-.001				
LOR	.108	-.234					.236	-.263		-.010
LPB	.166						.012	-.057	.111	-.034
LPS	-.167					.372	.021		-.067	-.114
LUB	.204					-.098			.364	
LY252	-.511	-.199	-.153	-.178	.089	.008				
LZH	-.279	-.048	-.065	-.039	-.335	.083				
MA265	-.133					-.078				
MAIO	.457					-.101				
MAJO	-.233	-.381	-.602	-.582	-.438	-.117	.359			.395
MAL	-.015					.177	-.046	-.092		-.062
MAT	-.069	-.518	-.676	-.657	-.482	-.142	.245	.330		.309
MBC	.067									-.024
MDS	-.012					.077	.186	-.116	-.323	.104
MI269	.095	.247	.221	.205	-.175	-.278				
MSO	-.247	-.049	-.056	-.154		.101				
MUN	.257	-.004	-.107	-.026	.001					
N04C2	-.008	.511	.744	.645	.315		-.359			-.377

1) the station bias which needs to be corrected (in addition to the path effect).

2) BSW = SW subsite, Balapan; BNE = NE subsite, Balapan; BTZ = transition zone, Balapan; Deg = Degelen Mountain; NNZ = northern island, Novaya Zemlya; PMA = Pahute Mesa, NTS; YFT = Yucca Flat, NTS; RNA = Rainier Mesa, NTS; Sahara = Ahaggar, French Sahara.

Table 6. m_b Receiver and Path Terms for Eurasian Nuclear Test Sites (cont)										
Station Term [S]		Path Terms [F]								
Code	Rcv[1]	BNE	BSW	BTZ	Deg	NNZ	PMA	RNA	Sahara	YFT
NA0	-.191					-.754	-.017			.094
NAI	-.122	-.078	-.065	.018	-.118	.283			-.121	
NAT	.189					-.229	-.040			.045
NDI	.170	-.037		-.519	-.046	.267			-.374	
NNA	-.109						.013	-.296	.031	-.044
NOR	-.491	.229			.881		-.322		-.042	-.055
NRA0	.088		.621	.395	.351		-.459			-.449
NUR	.093	.545	.415	.735	-.049		-.298		-.395	-.108
NVS	.315					-.010				
NWAO	.184	-.082	-.051	-.027	.014					
OBN	.286	-.184	-.110	.164	.168					
OGD	-.177	-.298		-.047		.112	.122	.170		-.160
OTT	.275						-.039			
OXF	.077	.251				.154	.251	-.198	.479	-.057
PDA	.296					-.003	-.504		.003	
PEL	-.063						.010	-.249		-.047
PHC	-.231					-.036				
PMG	.191	-.022	-.181	-.301	-.024					
PO275	-.262	-.192		-.222	-.088	.251				
POO	.069	-.146	.225	.104	-.047	-.057			-.218	
PRE	-.185	.036	-.019	.064	-.089				-.023	
PTO	-.026	-.101				.052	-.019		-.435	-.041
QUE	-.530	-.233			-.066	.352			-.203	
RAB	.447						-.034			-.068
RAR	-.163						-.100			.073
RES	-.090				-.416		-.204			.080
RSCP	-.166	.047	.035	-.033	.088	.215	-.014	-.388		-.168
RSNY	-.007	.382	.300	.269	-.056	-.145	-.065			-.487
RSON	.145	.120	.145	.060	-.119	.289	-.373			-.053
RSSD	.272	-.015	-.034	-.142	.050	-.070				
SCH	.109						-.080			.004
SCP	-.067	-.034	-.117	-.059		.190	.072	-.213	.101	-.085
SDB	.164	-.275			.006	-.007			-.259	
SEO	.203					-.025	.125			-.181
SH276	-.493					-.093				
SHA	.286					.046	-.062		.068	-.306
SHI	.139	-.302	-.250	-.296	.006	.094			.155	
SHK	.050	-.481	-.544	-.513	-.614	-.695	.311	-.017		.071
SHL	-.063				-.056	.228			-.230	

1) the station bias which needs to be corrected (in addition to the path effect).
2) BSW = SW subsite, Balapan; BNE = NE subsite, Balapan; BTZ = transition zone, Balapan; Deg = Degelen Mountain; NNZ = northern island, Novaya Zemlya; PMA = Pahute Mesa, NTS; YFT = Yucca Flat, NTS; RNA = Rainier Mesa, NTS; Sahara = Ahaggar, French Sahara.

Table 6. m_b Receiver and Path Terms for Eurasian Nuclear Test Sites (cont)										
Station Term [S]		Path Terms [F]								
Code	Rcv[1]	BNE	BSW	BTZ	Deg	NNZ	PMA	RNA	Sahara	YFT
SJG	.177					-.586	.113	-.368	-.297	.059
SLR	-.482		-.038							
SNG	.006	-.153	-.059	-.126		.033				
SO286	-.068	-.116	-.101	.066	-.079	.264				
STJ	.388									-.011
STU	.071	-.038	-.050	.015	.175	.038	-.262	-.295	-.054	-.282
TAB	.520					-.039				
TATO	-.322	.189	-.130	.082		.345				
TLY	-.289					-.034				
TOL	.131	-.213	-.181	-.043	-.144	.502	.072			.087
TRI	-.106	-.053			.308	.231	-.473		-.159	-.649
TRN	.008					.341	-.016	-.121	-.280	-.175
TT297	-.261	.039	.002	.028	-.095	-.023				
TUC	-.051	-.383				-.023			.210	
TUP	-.369	.142	-.230							
UME	.110	.297	.356	.500	-.071		-.188	-.452	-.424	.034
UPA	-.389						.020			-.204
UZH	-.135	-.330	-.125	-.191	-.211	.599				
VAL	.031	-.140		.079		.179	-.354		-.325	-.215
WES	-.251					.113	.037			-.414
WMQ	.375					-.031				
WRAR1	.398	-.016	.102	-.193	-.131					
YKAB5	-.032	.345		.401	.155	-.231	-.211			-.241
YKC	-.009						.066			-.068
ZOBO	-.101						.039	-.307		-.086

1) the station bias which needs to be corrected (in addition to the path effect).

2) BSW = SW subsite, Balapan; BNE = NE subsite, Balapan; BTZ = transition zone, Balapan; Deg = Degelen Mountain; NNZ = northern island, Novaya Zemlya; PMA = Pahute Mesa, NTS; YFT = Yucca Flat, NTS; RNA = Rainier Mesa, NTS; Sahara = Ahaggar, French Sahara.

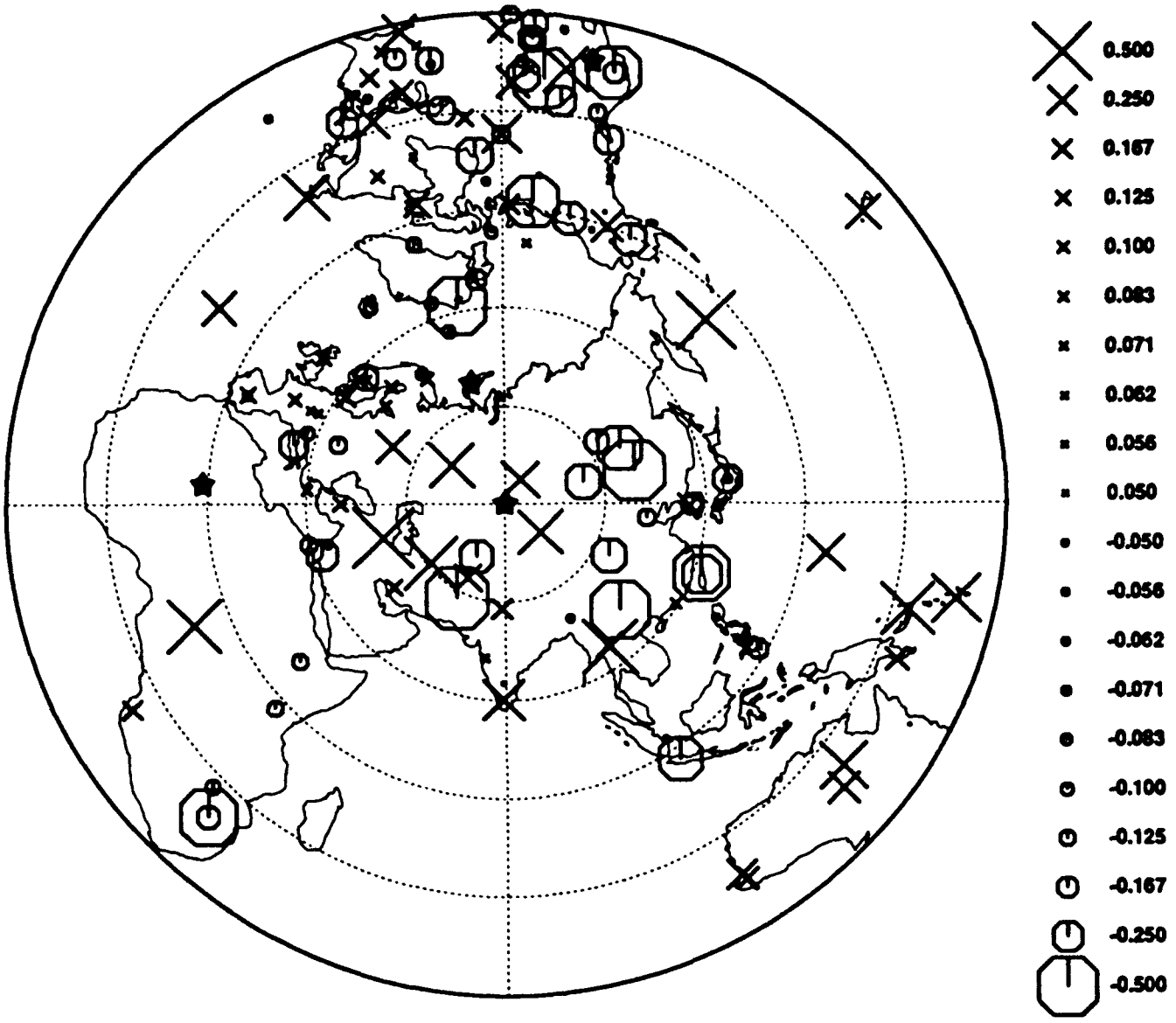

MEAN STATION AMPLIFICATION ON MB

Polar azimuthal equidistant projection, 78.00 , 50.00

Figure 7. Map of m_b station terms inferred from a GLM inversion solves for 3,306 unknowns with 35,211 linear equations. The high correlation between the tectonic type and the station terms suggests that these empirical corrections do reflect the upper mantle conditions underneath the receivers. The 4 darkened stars represent some of the nuclear test sites used in this study.

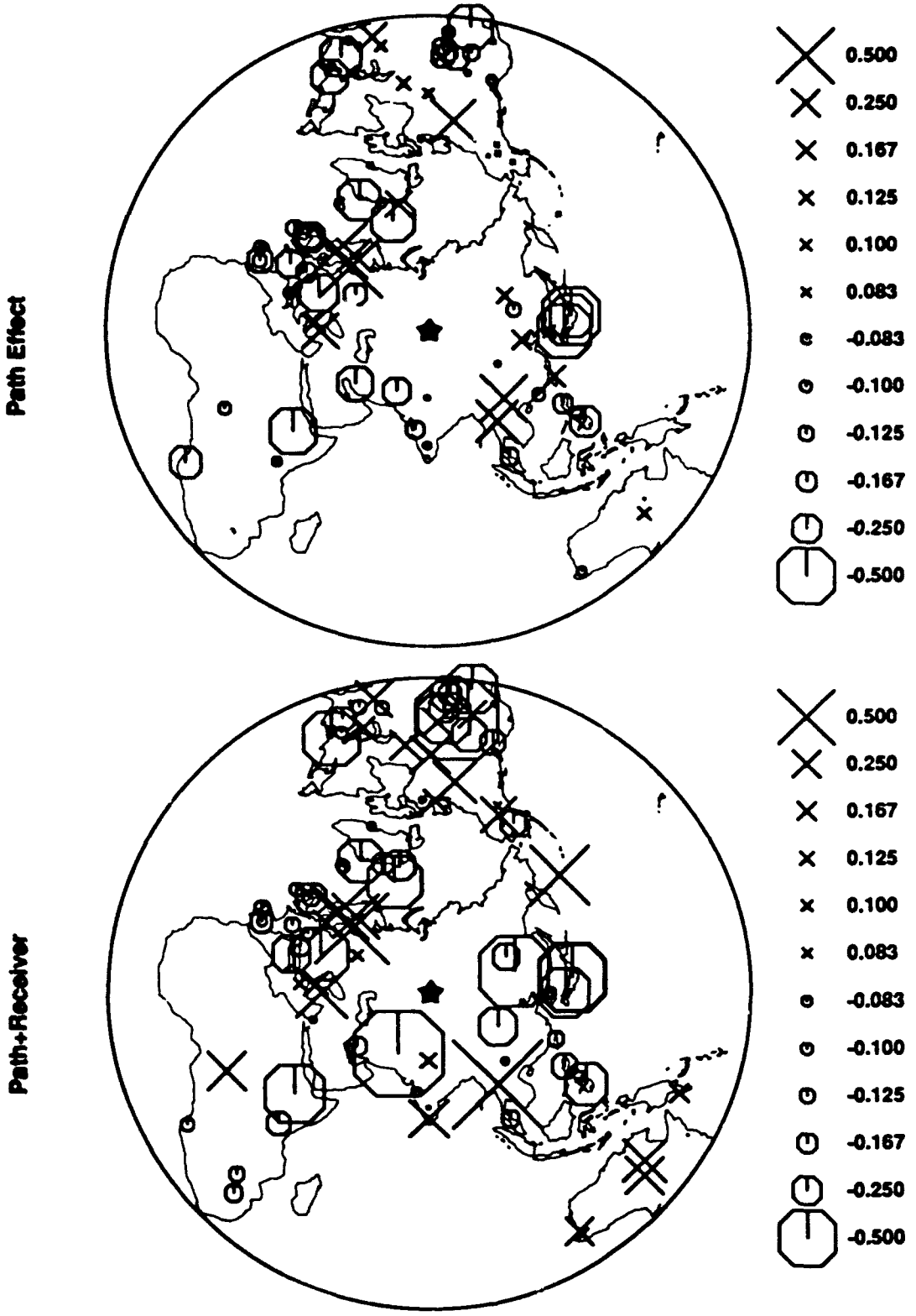

Figure 8. The map showing the "pure propagation effect" (top) and the combined station amplification (bottom) defined as the sum of the receiver term (Figure 7) and the path effect for NE Balkan explosions.

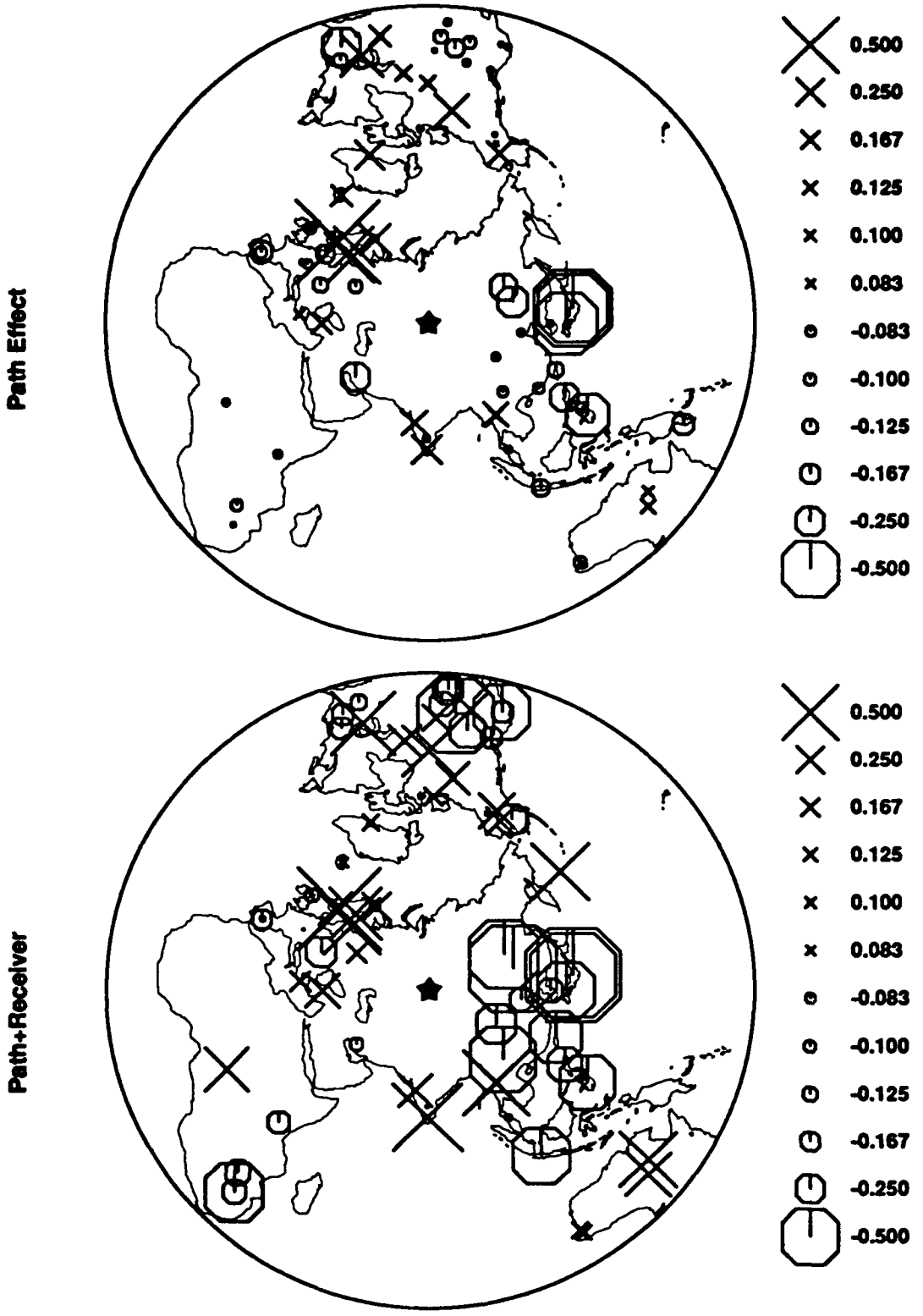

Figure 9. and the combined station amplification (bottom) defined as the sum of the receiver term (Figure 7) and the path effect for SW Balapan test site.

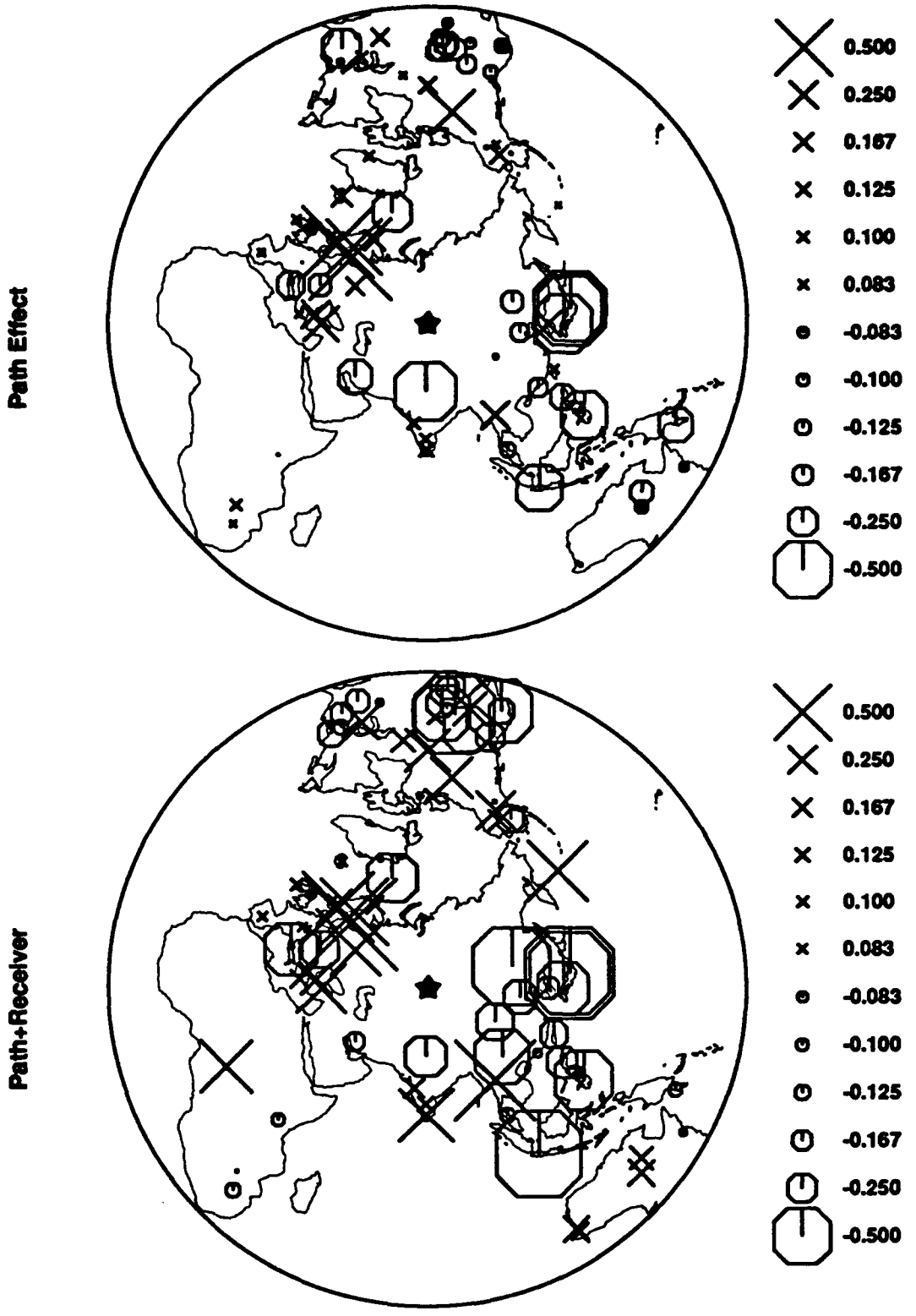

Figure 10. The map showing the "pure propagation effect" (top) and the combined station amplification (bottom) defined as the sum of the receiver term (Figure 7) and the path effect for TZ Balapan test site.

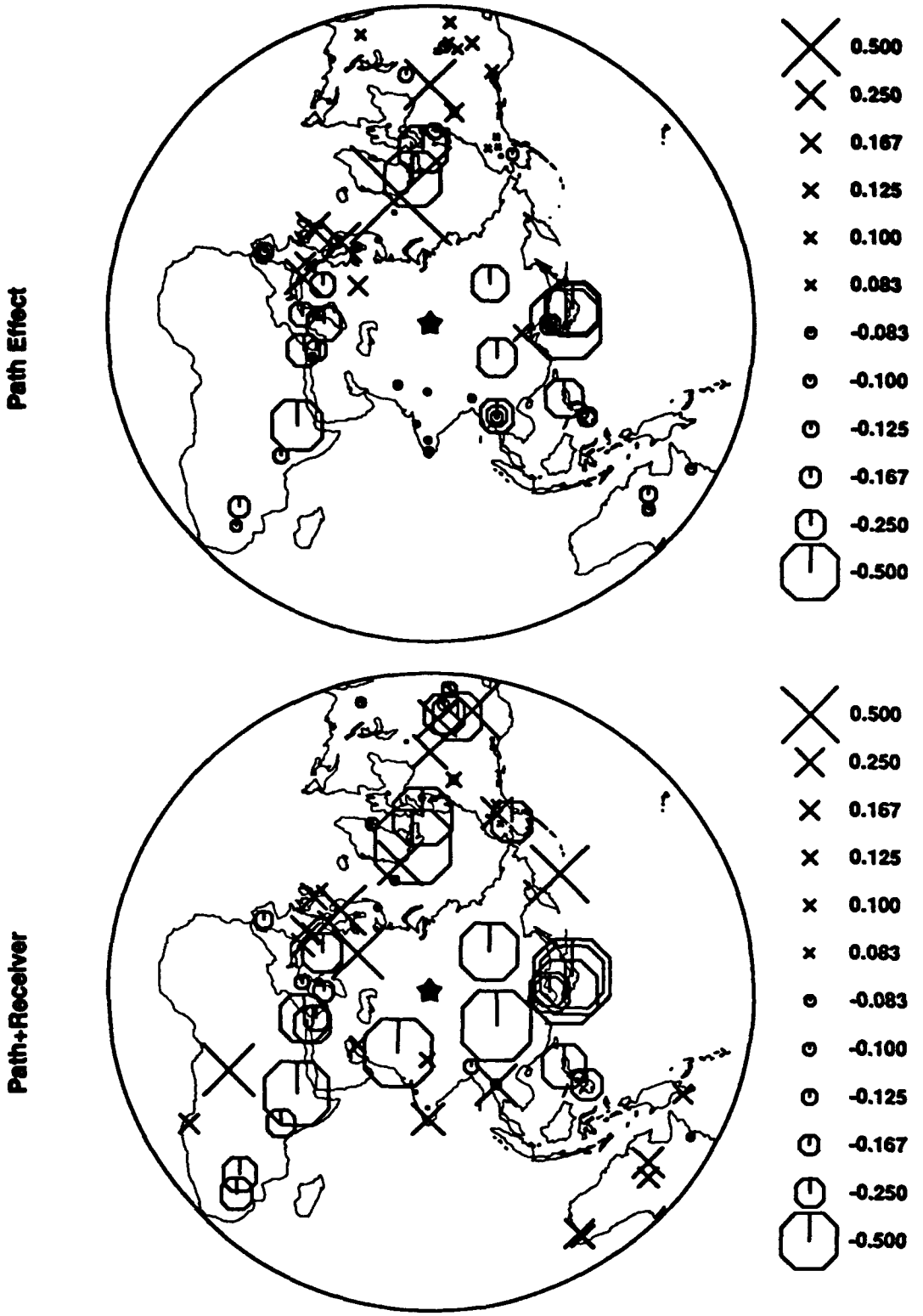

Figure 11. The map showing the "pure propagation effect" (top) and the combined station amplification (bottom) defined as the sum of the receiver term (Figure 7) and the path effect for Degelen test site.

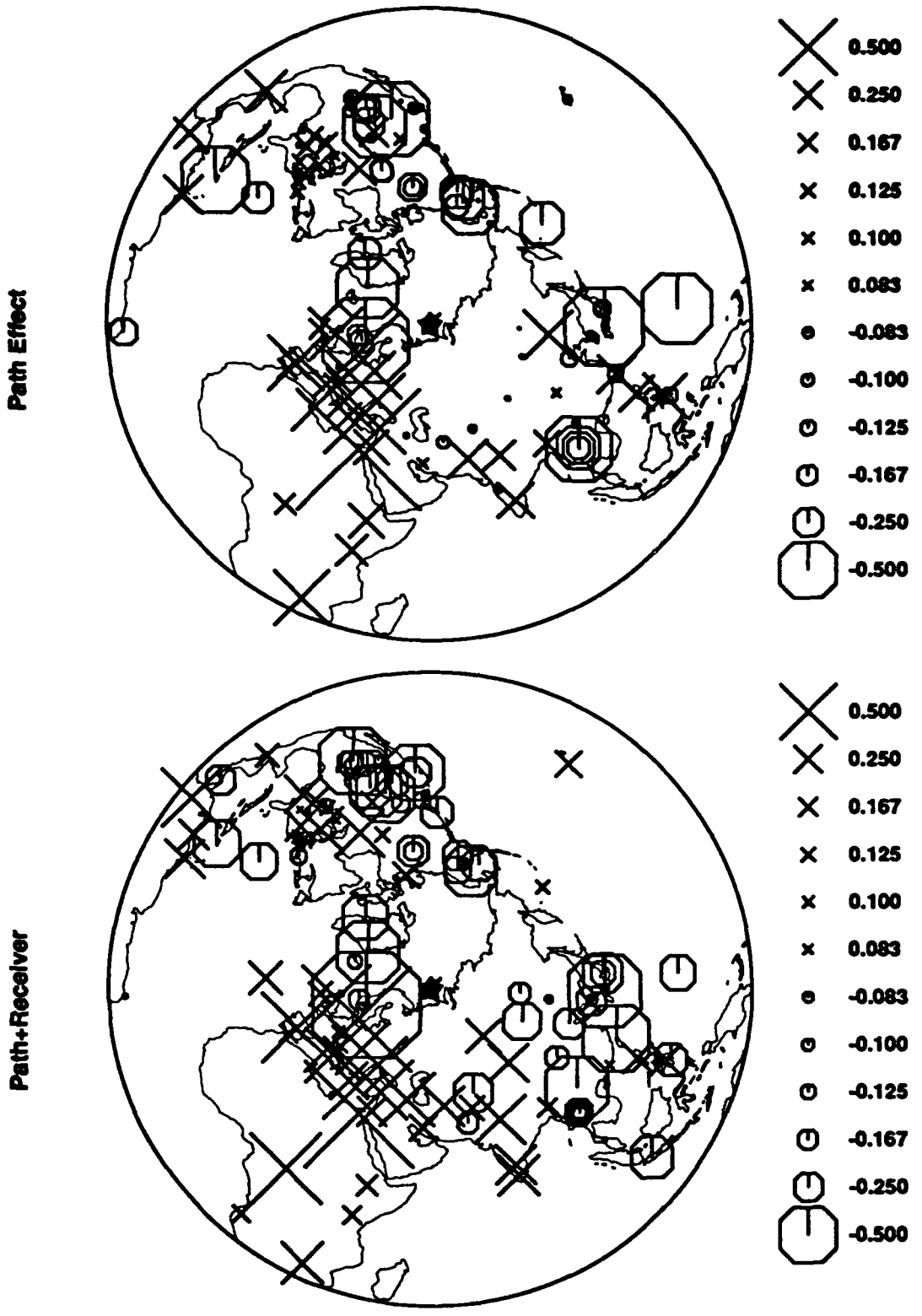

Figure 12. The map showing the "pure propagation effect" (top) and the combined station amplification (bottom) defined as the sum of the receiver term (Figure 7) and the path effect for Northern Novaya Zemlya.

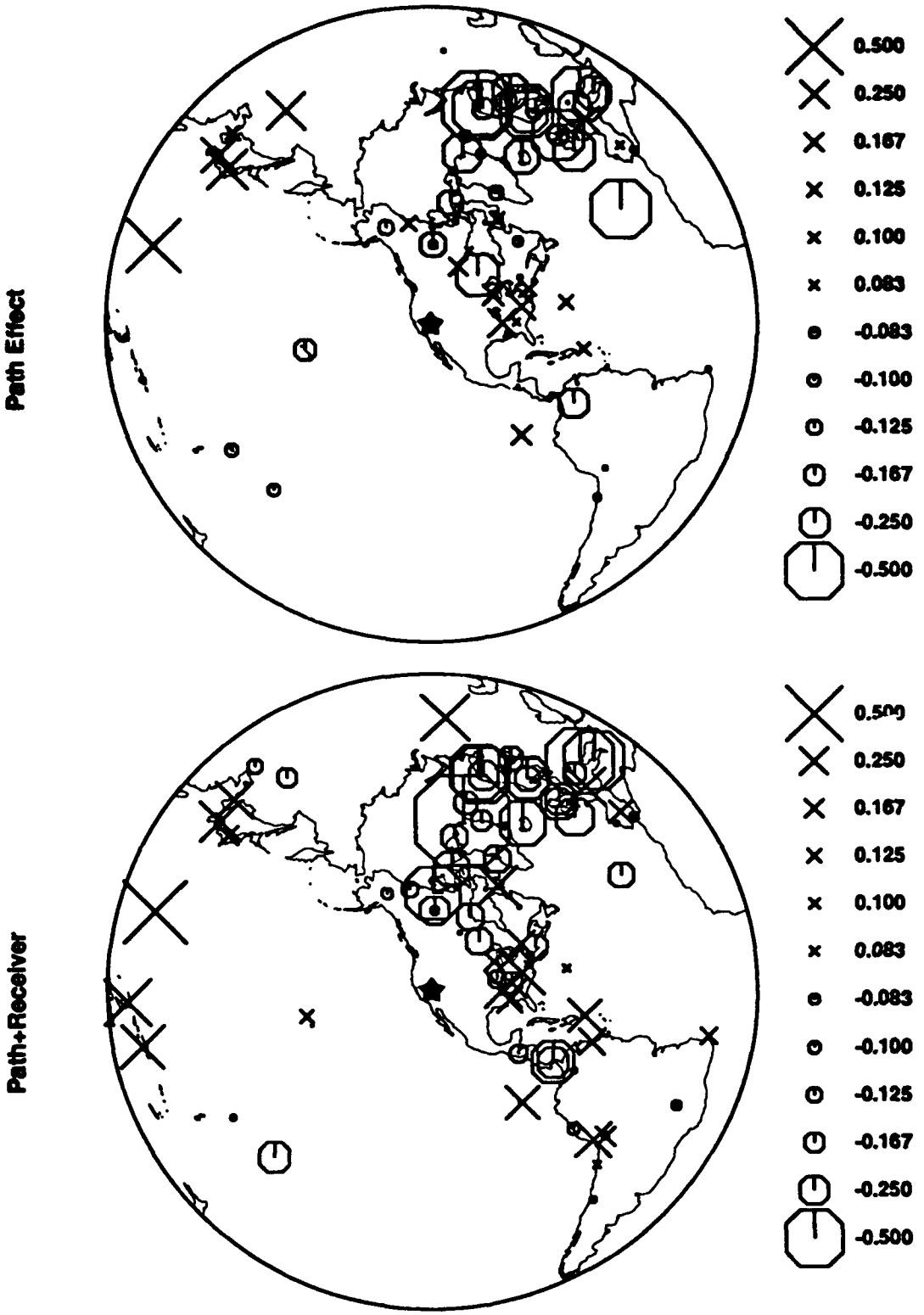

Figure 13. The map showing the "pure propagation effect" (top) and the combined station amplification (bottom) defined as the sum of the receiver term (Figure 7) and the path effect for Pahute Mesa.

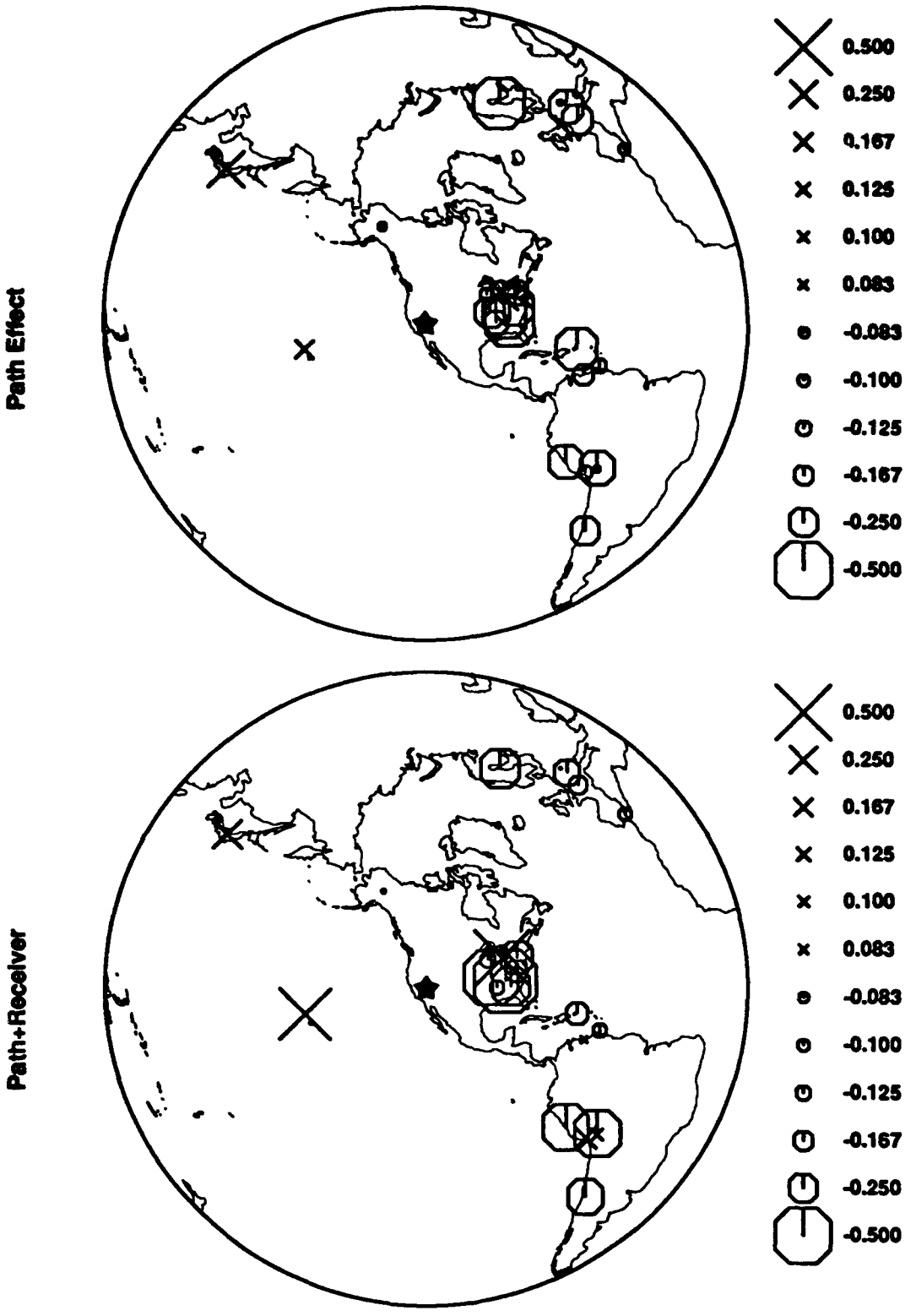

Figure 14. The map showing the "pure propagation effect" (top) and the combined station amplification (bottom) defined as the sum of the receiver term (Figure 7) and the path effect for Rainier Mesa.

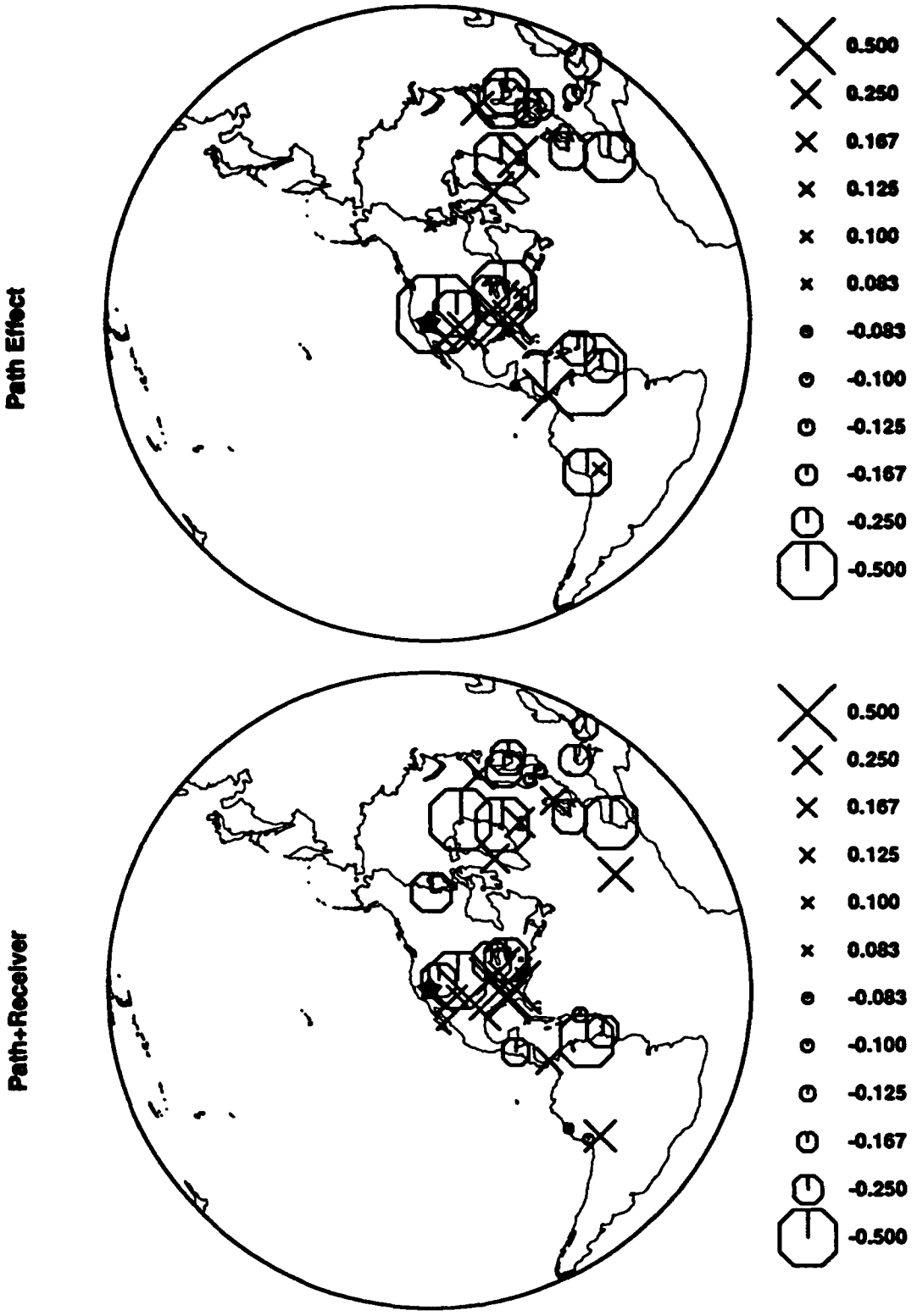

STATION AMPLIFICATION OF MB FOR YUCCA SHOTS

Polar azimuthal equidistant projection, -116.40 , 37.25

Figure 15. The map showing the "pure propagation effect" (top) and the combined station amplification (bottom) defined as the sum of the receiver term (Figure 7) and the path effect for Yucca Flat.

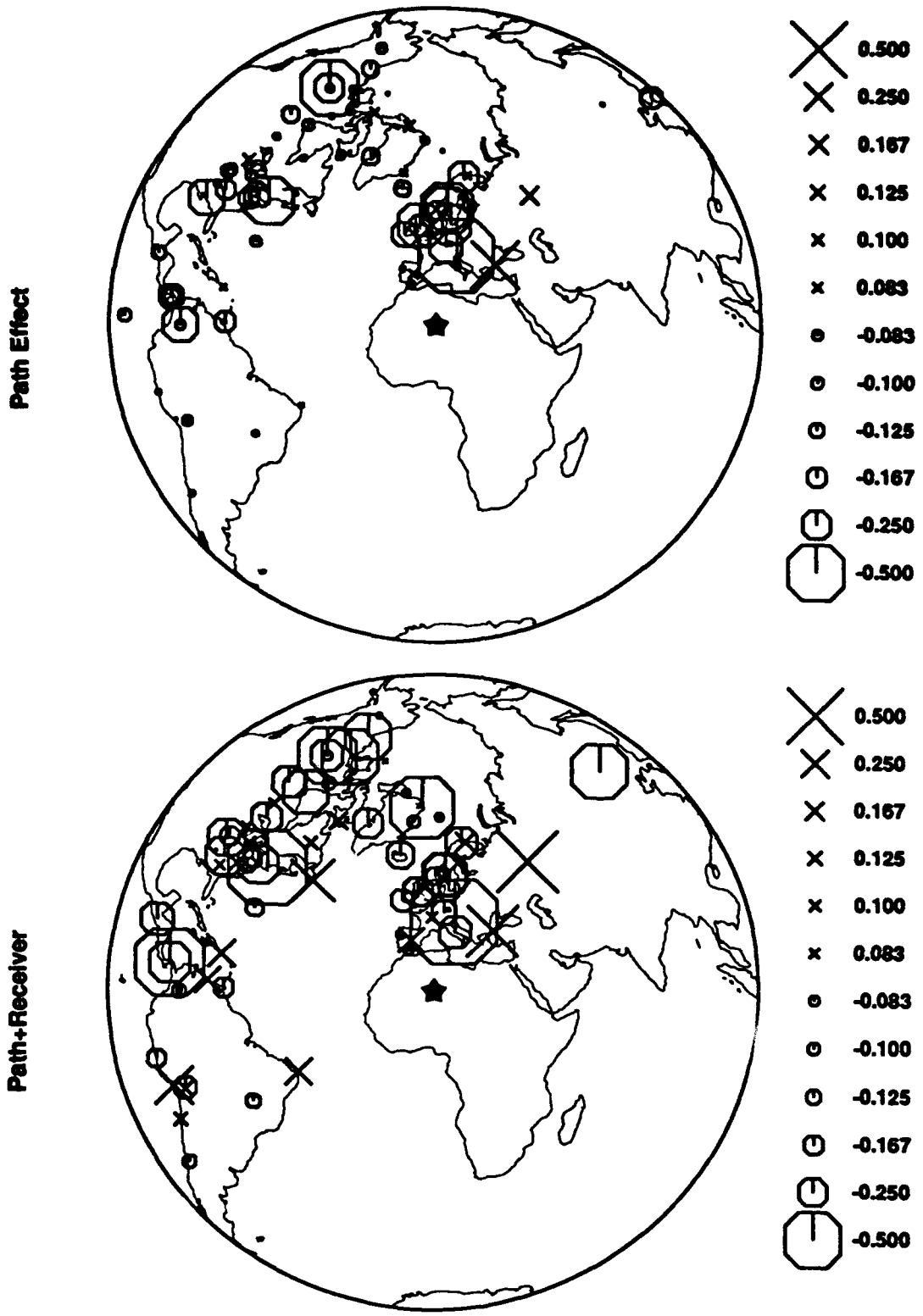

Figure 16. The map showing the "pure propagation effect" (top) and the combined station amplification (bottom) defined as the sum of the receiver term (Figure 7) and the path effect for French Sahara.

V. COMPARISON OF VARIOUS MAGNITUDES

V.1 Comparison of Various GLM Magnitudes

Table 7 compares $m_b(P_{max})$ and $m_b(P_b)$ relative to $m_b(P_a)$ at several nuclear test sites.

Table 7. $m_b(P_{max})$ and $m_b(P_b)$ vs. $m_b(P_a)$		
Test Site	$m_b(P_{max})-m_b(P_a)$ #	$m_b(P_b)-m_b(P_a)$ #
PMA	0.569±0.016 58	0.280±0.010 58
RNA	0.590±0.047 15	0.222±0.042 15
YFT	0.601±0.015 141	0.231±0.013 141
NTS	0.592±0.011 214	0.243±0.009 214
Deg	0.446±0.008 98	0.248±0.007 98
BNE	0.478±0.011 30	0.255±0.009 30
BTZ	0.495±0.014 19	0.282±0.007 19
BSW	0.481±0.005 48	0.281±0.004 48
KTS	0.464±0.005 195	0.261±0.004 195
NNZ	0.407±0.012 30	0.226±0.007 30
Sahara	0.422±0.050 7	0.125±0.053 7

Before Bocharov *et al.* (1989) published the yields and other source information of 98 historical Soviet events, several attempts had been made to investigate the characteristics of cratering explosions in that region. For instance, McLaughlin *et al.* (1985) studied the ratio of the P_a phase and P_{max} phase of presumed Balapan contained and cratering explosions by comparing the WWSSN station m_b's. The motivation was that the logarithm of amplitude ratio of P_{max}/P_a of event SH650115 was significantly smaller than other presumed contained explosions in the vicinity. Assuming the phase P_a is unaffected by the influence of the non-linear free-surface interference, then an adjustment to the m_b (P_{max}) should be able to convert that to a contained explosion of the same yield. McLaughlin *et al.* (1985) concluded that a correction between 0.17 and 0.27 is needed for this conversion, assuming a yield of 125KT.

Der *et al.* (1985) deconvolved four contained and the cratering Balapan events SH650115 recorded at EKA, and then they convolved the Green's functions with an appropriate attenuation operator as well as the source-time function of various yields of interest. By comparing the phases P_a and P_{max} of the synthetics, they obtained a cratering-to-contained correction of 0.15, 0.15, and 0.18 at 60, 125, and 300KT, respectively.

Day *et al.* (1986) did a theoretical study with nonlinear source calculations to account for coupling variations with depth. Their results are summarized as follows:

m_b (contained) - m_b (cratering) ≈ - (0.1 to 0.15) direct coupling
+ (0.1 to 0.25) surface interaction effects
≈ (0 to 0.15) total bias.

Based on 46 Balapan explosions recorded at EKA, Ringdal *et al.* (1992) derived a value of 0.75 as their mean $\log(P_{max}/P_a)$ across the EKA array using the same techniques as used in McLaughlin *et al.* (1985). The cratering event SH650115 had $m_b(P_{max}) - m_b(P_a) = 0.62$ at EKA, and hence they apply a correction of 5.87 + (0.75 - 0.62) = 6.00 for a hypothetical contained explosion with equivalent yield.

For event SH650115, our $m_b(P_{max}) - m_b(P_a) = 0.36$ (*cf.* Table 5), which is about 0.10 to 0.14 m.u. lower than the average $m_b(P_{max}) - m_b(P_a)$ value of 0.464 (KTS) or 0.495 (BTZ, where this event is located) shown in Table 7. Thus statistics in Table 7 suggest that our correction is in better agreement with those derived by Ringdal *et al.* (1992) and Day *et al.* (1986). It is also in agreement with the result in Jih *et al.* (1993) using primarily WWSSN data.

The cratering-to-contained conversions cited above typically require extra information about the general behavior of contained explosions in the same source region. For the purpose of estimating the yield of a cratering shot in an isolated region, directly using P_a could be a much easier approach (Jih *et al.*, 1993).

Without access to official yields, the simplest way to examine the transportability of scaling laws between different test sites would be to relate the seismic phase of interest to the generally more transportable M_S. Table 8 gives the results of regressing $m_b(P_{max})$, $m_b(P_b)$, and $m_b(P_a)$ on M_S (LR) at major test sites with the slope fixed at 1. It is interesting to note that $m_b(P_{max})-M_S$ at KTS is 0.55 m.u. larger than that at NTS, and that NNZ has an intermediate value between those of KTS and NTS.

Tables 9 and 10 compare m_b against L_g and P_n, respectively. The m_b-L_g bias between KTS and NTS is 0.38 m.u., which is in good agreement with the commonly quoted m_b bias of 0.35 m.u. at 150 kt level between KTS and NTS (*e.g.*, Jih *et al.*, 1993; U.S. Congress/Office of Technology Assessment, 1988; and many others). In his pioneering L_g study, Nuttli (1988, 1986ab, 1987) suggested that L_g excitation from explosions may be independent of the source material, and hence $m_b(L_g)$ can be used to calibrate m_b which is susceptible to the upper-mantle attenuation. Nuttli derived his $m_b(L_g)$-yield relationship with NTS explosions and applied the same formula to estimate the yields of Semipalatinsk explosions, and the resulting yield estimates are very good. This has led to numerous follow-up research in recent years using L_g as an excellent relative yield estimator. It should be noted, however, that the absolute $m_b(L_g)$ (or *RMS* L_g) scale is still subject to the source region bias. As Table 9 indicates, $m_b-m_b(L_g)$ at NNZ is even smaller than that at NTS. The same $m_b(L_g)$ formula was used for all test sites, and the path corrections we used are either based on Nuttli's calculation or based on a scheme which produces path attenuation equivalent to what Nuttli would give. In Nuttli's earlier L_g work for earthquakes, the time-domain approach was use in determining the L_g attenuation. Assuming the path attenuation parameters obtained with the coda-Q method is appropriate for NNZ explosions, then Table 9 would suggest that a L_g bias of approximately 0.3 m.u. is necessary to bring L_g scaling in alignment with that of M_S (*cf.* Table 8). That is to say, NNZ $m_b(L_g)$ are probably somewhat overestimated.

Table 8. m_b (GLM) vs. M_S (GLM) at Various Sites			
Test Site	$m_b(P_a)$–LR, #	$m_b(P_b)$–LR, #	$m_b(P_{max})$–LR, #
PMA	0.395±0.031 53	0.676±0.028 53	0.959±0.027 53
RNA	0.854±0.093 2	1.112±0.121 3	1.466±0.124 3
YFT	0.527±0.023 84	0.799±0.021 84	1.148±0.023 84
NTS	0.481±0.019 139	0.759±0.018 140	1.083±0.019 140
Deg	1.108±0.041 63	1.352±0.041 63	1.545±0.040 63
BNE	1.272±0.040 26	1.531±0.042 26	1.747±0.043 26
BTZ	1.220±0.060 18	1.503±0.058 18	1.714±0.059 18
BSW	1.190±0.031 47	1.471±0.031 47	1.670±0.029 47
KTS	1.174±0.022 154	1.436±0.022 154	1.637±0.022 154
NNZ	0.856±0.036 29	1.083±0.036 29	1.264±0.035 29

Table 9. m_b (GLM) vs. L_g (GLM) at Various Sites			
Test Site	$m_b(P_a)-L_g$, #	$m_b(P_b)-L_g$, #	$m_b(P_{max})-L_g$, #
PMA	-0.791±0.024 48	-0.512±0.023 48	-0.215±0.020 48
RNA	-0.585±0.054 15	-0.370±0.035 18	-0.009±0.032 22
YFT	-0.873±0.027 107	-0.638±0.027 108	-0.258±0.027 113
NTS	-0.825±0.020 170	-0.576±0.019 174	-0.217±0.019 183
Deg	-0.255±0.041 12	-0.015±0.037 12	0.167±0.035 12
BNE	-0.346±0.037 20	-0.088±0.037 20	0.127±0.033 20
BTZ	-0.346±0.039 15	-0.068±0.038 15	0.145±0.038 15
BSW	-0.288±0.024 27	0.000±0.023 27	0.197±0.024 27
KTS	-0.310±0.017 74	-0.040±0.016 74	0.163±0.015 74
NNZ	-0.620±0.043 24	-0.401±0.046 24	-0.237±0.041 24

Table 10. m_b (GLM) vs. P_n (GLM) at Various Sites			
Test Site	$m_b(P_a)-P_n$, #	$m_b(P_b)-P_n$, #	$m_b(P_{max})-P_n$, #
PMA	-0.515±0.018 54	-0.234±0.014 54	0.059±0.012 54
RNA	-0.055±0.056 15	0.163±0.026 18	0.522±0.032 22
YFT	-0.370±0.022 138	-0.143±0.022 139	0.231±0.022 145
NTS	-0.385±0.018 207	-0.140±0.017 211	0.218±0.017 221
Deg	-0.334±0.047 55	-0.086±0.043 55	0.103±0.043 55
BNE	-0.176±0.123 20	0.084±0.119 20	0.306±0.123 20
BTZ	-0.562±0.110 6	-0.291±0.113 6	-0.090±0.111 6
BSW	-0.452±0.064 32	-0.176±0.063 32	0.022±0.064 32
KTS	-0.351±0.037 113	-0.093±0.035 113	0.106±0.036 113
NNZ	-0.940±0.058 20	-0.721±0.058 20	-0.525±0.056 20

V.2 m_b-L_g Variability within Balapan Test Site

Marshall *et al.* (1984) found that explosions in the northeast and southwest portions of Balapan test site produce distinctly different waveforms when recorded at the UK seismological array stations, suggesting that Balapan test site can be subdivided into two areas characterized by different geophysical properties. Ringdal and Hokland (1987) find that this pattern is persistently present whether m_b based on worldwide network or m_b (*P*coda) of NORSAR is used. They inferred the average $m_b - L_g$ between SW and NE subregions as 0.17 m.u. In a follow-up study, Ringdal and Fyen (1988) suggest that there appears to be a transition zone between the NE and SW subregions. Ringdal *et al.* (1992) recomputed the SW-NE bias as 0.15 m.u. with 101 Balapan events recorded at ISC stations and NORSAR. Although Ringdal *et al.* (1992) agree that the possibility of a $m_b(L_g)$ bias contributing to this difference between SW and NE cannot be entirely ruled out, they propose an empirical approach to correct for this bias by assuming this bias is solely due to a relative m_b bias between these two areas.

We followed the zoning of Ringdal *et al.* (1992) in partitioning Balapan test site into three regions: southwest (SW), transition zone (TZ), and northeast (NE). Figure 17 shows the spatial pattern of m_b - L_g residuals of Semipalatinsk explosions based on Geotech's m_b values and RMS L_g values reported at NORSAR. There is a significant difference in the source medium across the Chinrau fault separating the northeastern and southwestern portion of Balapan test site, as reported by Ringdal *et al.* (1992) and Marshall *et al.* (1984). The mean m_b -L_g bias between SW and NE Balapan is about 0.07 m.u.

Note that the $m_b(P_{max}) - L_g$ bias of 0.08 m.u. between SW and NE (*cf.* Table 12) is significantly smaller than that of previous studies. Regressing the *RMS* L_g furnished by Israelson (1992) and our $\overline{m}_G$ on the yields published by Bocharov *et al.* (1989) (and Vergino, 1989) shows that NE explosions have positive L_g residuals and negative m_b residuals, whereas SW explosions show the opposite trend (Figure 10 of Jih *et al.*, 1993). A three-dimensional geological model of the Balapan test site by Leith and Unger (1989) shows a distinct difference between the NE and SW portions of the test site, with the granites closer to the surface and the alluvium thinner in the southwest. The thicker alluvium layer in NE region could increase the waveform complexity and reduce the magnitudes measured with P_{max}. The first motion should be least affected by this factor, however. Jih *et al.* (1993) suggest that the $m_b - L_g$ bias between SW and NE Balapan can be tentatively decomposed into several parts:

[I] Difference in *pP* between SW and NE,
[II] Difference in m_b coupling, *i.e.*, m_b (SW) > m_b (NE),
[III] Difference in L_g coupling, *i.e.*, L_g (NE) > L_g (SW),
[IV] Effects due to the station-station correlation structure,
[V] Effects due to the uneven geographical clustering of stations, as well as any path effect which is not fully accounted for through the network averaging.

The bias of 0.08 m.u. for $m_b(P_{max})$ -*RMS* L_g between SW and NE Balapan (Table 12) is essentially the sum of [I] through [III]. However, if the time-domain L_g magnitude is used instead, the bias between SW and NE Balapan is insignificant (Table 11).

For ISC data, we estimate that [V] is about 0.02 m.u. if $\overline{m}_{2.2}$ derived by the conventional LSMF are used. When $\overline{m}_G$ is used, this term is eliminated, and hence a smaller $m_b - L_g$ bias is obtained. [II] and [III] can be easily illustrated with regressions on Bocharov's published yields, as explained earlier.

There are only a handful of Balapan events with published yields in Bocharov *et al.* (1989). However, the 5 large historical events (for which the yields were exchanged during JVE) can also provide some supplementary clue in support of our postulated hypotheses [I] through [III]. The yield estimate based on P_{max} for two (out of three) historical events in SW subregion (790804B and 791223B) is larger than that based on P_a. On the other hand, the two events in NE subregion (791028B and 840526B) have a smaller yield estimate based on P_{max} as compared to P_a. The larger bias of 0.15 m.u. that Ringdal *et al.* (1992) obtained with m_b (ISC) could have been slightly "enhanced" due to [IV] and [V]. The m_b determination procedure presented in this study does not correct for [IV] either. However, the contribution of inter-station correlation alone is believed to be insignificant if WWSSN is used.

In Figure 19 we show the difference of path effects between BSW and BNE at each WWSSN station, which is a measure of the relative bias between BSW and BNE along each path. Positive symbols represent the stations where BSW events are enhanced relative to BNE events. If the raw station magnitudes are used in the network averaging without fully accounting for such path-effect differential, significant bias (relative to the L_g magnitude) will be present. ISC network is dominated by western European stations, and hence the effect due to [V] would be more severe than that on WWSSN.

Nuttli (1987, 1988) suggests that there is a m_b bias of about 0.2 m.u. between Degelen and Balapan, with Degelen explosions having even larger m_b excitation (relative to L_g). We do not see such Degelen-Balapan bias with Nuttli's $m_b(L_g)$ (Table 11) or *RMS* L_g measured at NORSAR (Table 12).

Table 11. $\overline{m}_G$ (GLM) vs. $m_b(L_g)$ (Nuttli) at Various Sites

Test Site	$m_b(P_a)$–Nuttli, #	$m_b(P_b)$–Nuttli, #	$m_b(P_{max})$–Nuttli, #	$m_b(L_g)$–Nuttli
PMA	-0.894±0.054 16	-0.630±0.053 16	-0.326±0.044 16	-0.062±0.042 13
RNA	-0.627±0.066 6	-0.458±0.035 7	-0.057±0.035 8	-0.071±0.062 9
YFT	-0.841±0.046 56	-0.636±0.049 57	-0.273±0.048 59	0.167±0.121 44
NTS	-0.836±0.036 78	-0.619±0.037 80	-0.263±0.036 83	0.090±0.082 66
BSW	-0.406±0.020 26	-0.120±0.020 26	0.080±0.020 26	-0.104±0.032 18
BNE	-0.415±0.026 21	-0.150±0.026 21	0.059±0.026 21	-0.087±0.050 17
BTZ	-0.415±0.029 12	-0.133±0.025 12	0.077±0.030 12	-0.036±0.059 9
Deg	-0.350±0.054 20	-0.100±0.058 20	0.102±0.057 20	
KTS	-0.395±0.017 79	-0.125±0.017 79	0.079±0.017 79	-0.081±0.025 45
NNZ	-0.589±0.035 25	-0.363±0.037 25	-0.188±0.032 25	0.021±0.024 20

Table 12. $\overline{m}_G$ (GLM) vs. *RMS* L_g (NORSAR) at Various Sites

Test Site	$m_b(P_a)$–*RMS* L_g, #	$m_b(P_b)$–*RMS* L_g, #	$m_b(P_{max})$–*RMS* L_g, #	$m_b(L_g)$–*RMS* L_g
BSW	-0.367±0.009 39	-0.084±0.008 39	0.114±0.009 39	-0.103±0.019 24
BNE	-0.449±0.013 23	-0.192±0.012 23	0.028±0.014 23	-0.131±0.032 18
BTZ	-0.466±0.018 13	-0.178±0.015 13	0.033±0.015 13	-0.143±0.033 9
Deg	-0.333±0.028 5	-0.106±0.028 5	0.074±0.029 5	-0.122±0.118 2
KTS	-0.404±0.008 80	-0.132±0.008 80	0.074±0.008 80	-0.120±0.015 53
NNZ	-0.577±0.019 15	-0.346±0.022 15	-0.143±0.023 15	0.124±0.051 10

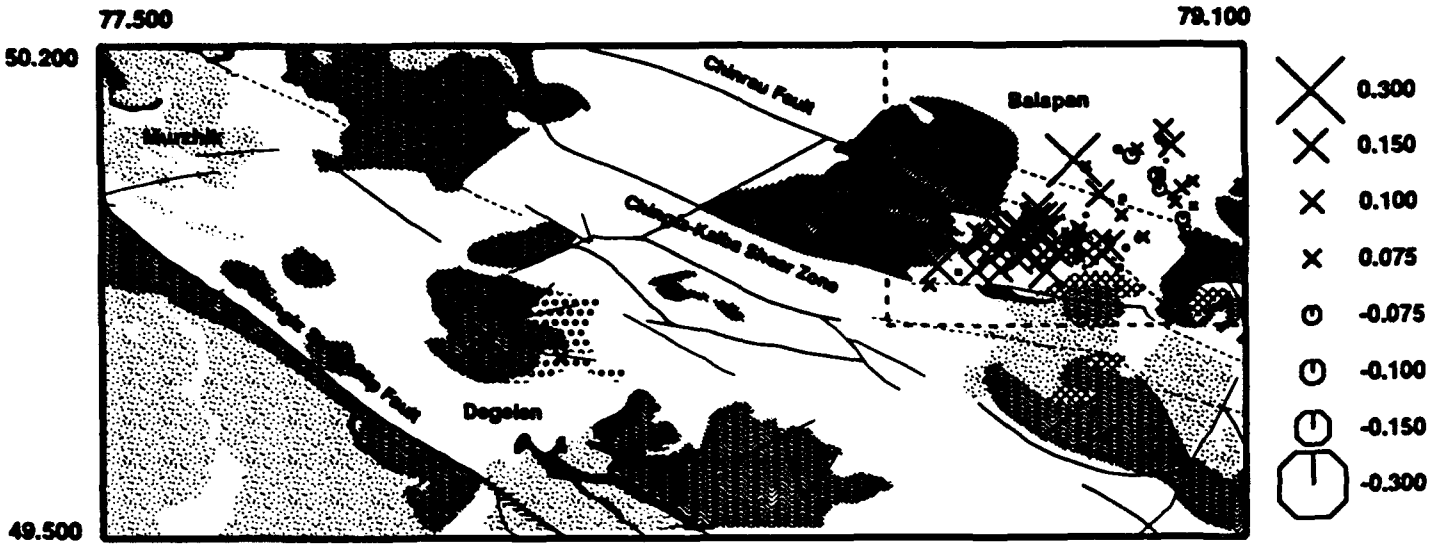

SPATIAL PATTERN OF SEMIPALATINSK mb-Lg RESIDUALS

- Sedimentary & volcanic rocks
- Devonian & Carboniferous rocks
- Granitic rocks
- Limestone
- Lower Metamorphic rocks
- Upper Paleozoic sedimentary rocks
- Migmatite
- Metamorphic rocks
- Cataclastic rocks

Figure 17. The spatial pattern of m_b-L_g residuals of Semipalatinsk explosions using the m_o (P_{max}) of this study (Table 5) and RMS L_g values reported by Ringdal *et al.* (1992). The locations are based on Bocharov *et al.* (1989) and Thurber, Quin, and Richards (1993), and the tectonics are based on Bonham *et al.* (1980) and Leith (1987). The pattern suggests some difference in the source medium across the Chinrau fault separating the northeastern and southwestern portion of the test site. The mean m_b-L_g bias between SW and NE Balapan is about 0.08 m.u.

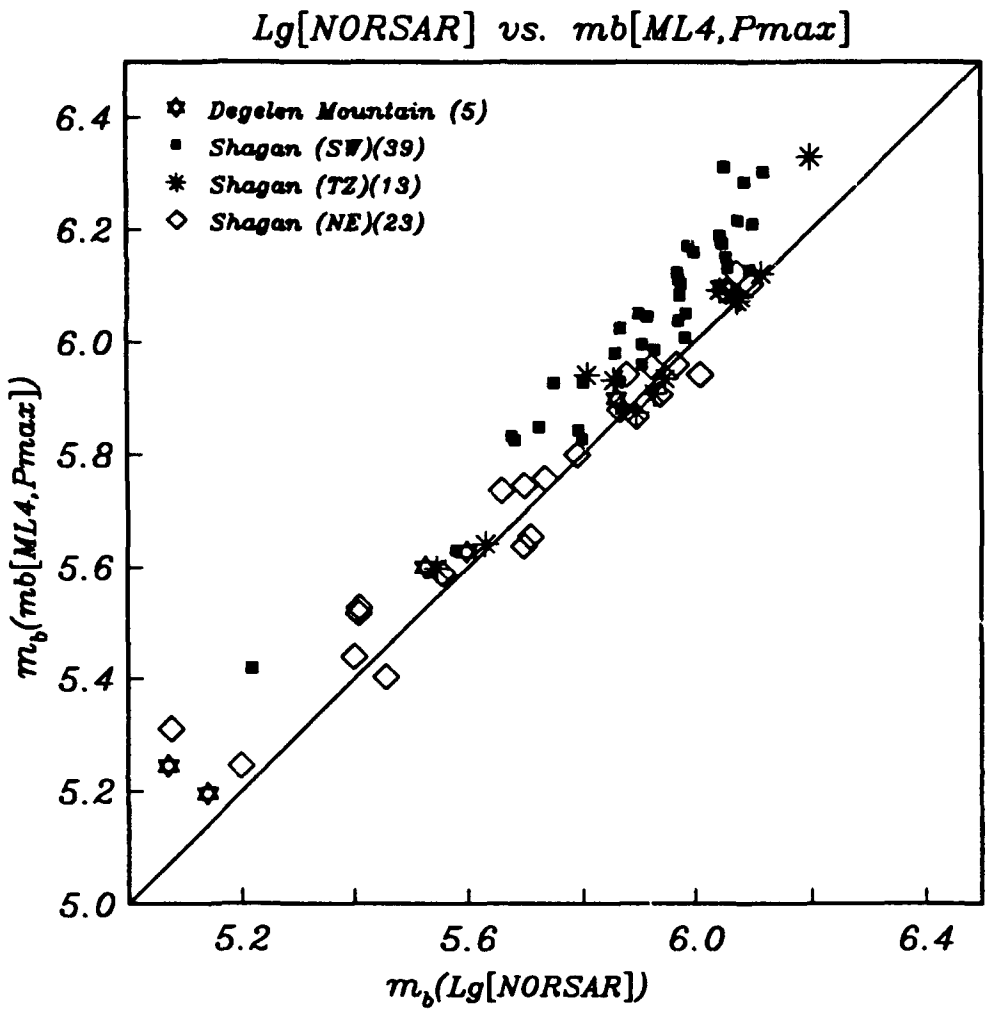

Figure 18. Comparison of m_b (P_{max}) against *RMS* L_g (NORSAR) reported by Ringdal *et al.* (1992). The slope is fixed at 1.

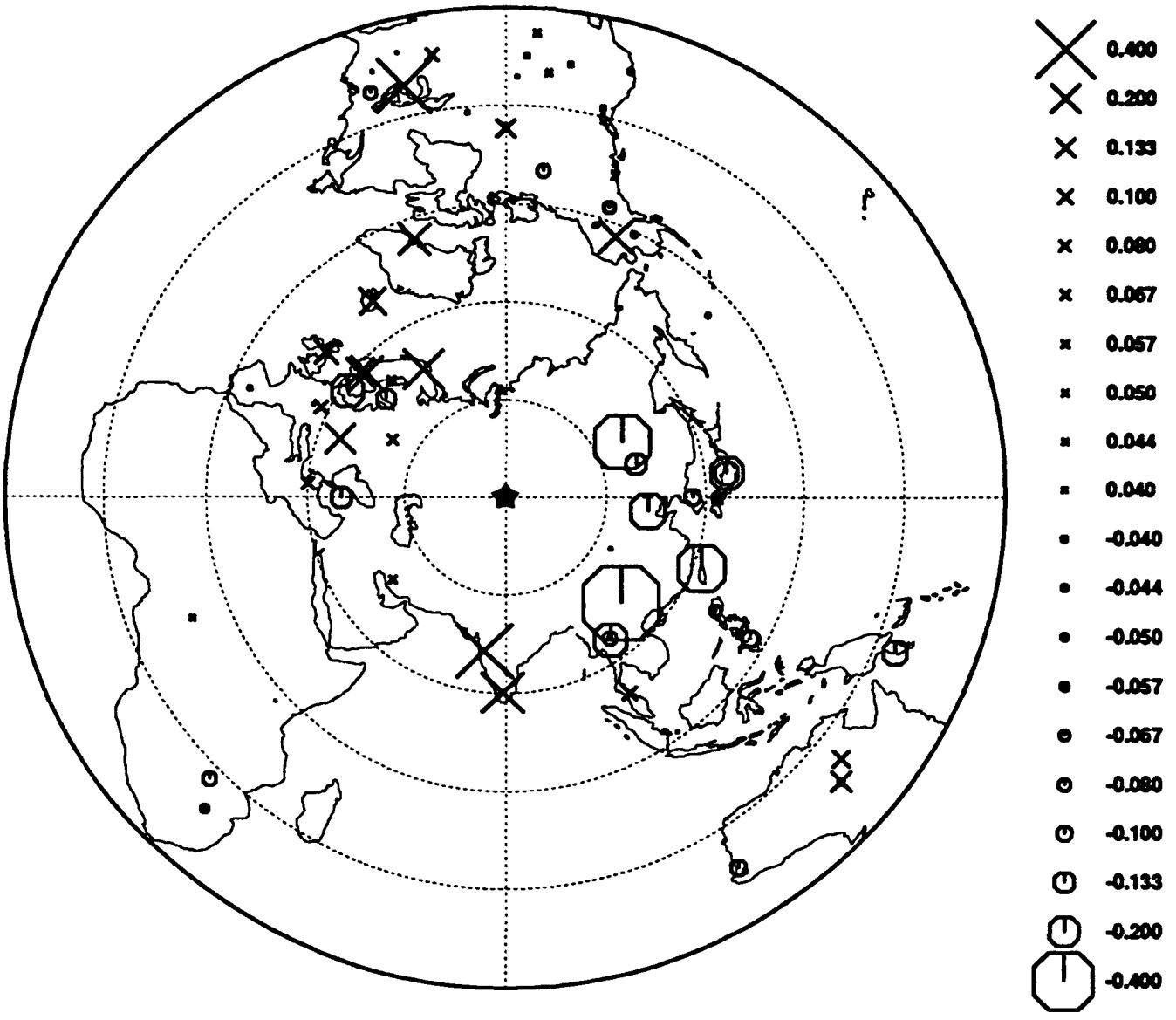

Figure 19. Averaged SW-NE bias at each WWSSN station. Positive symbols represent the stations where amplitude of BSW events is enhanced relative to that of BNE events of the same source strength. This pattern reflects the difference of path effects on these two adjacent test sites. For network with an uneven geographical distribution of stations (such as ISC), the simple network averaging of station magnitudes can only eliminate the path effect to certain extent.

V.3 Magnitude-magnitude Regression with Uncertain Data

The standard approach of yield estimation is to use known-yield events to construct a magnitude-yield relationship which is then utilized to estimate the yield of other events. Typically either the yield or the m_b is assumed to be exact in the regression. The magnitude-magnitude regressions of Sections V.1 and V.2 are such that the independent variable is assumed to be exact and that the slope is fixed at 1. In reality, however, both the yields and the magnitudes are subject to error. The regression result could be misleading if we simply assume that the yields of 19 Semipalatinsk explosions published in Soviet literature are exact. It has been specu oviets might have rounded 8 of the announced 19 yields to the nearest 5 kt or 10 kt. Thus an announced yield of 100 kt could mean something actually measured between 95 kt and 104 kt if rounding is the only source of error. It could also indicate that perhaps 100 kt was the designed energy release, and the actual yield was somewhere nearby. Unlike the magnitude-yield regression, the rounding errors can be controlled in the magnitude-magnitude regression models. The standard errors, however, still can not be ignored.

A more general regression routine is given in this section to take the standard errors in the magnitudes into account. For each (X, Y) pair (where X and Y are two different magnitudes), we use a random number generator to produce a perturbed (X, Y) pair according to their uncertainty distribution. A standard least-squared regression is then performed for each data set of perturbed pseudo-observations. The procedure is repeated for several hundred iterations, and all the resulting calibration curves are then used to infer the ensemble behavior. This "doubly-weighted least-squares scheme" [DWLSQ] is an extension to the "ordinary weighted least-squares" [OWLS] in which only errors in the Ys would be used to adjust the inferred parameters.

The "upper 95% confidence limit" of the predicted m_b at a given X (say, X_0) can be computed as follows:

$$\hat{Y}(\max) + t(\text{D.O.F.},0.975)[\sigma^2(Y) + \sigma^2(\text{regression})(\frac{1}{N} + \frac{(X_0 - \bar{X})^2}{\sum(X_i - \bar{X})^2})]^{0.5} \quad , \qquad [19]$$

where N = number of data points used in the regression, D.O.F. = N-2, $\sigma(Y)$ = the mean S.E. in the network m_b [2] used in the regression, σ(regression) = the σ of residuals, $\hat{m}_b(\max)$ = estimate of the largest possible mean m_b [2] at the given X, $\bar{X}$ is the mean X used in the regression, and t(D.O.F., 0.975) is the 97.5 percentile of Student's *t* distribution at "D.O.F." degrees of freedom. Most statistics textbooks have a table of such values after Fisher and Yates (1963). Several commonly quoted t(D.O.F., 0.975) values are listed in Table 13.

Table 13. 97.5 Percentile of *t* Distribution

D.O.F.	5	10	20	30	40	60	∞
t(D.O.F.)	2.571	2.228	2.086	2.042	2.021	2.000	1.960

The "lower 95%-confidence limit" can be computed in a similar way:

$$\hat{Y}(min) - t(D.O.F.,0.975)[\sigma^2(Y) + \sigma^2(regression)(\frac{1}{N} + \frac{(X_0 - \bar{X})^2}{\sum(X_i - \bar{X})^2})]^{0.5} \quad . \qquad [20]$$

In the case where each error range in the X and the Y is reduced to zero, then all the random resamplings will simply produce identical replica of the original data set. Consequently, the several hundred regressions will all give the result identical to a single call of the standard least-squares. This illustrates how the "doubly weighted least-squares" [DWLSQ] would degenerate to the standard least-squares when the uncertainties in the X and Y shrink to zero. By the same reasoning, this "doubly weighted least squares" regression method is also an extension to the conventional "weighted least-squares" in which only the errors in the Y's would be used to adjust the inferred parameters.

Table 14 summarize the magnitude-magnitude regression models for all test sites with the algorithm described above. $m_b(P_{max})$ is used as the independent variable in all regressions. The standard errors associated with the event magnitudes as listed in Table 5 are taken into account. Outliers are rejected and then the regression was repeated until no outlier was detected. Figures 20 through 24 show the regressions of different phases on $m_b(P_{max})$ at major test sites. Figure 21 show the $m_b(P_{max})$:LR regression with the outliers retained. The uncertainties in both X and Y variables were accounted for by the same bootstrap resampling procedure.

For comparison, Figures 25 and 27 show the standard least-square regression, ignoring the standard errors in $m_b(P_{max})$ and M_S. The regression results using other phases are summarized in the Appendix D.

Table 14. Magnitude:magnitude Regression Results							
Uncertain X & Y, Bootstrap Used, Outlier Rejected							
Site	X	Y	N	Slope	Intercept	σ(Y)	ρ
NTS	Pmax	Pb	192	1.043±0.021	-0.558±0.116	0.073	0.98
PMA	Pmax	Pb	56	1.050±0.031	-0.574±0.171	0.065	0.98
RNA	Pmax	Pb	18	0.756±0.167	0.877±0.855	0.102	0.86
YFT	Pmax	Pb	130	1.047±0.028	-0.605±0.153	0.095	0.98
KTS	Pmax	Pb	184	0.982±0.010	-0.096±0.057	0.036	1.00
Deg	Pmax	Pb	95	0.965±0.024	-0.008±0.130	0.043	0.99
BNE	Pmax	Pb	30	1.051±0.040	-0.513±0.228	0.047	0.99
BTZ	Pmax	Pb	19	0.999±0.049	-0.209±0.288	0.043	0.99
BSW	Pmax	Pb	48	0.990±0.053	-0.140±0.322	0.025	1.00
NNZ	Pmax	Pb	29	1.050±0.017	-0.469±0.101	0.034	1.00
Sahara	Pmax	Pb	7	0.991±0.125	-0.255±0.683	0.113	0.97
NTS	Pmax	Pa	192	1.036±0.019	-0.786±0.104	0.108	0.96
PMA	Pmax	Pa	53	1.009±0.031	-0.611±0.173	0.085	0.96
RNA	Pmax	Pa	15	0.902±0.201	-0.087±1.034	0.185	0.73
YFT	Pmax	Pa	126	1.031±0.023	-0.766±0.129	0.113	0.96
KTS	Pmax	Pa	184	0.954±0.009	-0.208±0.050	0.050	0.99
Deg	Pmax	Pa	91	0.980±0.017	-0.336±0.092	0.056	0.98
BNE	Pmax	Pa	30	1.014±0.040	-0.559±0.226	0.058	0.98
BTZ	Pmax	Pa	19	0.977±0.049	-0.359±0.293	0.062	0.97
BSW	Pmax	Pa	48	1.003±0.054	-0.497±0.328	0.036	0.99
NNZ	Pmax	Pa	29	1.026±0.017	-0.553±0.099	0.057	1.00
Sahara	Pmax	Pa	7	0.733±0.108	0.980±0.591	0.066	0.98
NTS	Pmax	Pn	204	1.054±0.029	-0.464±0.153	0.137	0.95
PMA	Pmax	Pn	54	0.962±0.068	0.153±0.371	0.090	0.95
RNA	Pmax	Pn	22	0.638±0.183	1.315±0.930	0.148	0.72
YFT	Pmax	Pn	141	1.002±0.033	-0.216±0.172	0.125	0.96
KTS	Pmax	Pn	100	0.925±0.048	0.374±0.268	0.243	0.86
Deg	Pmax	Pn	52	0.834±0.100	0.822±0.528	0.263	0.72
BNE	Pmax	Pn	20	0.685±0.177	1.500±1.012	0.542	0.35
BTZ	Pmax	Pn	6	0.418±0.362	3.493±2.141	0.170	0.67
BSW	Pmax	Pn	30	0.742±0.209	1.471±1.261	0.218	0.58
NNZ	Pmax	Pn	20	0.921±0.086	0.966±0.465	0.248	0.84
NTS	Pmax	Lg	168	0.849±0.029	1.066±0.156	0.151	0.91
PMA	Pmax	Lg	47	0.805±0.070	1.302±0.391	0.118	0.89
RNA	Pmax	Lg	22	0.776±0.183	1.146±0.928	0.153	0.78
YFT	Pmax	Lg	107	0.834±0.036	1.178±0.191	0.151	0.92
KTS	Pmax	Lg	74	0.725±0.066	1.459±0.390	0.113	0.86

Table 14. Magnitude:magnitude Regression Results (Cont)							
Uncertain X & Y, Bootstrap Used, Outlier Rejected							
Site	X	Y	N	Slope	Intercept	σ(Y)	ρ
Deg	Pmax	Lg	12	0.826±0.148	0.825±0.846	0.111	0.91
BNE	Pmax	Lg	20	0.647±0.138	1.920±0.806	0.126	0.78
BTZ	Pmax	Lg	15	0.644±0.126	1.951±0.748	0.107	0.88
BSW	Pmax	Lg	27	0.557±0.221	2.486±1.335	0.107	0.63
NNZ	Pmax	Lg	24	0.710±0.051	1.950±0.304	0.109	0.97
NTS	Pmax	LR	134	1.173±0.031	-2.042±0.174	0.189	0.90
PMA	Pmax	LR	51	1.113±0.049	-1.590±0.275	0.169	0.88
YFT	Pmax	LR	80	1.121±0.039	-1.818±0.214	0.170	0.92
KTS	Pmax	LR	138	0.972±0.017	-1.501±0.102	0.191	0.89
Deg	Pmax	LR	55	1.312±0.045	-3.310±0.242	0.196	0.89
BNE	Pmax	LR	26	1.212±0.069	-2.962±0.399	0.209	0.86
BTZ	Pmax	LR	18	1.252±0.099	-3.202±0.595	0.238	0.83
BSW	Pmax	LR	42	0.479±0.033	1.506±0.197	0.126	0.66
NNZ	Pmax	LR	29	0.996±0.023	-1.238±0.140	0.189	0.95

At M_S = 4.0, the corresponding $m_b(P_{max})$ at NTS, KTS, and NNZ are 5.151, 5.659, and 5.259, respectively. Once again, under the assumption that M_S is relatively less susceptible to source medium and propagation effect than other phases, then M_S -m_b bias would reflect primarily the m_b bias, and our results would support the claim that m_b excitation at NNZ is intermediate between that of NTS and KTS, with m_b the largest, given the same M_S level. This result is in agreement with that based on fixed-slope regression as did in the previous section.

The $m_b(P_{max})$:$m_b(L_g)$ regression models appear to lead some inconsistency with the $m_b(P_{max})$:M_S models. At $m_b(L_g)$ of 5.5, the corresponding $m_b(P_{max})$ at NTS, KTS, and NNZ are 5.223, 5.574, and 5.000, respectively. This is in conflict with the m_b excitation relative to M_S. We have noticed this inconsistency in the previous section. It would seem that our $m_b(L_g)$ values are too high for NNZ explosions. To remove this inconsistency, at least two simple approaches can be adopted. The first one is to revise Nuttli's path attenuation parameters for NNZ explosions. Perhaps his Q values based on the coda-Q method are too low which caused the over-compensation of the attenuation effect. An 10%-15% increase in the Q values would bring the $m_b(L_g)$ values down by 0.2-0.3 m.u., which would be sufficient to remove the inconsistency. Alternatively, assuming the Q values derived by the coda-Q method do match perfectly with those derived with the time-domain amplitude decay relationship, then probably the apparently strongest $m_b(L_g)$ excitation at NNZ is due to erroneous scaling constant in the $m_b(L_g)$ formula. In this study, we have used a single formula to compute the station $m_b(L_g)$, Equation [1], which is the same formula that Nuttli used in his L_g study of NTS, KTS, and NNZ explosions:

$$m_b(L_g) = 4.0272 + \log A(\Delta) + \frac{1}{3}\log(\Delta(\mathrm{km})) + \frac{1}{2}\log[\sin(\frac{\Delta(\mathrm{km})}{111.1(\mathrm{km/deg})})] + \frac{\gamma(\Delta-10\mathrm{km})}{\ln(10)} .$$

This formula is scaled so that a seismic source with 1-sec L_g amplitude of 110 μm at 10 km epicentral distance would correspond to a $m_b(L_g)$ of 4.0272 + 2.0414 + 0.3333 - 1.4019 + 0.0000 = 5.000, which was suggested to be appropriate for eastern North America and Semipalatinsk. However, Nuttli (1980) also suggested that a seismic source in Iran with the ISC bulletin m_b 5.0 should excite L_g amplitude of 270 microns at a 10-km extrapolated distance. Possible explanations for this apparent bias of 0.26–0.39 m.u. include [1] uncertainty in the ISC bulletin m_b values (Nuttli, 1981), [2] differences in L_g excitation relative to m_b, or [3] differences in the upper mantle property which could cause a bias in m_b. Many L_g studies have used the ISC m_b for "normalizing" their L_g magnitude scale (*e.g.*, page 2146 of Nuttli, 1986a; page 128 of Israelson, 1992). Without careful re-processing, the ISC bulletin m_b values typically would be associated with large uncertainty. The m_b used in this study are those that have been corrected for the station amplifications as well as the path effects, and therefore we can rule out the possibility of large uncertainty in m_b. It would seem plausible that NNZ might have a L_g scale similar to that in Iran:

$$m_b(L_g) = 3.6372 + \log A(\Delta) + \frac{1}{3}\log(\Delta(\mathrm{km})) + \frac{1}{2}\log\left[\sin\left(\frac{\Delta(\mathrm{km})}{111.1(\mathrm{km/deg})}\right)\right] + \frac{\gamma(\Delta - 10\mathrm{km})}{\ln(10)} .$$

With a reduction of 0.39 m.u. in the $m_b(L_g)$ scaling constant, it is sufficient to make the m_b :L_g and m_b :M_S models consistent across the three test sites we discussed. This adjustment would, however, raise a doubt whether the L_g scaling appropriate for eastern U.S. and Semipalatinsk is really transportable to Novaya Zemlya as is M_S.

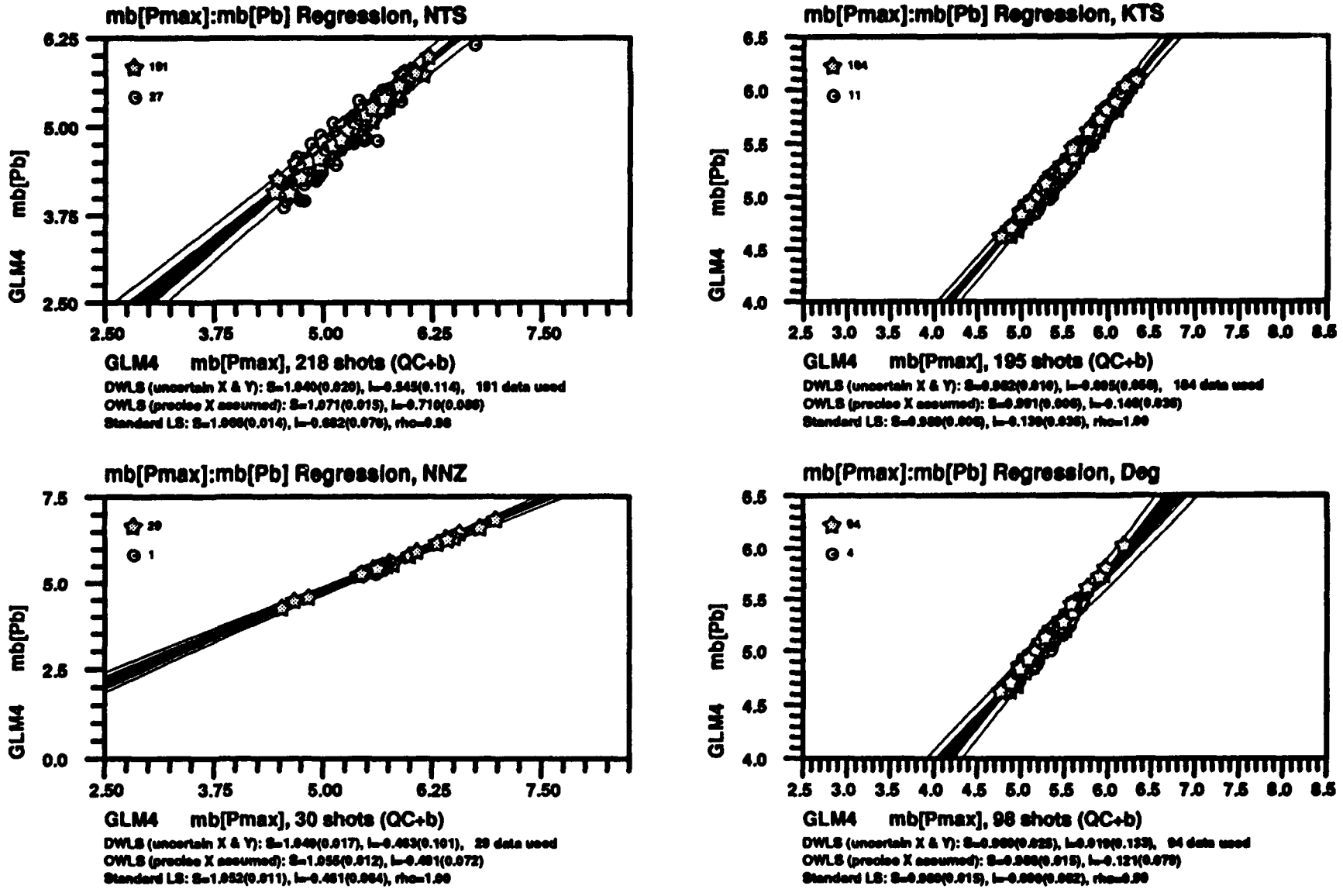

Figure 20. Regressing $m_b(P_b)$ on $m_b(P_{max})$ with outliers excluded. The uncertainty in each individual event magnitude is taken into account. Each Soviet test site appears to be more homogeneous in terms of geological / geophysical characteristics, as indicated by the small scatter around the $m_b(P_b):m_b(P_{max})$ calibration curves.

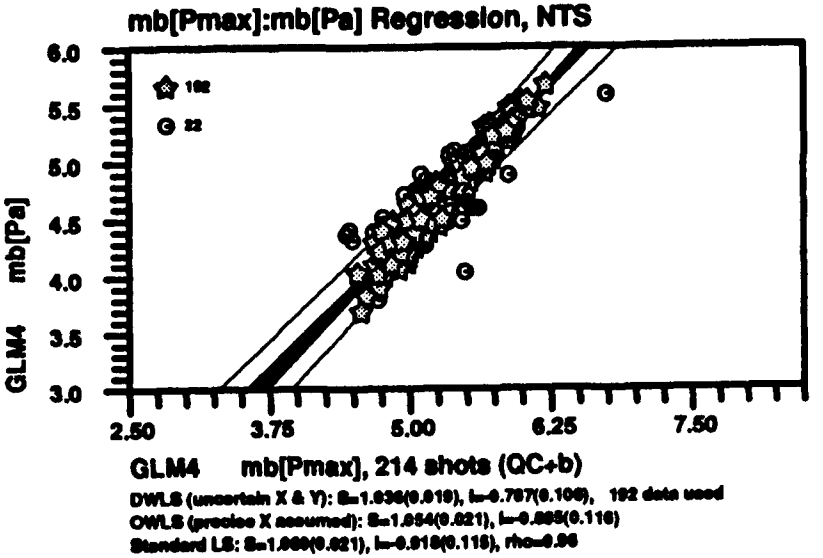

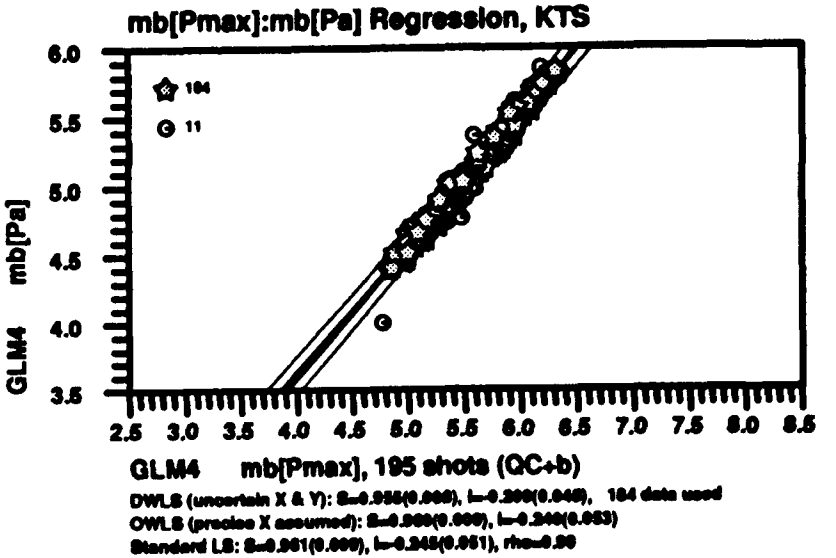

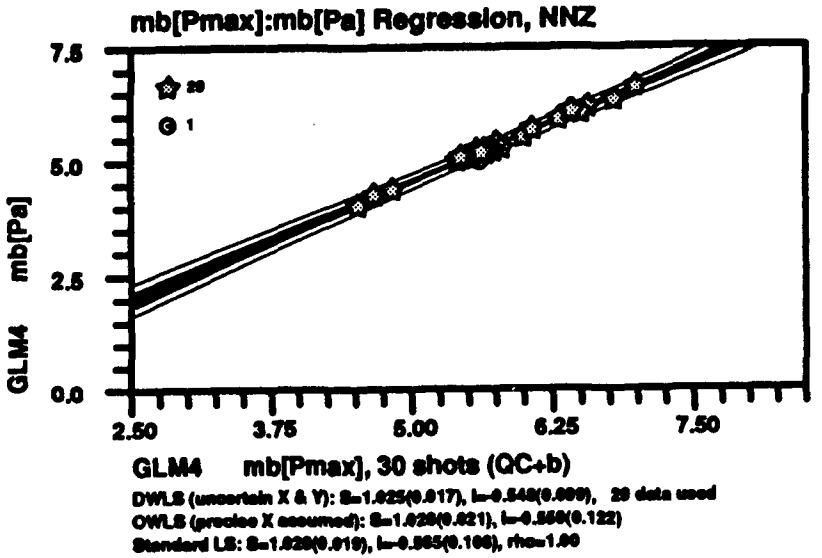

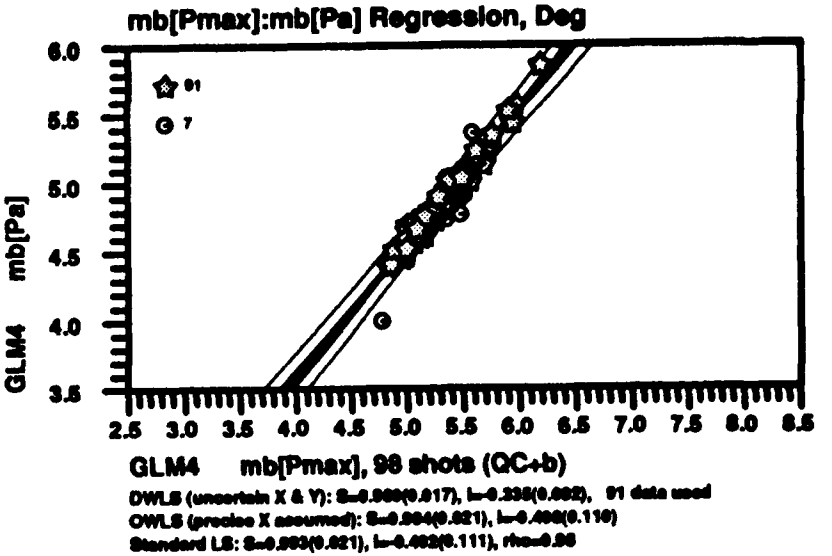

Figure 21. Regressing $m_b(P_a)$ on $m_b(P_{max})$ with outliers excluded.

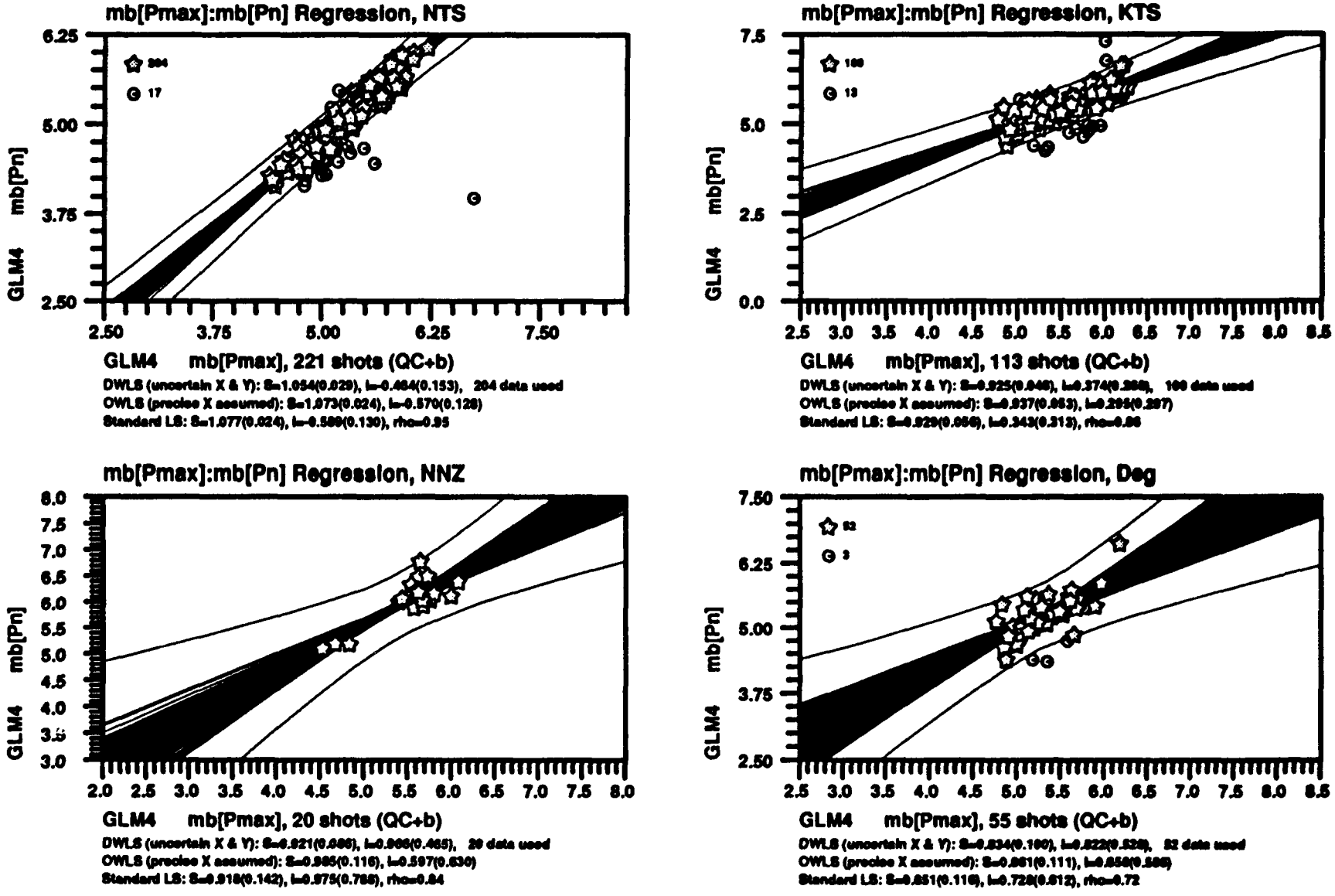

Figure 22. Regressing mPn on $m_b(P_{max})$ with outliers excluded. The darkened bundle in each regression represents 800 possible calibration curves.

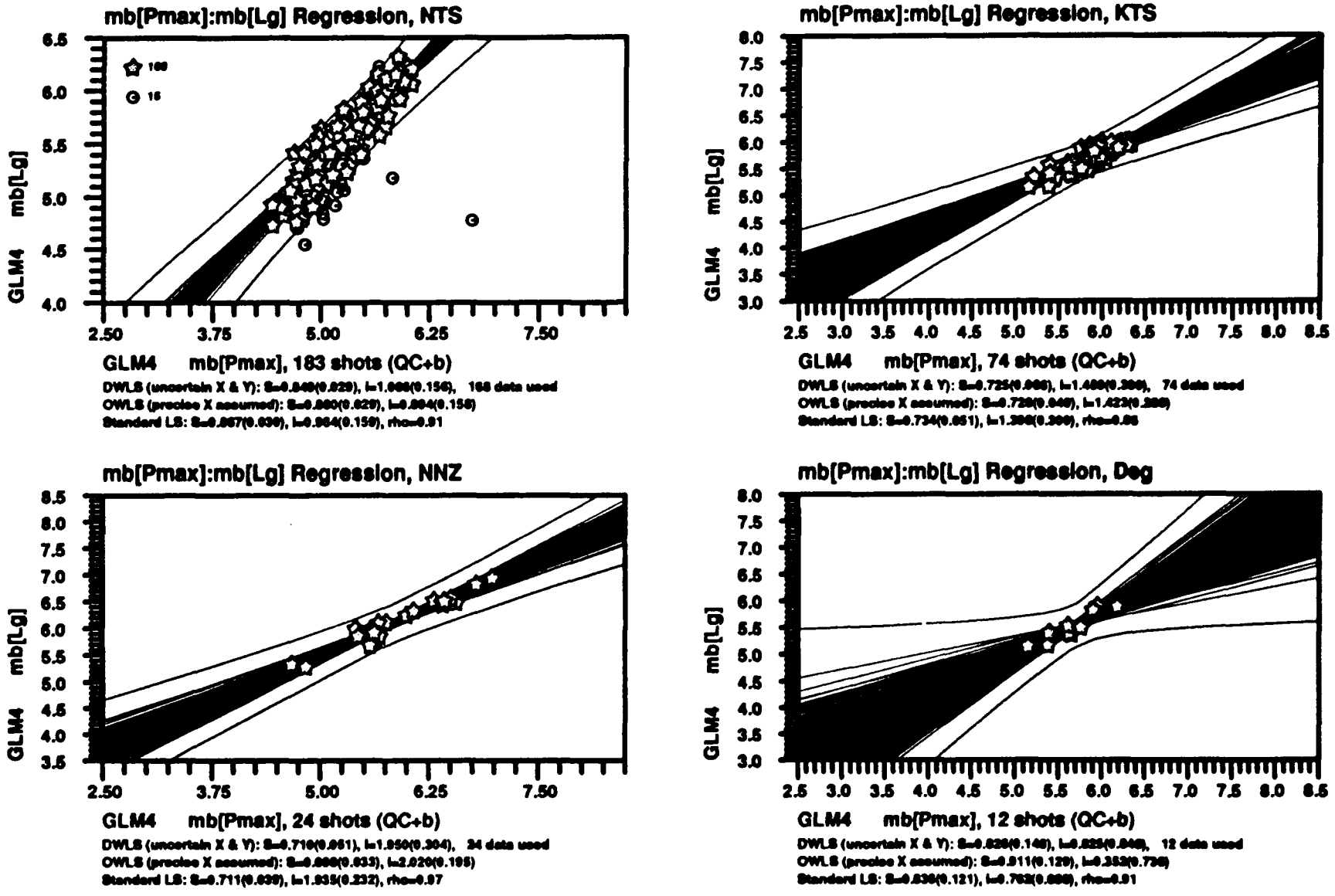

Figure 23. Regressing $m_b(L_g)$ on $m_b(P_{max})$ with outliers excluded.

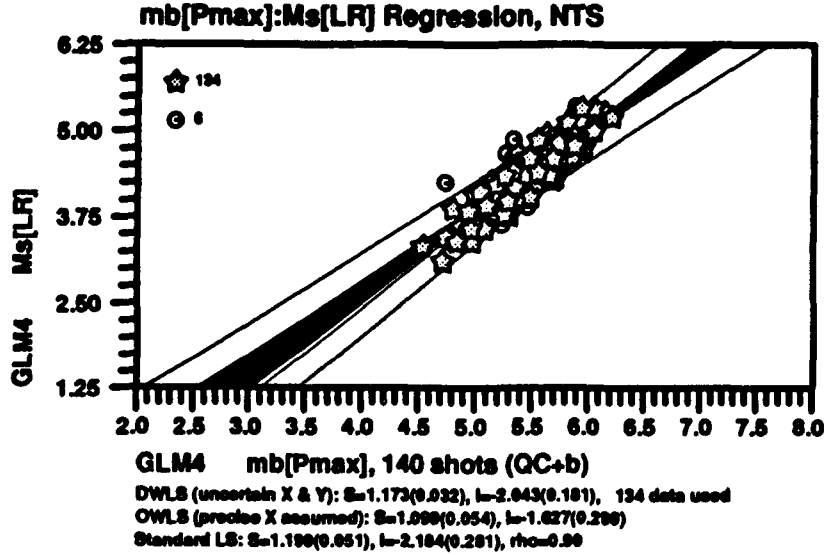

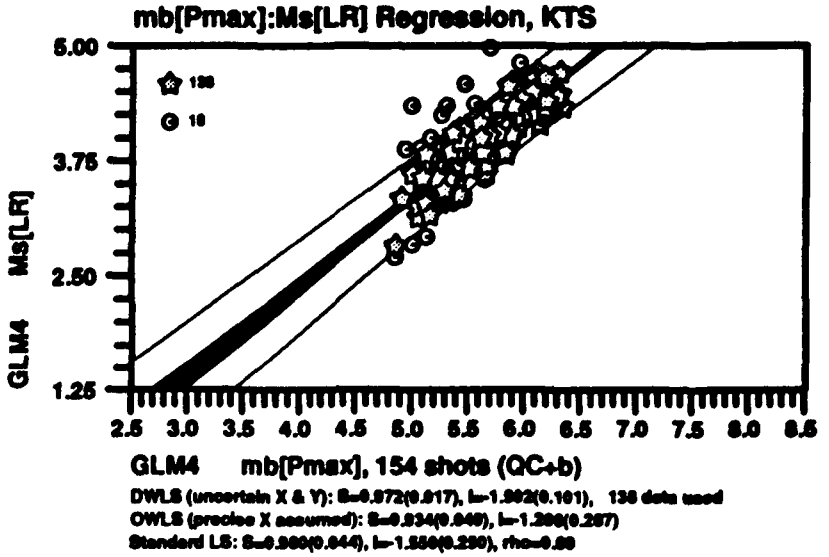

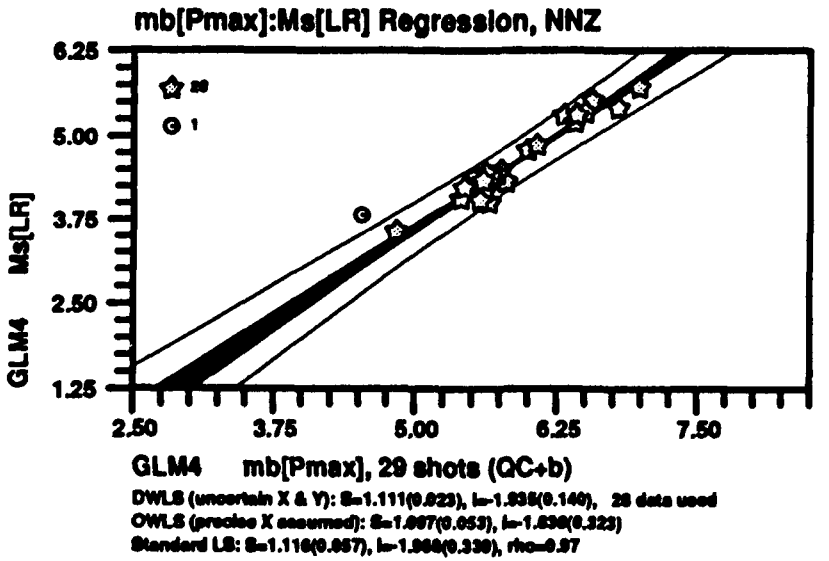

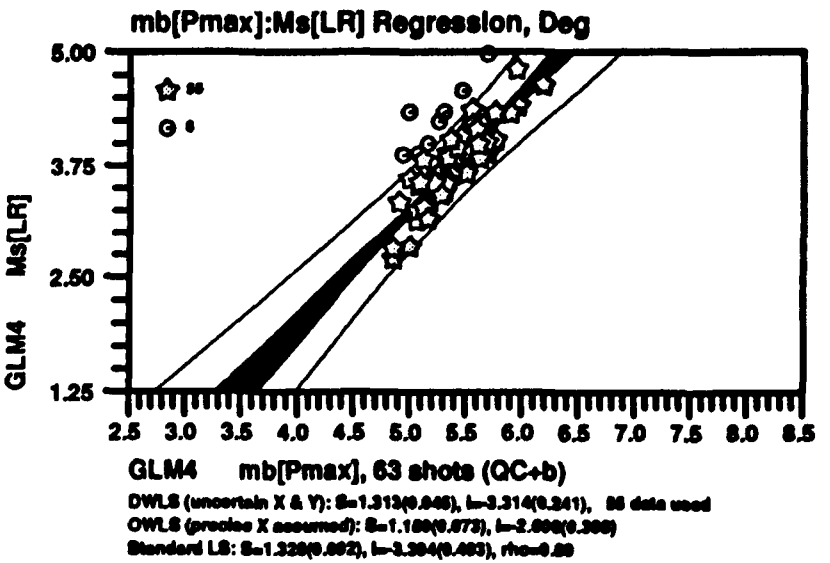

Figure 24. Regressing M_S on $m_b(P_{max})$ with outliers excluded.

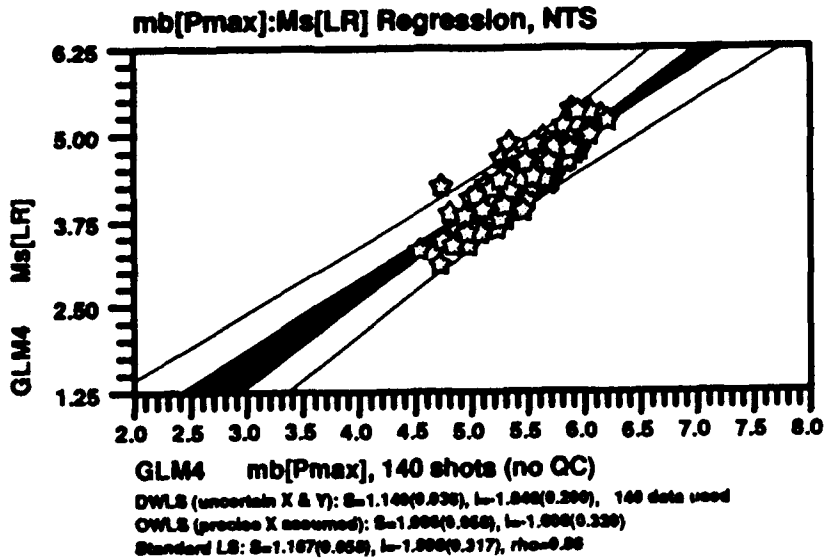

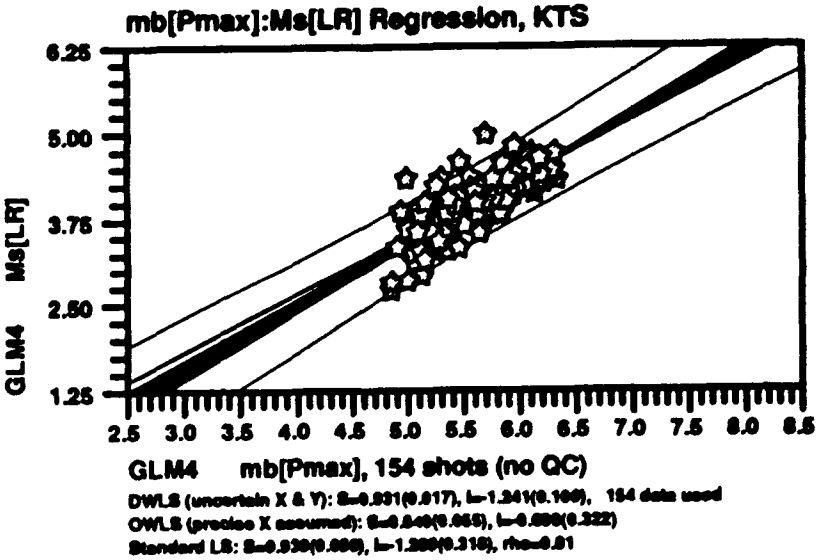

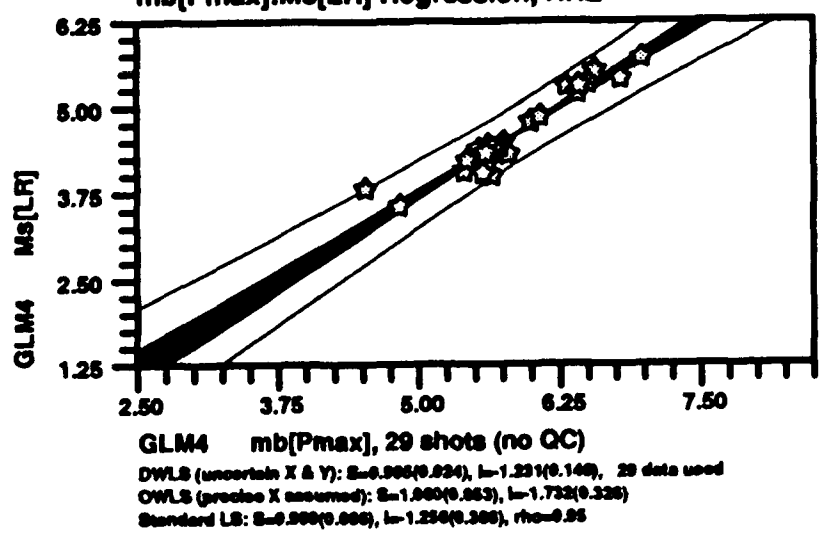

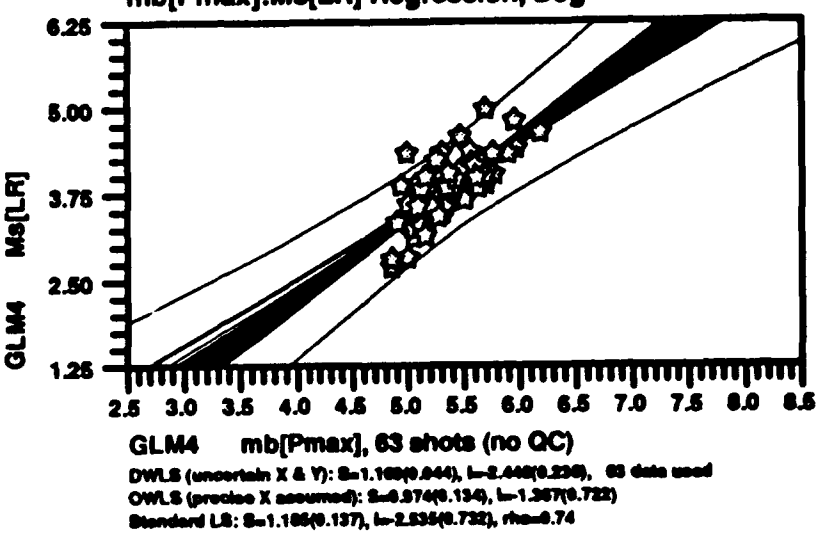

Figure 25. Regressing M_S on $m_b(P_{max})$ with outliers retained.

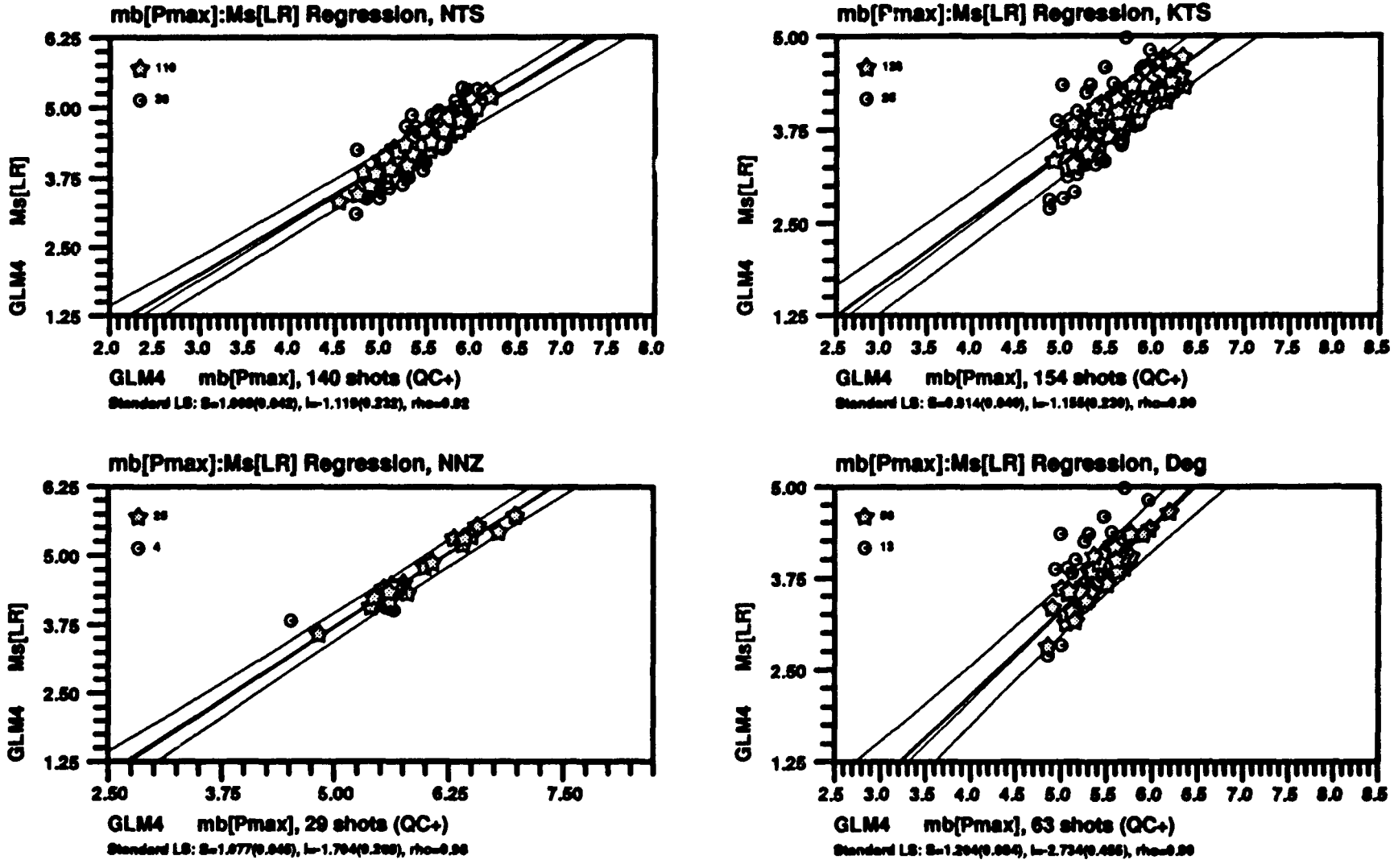

Figure 26. Regressing M_S on $m_b(P_{max})$ with the standard least squares method.

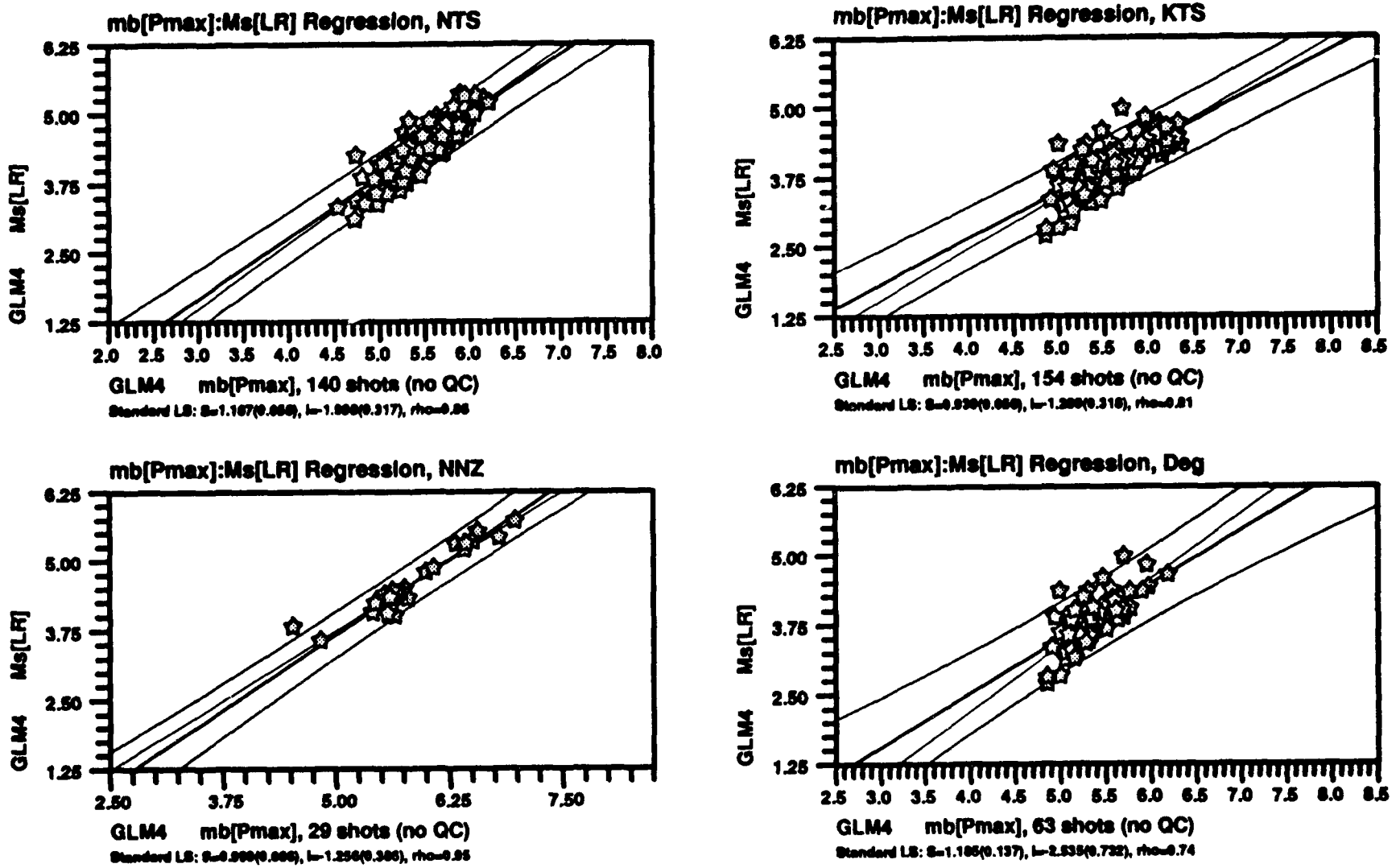

Figure 27. Regressing M_S on $m_b(P_{max})$ with the standard least squares method and outliers retained.

VI. CONCLUSION AND RECOMMENDATIONS

The most important goal of this contract was to provide AFTAC/TT a huge explosion database of quality measurements with which AFTAC/TTR can conduct various follow on research and analysis. This goal has been accomplished under Task 1 (*cf.* Baumstark and Wagner, 1994). Furthermore, the delivered product also includes all the digital waveforms, fully documented and converted to CSS 3.0 format, which were used in making the measurements. The measurements made by Teledyne analysts can be verified or revised by bringing up the waveforms with an interactive display routine "geotool" developed by Teledyne and SAIC (Henson and Coyne, 1993). The detailed description of the measured parameters as well as the procedure used in making those measurements can be found in an accompany final report (Baumstark and Wagner, 1994).

To fully digest the huge explosion dataset would require a significant amount of time and labor which are certainly beyond the level of efforts allocated to this Task 3. The results presented in this report should be regarded as preliminary in nature with many topics remaining to be explored. That is, this part of the final report is a pilot study which only serves to illustrate how these carefully measured parameters can be used in some magnitude:yield analysis with the statistical software package developed at Teledyne. In Sections II and III, we presented the methodlogies used in determining the station magnitudes and the event magnitudes, respectively. The GLM algorithm not only produces the network-averaged magnitudes, which are optimal in the maximum-likelihood sense, it also generates two types of by-products: the station corrections and the path corrections. For explosions clustered in a region of the "same" geological / geophysical characteristics, the residuals (after the mean event magnitude and the station effect have been removed) typically exhibit some coherent pattern reflecting the propagation effect (*cf.* Jih and Wagner, 1991, for detailed discussion). The GLM algorithm has been upgraded during the past several years to include the path terms in the joint inversion. This GLM routine has been fully tested and it has been applied to all time-domain magnitudes used in this study, although much attention was paid to m_b for illustrative purpose as explained before. The explosion data set established under this contract has a very broad spatial coverage. As a result, the m_b station corrections derived by GLM routine appear to match with the (receivers') tectonics fairly well. These station corrections have been used in computing the event magnitudes of those isolated explosions that were not included in the GLM inversion. Thus the event magnitudes of PNEs and explosions in Amchitka, South Novaya Zemlya, Colorado, and Mississippi are "sub-optimal" in the sense that only receiver effects were removed, but not the path effects. Another non-standard algorithm we used in this study is a magnitude-magnitude regression routine which accounts for the uncertainties in the event magnitudes through Monte-Carlo resampling. A feature of automatic outlier rejection has been added to this routine. This feature should be used carefully, since "outliers" of the magnitude-magnitude regression (or magnitude-yield regression) may sometimes be diagnostic of the peculiar testing practice or the emplacement media.

The m_b results presented in this report are very consistent with those of our previous study (*cf.* Jih *et al.*, 1993) using essentially the same technologies and different explosion dataset. In comparing m_b, M_S, and $m_b(L_g)$, we observe some inconsistency in the scaling relationships. The systematic bias in the L_g scale can be removed either by raising Nuttli's path attenuation coefficients (which were derived with the coda Q method), or by revising the absolute L_g excitation level for Novaya Zemlya

explosions. Whichever approach adopted, there would be some question about whether the L_g scale is really as transportable as Nuttli suggested. The good results of applying Nuttli's NTS L_g yield formula to Semipalatinsk explosions may turn out to be a special case rather than a general rule. If the L_g scale suitable for Iranian Plateau were used in computing the $m_b(L_g)$ of Novaya Zemlya explosions, then the magnitude-yield relationships based on m_b, M_S, and L_g would be consistent.

Under this contract, the Moscow-Prague formula has been used in computing M_S when Δ is larger than 25 degrees. Recently Herak and Herak (1993) suggest that the amplitude of 20-second Rayleigh wave should decrease as $\Delta^{-1.094}$, instead of $\Delta^{-1.66}$ as in the Moscow-Prague formula. Herak's new formula is very similar to that of von Seggern (1977). It would also be more consistent with the formula Nuttli and Kim (1975) suggested for $10° < \Delta < 25°$.

VII. ACKNOWLEDGEMENTS

All the raw station magnitudes used in this study are based on the measurements (amplitudes, periods, group velocity *etc.*) furnished by Task 1 assignees, Richard R. Baumstark and Robert A. Wagner, during the original contract period (January 1991 - November 1993) at Teledyne Geotech Alexandria Laboratory [TGAL] under Wilmer Rivers' management. Earlier TGAL's research on magnitude determination conducted by Robert R. Blandford (now at AFTAC/CSS) and Robert H. Shumway (now at Univ. of California) in early eighties laid the cornerstones for major GLM [General Linear Models] algorithms currently in use. The GLM routine and other statistical software tools used in this study were upgraded or developed at TGAL under several research contracts issued by Advanced Research Projects Agency [ARPA/NMRO] and Phillips Laboratory [PL/GPE] during the past eight years.

This project was sponsored and monitored by AFTAC/TT under contract F08606-91-C-0005 (AFTAC PA T/0122) through November 1993. The results presented in this report were obtained during the extended contract period (January 1994 - March 1994) with partial financial support from Teledyne Corporate after the original contract expired and TGAL relocated to Arlington, Virginia, in December 1993. The views and conclusions contained in this report are those of the authors and should not be interpreted as representing the official policies, either expressed or implied, of the United States Air Force or the U.S. Government.

VIII. REFERENCES

Bache, T. C. (1982). Estimating the yield of underground nuclear explosions, *Bull. Seism. Soc. Am.*, **72-6**, S131-168.

Baumstark, R. R. and R. A. Wagner (1994). Measurements and statistics of underground nuclear explosions, *Report TBE-4617-1/TGAL-94-01*, Teledyne Brown Engineering, Arlington, VA.

Bennett, T. J., J. F. Scheimer, A. K. Campanella, and J. R. Murphy (1990). Regional discrimination research and methodology implementation: analyses of CDSN and Soviet IRIS data, *Report GL-TR-90-0194*, Geophysics Laboratory, Hanscom AFB, MA.

Blandford, R. R., and R. H. Shumway (1982). Magnitude:yield for nuclear explosions in granite at the Nevada Test Site and Algeria: joint determination with station effects and with data containing clipped and low-amplitude signals, *Report VSC-TR-82-12*, Teledyne Geotech, Alexandria, Virginia.

Blandford, R. R., R. H. Shumway, R. Wagner, and K. L. McLaughlin (1983). Magnitude:yield for nuclear explosions at several test sites with allowance for effects of truncated data, amplitude correlation between events within test sites, absorption, and pP, *Report TGAL-TR-83-06*, Teledyne Geotech, Alexandria, Virginia.

Bocharov, V. S., S. A. Zelentsoz, and V. Mikhailov (1989). Characteristics of 96 underground nuclear explosions at the Semipalatinsk test site, *Atomic Energy*, **67**, 210-214

Bonham, S., W. J. Dempsey, J. Rachlin (1980). Geologic environment of the Semipalatinsk area, U.S.S.R. *(Preliminary Report)*, U.S. Geological Survey, Reston, VA 22092.

Booth, D. C., P. D. Marshall, and J. B. Young (1974). Long and short period *P*–wave amplitudes from earthquakes in the range 0°-114°, *Geophys. J.*, **39**, 523-537.

Burdick, L. J. (1981). The changing results on attenuation of *P* waves, in *"A technical assessment of seismic yield estimation," Report DARPA-NMR-81-01, Appendix*, DARPA, Arlington, VA.

Butler, R. (1981). Estimation of body wave magnitudes and site specific propagation effects, in *"A technical assessment of seismic yield estimation," Report DARPA-NMR-81-01, Appendix*, DARPA, Arlington, VA.

Butler, R. and L. Ruff (1980). Teleseismic short-period amplitudes: source and receiver variations, *Bull. Seism. Soc. Am.*, **70-3**, 831-850.

DARPA (1981). A technical assessment of seismic yield estimation, *Report DARPA-NMR-81-02*, DARPA/NMRO, Arlington, VA.

Day, S. M., N. Rimer, T. G. Barker, E. J. Halda, and B. Shkoller (1986). Numerical study of depth of burial effects on the seismic signature of underground explosions, *Report DNA-TR-86-114 (=SSS-R-86-7398)*, S-cubed, La Jolla, CA.

Dempster, A. P., N. M. Laird, and D. B. Rubin (1977). Maximum:likelihood estimation from incomplete data via the EM algorithm, *J. Roy. Statist. Soc. B.*, **39**, 1-38.

Der, Z. A., R. H. Shumway, A. C. Lees, and E. Smart (1985). Multichannel deconvolution of *P* waves at seismic arrays, *Report TGAL-85-04*, Teledyne Geotech, Alexandria, VA.

Douglas, A. (1966). A special purpose least squares programme, *AWRE Report No. O-54/66*, HMSO,

London, UK.

Douglas, A. and P. D. Marshall (1983). Comments on "Teleseismic short-period amplitudes: source and receiver variations" by R. Butler and L. Ruff, ul Bull. Seism. Soc. Am., **73**, 667-671.

Evernden, J. F. and D. M. Clark (1970). Study of teleseismic *P*. II. Amplitude data, *Phys. Earth Planet. Interiors*, **4**, 24-31.

Evernden, J. F. and G. E. Marsh (1987). Yields of U.S. and Soviet nuclear tests, *Physics Today*, **8-1**, 37-44.

Fisher, R. A. and F. Yates (1963). *Statistical Tables for Biological, Agricultural, and Medical Research*, Hafner Publishing Co., New York.

Gutenberg, B. (1945). Amplitudes of surface waves and magnitude of shallow earthquakes, *Bull. Seism. Soc. Am.*, **35**, 3-12.

Gutenberg, B. and C. F. Richter (1956). Magnitude and energy of earthquakes, *Annali Geofis*, **9**, 1-15.

Henson, I. and J. Coyne (1993). The geotool seismic analysis system, *Proceedings of the 15th ARPA/PL Seismic Research Symposium, (8-10 Sept 1993, Vail, Colorado)* (Eds J. Lewkowicz and J. McPhetres), *Report PL-TR-93-2160*, Phillips Laboratory, Hanscom Air Force Base, MA.

Herak, M. and D. Herak (1993). Distance dependence of M_S and calibrating function for 20-second Rayleigh waves, *Bull. Seism. Soc. Am.*, **83**, 1881-1892.

Herrmann, R. B. (1980). *Q* estimates using the coda of local earthquakes, *Bull. Seism. Soc. Am.*, **70**, 447-468.

Israelson, H. (1992). L_g as a yield estimator in Eurasia, *Final Report PL-TR-92-2117(I)*, Phillips Laboratory, Hanscom Air Force Base, MA.

Jih, R.-S. (1992). Simultaneous inversion of explosion size and path attenuation coefficient with crustal phases. *TGAL-92-11, Semi-annual Technical Report #2*, Teledyne Geotech, Alexandria, VA.

Jih, R.-S. (1993). Statistical characterization of rugged propagation paths with application to Rg scattering study, *TGAL-93-07, Semi-annual Technical Report #4*, Teledyne Geotech, Alexandria, VA.

Jih, R.-S. and C. S. Lynnes (1993). Studies of regional phase propagation in Eurasia. *Final Report PL-TR-93-2003 (=TGAL-93-01)*, Phillips Laboratory, Hanscom Air Force Base, MA.

Jih, R.-S. and R. A. Wagner (1991). Recent methodological developments in magnitude determination and yield estimation with applications to Semipalatinsk explosions, *PL-TR-91-2212(I) (=TGAL-91-05), Final Report*, Phillips Laboratory, Hanscom Air Force Base, MA.

Jih, R.-S. and R. A. Wagner (1992a). Path-corrected body-wave magnitudes and yield estimates of Novaya Zemlya explosions, *PL-TR-92-2042 (=TGAL-91-09), Scientific Report #1*, Phillips Laboratory, Hanscom Air Force Base, MA **(ADA251240)**.

Jih, R.-S. and R. A. Wagner (1992b). Path-corrected body-wave magnitudes and yield estimates of Semipalatinsk explosions, *TGAL-92-05, Semi-annual Technical Report #1*, Teledyne Geotech, Alexandria, VA.

Jih, R.-S., R. A. Wagner, and R. H. Shumway (1993). Statistical study of Soviet nuclear explosions: data, results, and software tools, *TGAL-93-05, Final Report*, Teledyne Geotech, Alexandria, VA.

Jih, R.-S. and R. H. Shumway (1989). Iterative network magnitude estimation and uncertainty assessment with noisy and clipped data, *Bull. Seism. Soc. Am.*, **79**, 1122-1141.

Leith, W. (1987a). Geology of NRDC seismic stations sites in Eastern Kazakhstan, USSR. *Open-File Report 87-597*, U.S. Geological Survey, Reston, VA 22092.

Leith, W. (1987b). Tectonics of Eastern Kazakhstan and implications for seismic source studies in the Shagan River area, *Proceedings of DARPA/FGL Annual Seismic Research Review*, 34-37, 15-18 June, 1987, Nantucket, MA.

Leith, W. and J. Unger (1989). Three-dimensional geological modeling of the Shagan River nuclear test site, paper presented at *DARPA/AFTAC Annual Seismic Research Review*, Patrick AFB, FL.

Lilwall, R. C. and J. M. Neary (1985). Redetermination of earthquake body-wave magnitudes using ISC Bulletin data, *AWRE Report No. O-21/85*, HMSO, London, UK.

Lilwall, R. C., P. D. Marshall, and D. W. Rivers (1988). Body wave magnitudes of some underground nuclear explosions at the Nevada (USA) and Shagan River (USSR) Test Sites, *AWE Report O-15/88*, HMSO, London, UK.

Lynnes, C. S. and T. Lay (1990). Effects of lateral heterogeneity under the Nevada Test Site on short-period *P* wave amplitudes and travel times, *Pure and Applied Geophysics*, **132**, 245-267.

Marshall, P. D. and D. L. Springer (1976). Is the velocity of P_n an indicator of Q? *Nature*, **264**, 531-533.

Marshall, P. D., D. L. Springer, and H. C. Rodean (1979). Magnitude corrections for attenuation in the upper mantle, *Geophys. J. R. astr. Soc.*, **57**, 609-638.

Marshall, P. D., T. C. Bache, and R. C. Lilwall, R. C. (1984). Body wave magnitudes and locations of Soviet underground explosions at the Semipalatinsk Test Site, *UK/AWE Report O-16/84*, HMSO, London, UK.

Marshall, P. D., D. Porter, and P. Peachell (1992). Analysis of seismograms from nuclear explosions of known yield at Degelen Mountain and Konystan in East Kazakhstan, USSR, *UK/AWE Report No. O-2/92*, HMSO, London, UK.

McLaughlin, K. L., I. N. Gupta, and R. A. Wagner (1985). Magnitude determination of cratering and non-cratering nuclear explosions, *Report TGAL-85-03*, Teledyne Geotech, Alexandria Laboratory, Alexandria, VA.

Murphy, J. R., B. W. Barker, and A. O'Donnell (1989). Network-averaged teleseismic *P*-wave spectra for underground explosions. Part I - Definitions and Examples, *Bull. Seism. Soc. Am.*, **79-1**, 141-155.

North, R. G. (1977). Station magnitude bias: its determination, causes, and effects, *ESD-TR-77-85*, Lincoln Laboratory, Lexington, Massachussetts.

Nuttli, O. W. (1973). Seismic wave attenuation and magnitude relations for eastern North America, *J. Geophys. Res.*, **78**, 876-885.

Nuttli, O. W. (1980). The excitation and attenuation of seismic crustal phases in Iran, *Bull. Seism. Soc. Am.*, **70**, 469-485.

Nuttli, O. W. (1981). On the attenuation of L_g waves in Western and Central Asia and their use as a

discriminant between earthquakes and explosions, *Bull. Seism. Soc. Am.*, 71, 249-261.

Nuttli, O. W. (1986a). Yield estimates of Nevada Test Site explosions obtained from seismic L_g waves, *J. Geophys. Res.*, 91, 2137-2151.

Nuttli, O. W. (1986b). L_g magnitudes of selected East Kazakhstan underground explosions, *Bull. Seism. Soc. Am.*, 76, 1241-1251.

Nuttli, O. W. (1987). L_g magnitudes of Degelen, East Kazakhstan, underground explosions, *Bull. Seism. Soc. Am.*, 77, 679-681.

Nuttli, O. W. (1988). L_g magnitudes and yield estimates for underground Novaya Zemlya nuclear explosions, *Bull. Seism. Soc. Am.*, 78, 873-884.

Nuttli, O. W. and S. G. Kim (1975). Surface-wave magnitudes of Eurasian earthquakes and explosions, *Bull. Seism. Soc. Am.*, 65, 693-709.

Patton, H. J. (1988). Application of Nuttli's method to estimate yield of Nevada Test Site explosions recorded on Lawrence Livermore National Laboratory's digital seismic system, *Bull. Seism. Soc. Am.*, 78, 1759-1772.

Richards, P. G., L. R. Sykes, and W. Tedards (1990). Evidence for reduced uncertainty in estimates of Soviet explosion yields, and for an increase in estimates of explosion detection capability (abstract), *EOS, Trans. A.G.U.*, 71-43, 1477.

Ringdal, F. (1976). Maximum likelihood estimation of seismic magnitude, *Bull. Seism. Soc. Am.*, 66, 789-802.

Ringdal, F. (1986). Study of magnitudes, seismicity, and earthquake detectability using a global network, *Bull. Seism. Soc. Am.*, 76, 1641-1659.

Ringdal, F. (1990). NORSAR detection and yield estimation studies, in *Proceedings of the 12th DARPA/GL Seismic Research Symposium, 18-20 Sept 1990, Key West, FL*, (Eds J. Lewkowicz and J. McPhetres), *Report GL-TR-90-0212*, Geophysics Laboratory, Hanscom Air Force Base, MA.

Ringdal, F. (1990). *P*-wave focusing effects at NORSAR for Novaya Zemlya explosions, in *NORSAR Basic Seismological Research, 1 Oct 1989 - 30 Sept 1990*, (S. Mykkeltveit, ed.), *Report GL-TR-90-0330*, Geophysics Laboratory, Hanscom AFB, MA.

Ringdal, F. and B. K. Hokland (1987). Magnitude of large Semipalatinsk explosions using *P* coda and L_g measurements at NORSAR, Semiannual Technical Summary, 1 April 1987 - 30 Sept 1987, *NORSAR Scientific Report No. 1-87/88*, NTNF/NORSAR, Kjeller, Norway.

Ringdal, F. and J. Fyen (1988). Comparative analysis of NORSAR and Grafenberg L_g magnitudes for Shagan River explosions, Semiannual Technical Summary, 1 Apr 1988 - 30 Sept 1988, *NORSAR Scientific Report No.1-88/89*, NTNF/NORSAR, Kjeller, Norway.

Ringdal, F. and J. Fyen (1991). *RMS* L_g analysis of Novaya Zemlya explosion recordings, Semiannual Technical Summary, 1 Oct 1990 - 31 Mar 1991, *NORSAR Scientific Report No.2-90/91*, NTNF/NORSAR, Kjeller, Norway.

Ringdal, F., P. D. Marshall, and R. Alewine (1992). Seismic yield determination of Soviet underground nuclear explosions at the Shagan River Test Site, *Geophys. J. Int.*, 109, 65-77.

Rodean, H. C. (1979), ISC events from 1964 to 1976 at and near the nuclear testing ground in eastern Kazakhstan, *UCRL-52856*, Lawrence Livermore Laboratory, University of California, CA.

Solomon, S. and M. N. Toksoz (1970). Lateral variation of attenuation of *P* and *S* waves beneath the United States, *Bull. Seism. Soc. Am.*, **60**, 819-838.

Thurber, C. H. and H. R. Quin (1992). Seismic event location at regional and teleseismic distances, *Final Report PL-TR-92-2304*, Phillips Laboratory, Hanscom Air Force Base, MA.

U.S. Congress/Office of Technology Assessment (1988). Seismic verification of nuclear testing treaties, *OTA-ISC-361*, U.S. Government Printing Office, Washington, D.C.

U.S. Department of Energy (1990). Announced United States nuclear tests: July 1945 through December 1989, *DOE/NV-209 (Rev. 10), April 1990*, Office of External Affairs, Nevada Operations Office.

Veith, K. F. and G. E. Clawson (1972). Magnitude from short-period *P*-wave data, *Bull. Seism. Soc. Am.*, **62**, 435-452.

Vergino, E. S. (1989). Soviet test yields, *EOS*, *Trans. A.G.U.*, Nov 28, 1989.

Vergino, E. S., and R. W. Mensing (1990). Yield estimation using regional m_b (P_n), *Bull. Seism. Soc. Amer.*, **80**, 656-674.

von Seggern, D. H. (1973). Joint magnitude determination and analysis of variance for explosion magnitude estimates, *Bull. Seism. Soc. Amer.*, **63**, 827-845.

von Seggern, D. H. (1977). Amplitude distance relation for 20-second Rayleigh waves, *Bull. Seism. Soc. Amer.*, **67**, 405-511.

von Seggern, D. H. and D. W. Rivers (1978). Comments on the use of truncated distribution theory for improved magnitude estimation, *Bull. Seism. Soc. Amer.*, **68**, 1543-1546.

APPENDIX A: PREREQUISITE MATHEMATICS FOR MAXIMUM-LIKELIHOOD ESTIMATOR

Proposition 1. Let X be a Gaussian random variable with the probability density function [p.d.f.] g and the cumulative distribution function [c.d.f] G, respectively. Its mean and variance are denoted by μ and σ^2, respectively. Then

$$\int_{-\infty}^{a} xg(x)dx = \mu G(a) - \sigma^2 g(a).$$

Proof.

$$\int_{-\infty}^{a} xg(x)dx = \frac{1}{\sigma\sqrt{2\pi}} \int_{-\infty}^{a} x \exp(-\frac{(x-\mu)^2}{2\sigma^2})dx$$

$$= \frac{1}{\sigma\sqrt{2\pi}} \int_{-\infty}^{a} \mu \exp(-\frac{(x-\mu)^2}{2\sigma^2})dx + \frac{\sigma}{\sqrt{2\pi}} \int_{-\infty}^{a} \frac{(x-\mu)}{\sigma^2} \exp(-\frac{(x-\mu)^2}{2\sigma^2})dx$$

$$= \mu G(a) - \sigma^2 g(a).$$

In particular, when $a = \infty$, this integral gives the mean of X, namely, μ.

Proposition 2. Let X be a Gaussian random variable with mean μ and variance σ^2, then $E[\, X \mid X < a \,] = \mu - \sigma^2 g(a)/G(a)$.

Proof. Let Y be the random variable $X \mid_{X<a}$, then

$$P(\, Y < b \,) = P(\, X < b \mid X < a \,) = \frac{P(\, X < b \text{ and } X < a \,)}{P(\, X < a \,)}$$

which is 1 if $b > a$, and $G(b)/G(a)$ if $b \le a$. Therefore, the p.d.f. of Y is:

$$h(x) = 0 \quad \text{if} \quad x > a\,, \qquad h(x) = g(x)/G(a) \quad \text{if} \quad x < a,$$

and the expectation of Y is

$$E(Y) = \int_{-\infty}^{\infty} xh(x)dx = \int_{-\infty}^{a} xg(x)/G(a)dx$$

$$= \frac{\mu G(a) - \sigma^2 g(a)}{G(a)} \quad \text{(by Proposition 1)}$$

$$= \mu - \sigma^2 g(a)/G(a)\,.$$

Similarly, it can be shown that $E[\, X \mid X > a \,] = \mu + \sigma^2 g(a)/G(-a)$. Note that the conditional expectation $E[\, X \mid X > a \,]$ is the "best" guess of X under the constraint that one knows only that $X > a$.

In computing $E[\, X \mid X > a \,]$, it is generally more convenient to transform the random variable X into the standard random variable, $Z \sim N(0, 1)$, for which the p.d.f. and c.d.f. are typically available as system-furnished functions or part of some utility libraries in the public domain. Let Φ and ϕ be the c.d.f. and p.d.f. of Z, respectively, then $G(a) = \Phi[\frac{a-\mu}{\sigma}]$ and $g(a) = \sigma\, \phi[\frac{a-\mu}{\sigma}]$. Therefore,

$$E[X \mid X < a] = \mu - \sigma \phi\left(\frac{a-\mu}{\sigma}\right)/\Phi\left[\frac{a-\mu}{\sigma}\right].$$

APPENDIX B. LINEAR REGRESSION WITH CENSORED OBSERVATIONS

Consider the situation where the independent variable can be precisely measured, and that we want to regress the dependent variable as a linear function of the independent variable. This is an extension to the single-event network magnitude determination discussed in Section I.3.

Suppose we have a linear model of the common form:

$$Y = \alpha + \beta X + v \ ,$$

where X is the independent variable which has a precision relatively much better than that of Y, the dependent variable. α and β are the intercept and slope, respectively, to be determined, and v is an error term. v is assumed to be a Gaussian random variable with mean zero and standard deviation σ. Furthermore, assume that there are four types of data available:

[0] the observed measurement, Y, is known as y_0,

[1] Y is only known to be less than certain level,

[2] Y is only known to be larger than certain level, and

[3] Y is only known to lie between two bounds.

Type 3 data are not uncommon. The majority of Soviet yields recently published by Bocharov *et al.* (1989) and Vergino (1989) actually fall in this category.

Elegant maximum-likelihood theory can be derived for this model. Suppose there are n_0, n_1, n_2, and n_3 measurements for each type, respectively. The conditional likelihood function of the censored observations (y_0, t_1, t_2, t_3) given the intercept α, slope β, and σ is

$$L\ (\ y_0, t_1, t_2, t_3 \mid \alpha, \beta, \sigma\ ) = \prod_{j=1}^{n_0} P(\ Y_j = y_{0j} \mid \alpha, \beta, \sigma\ ) \cdot \prod_{j=1}^{n_1} P(\ Y_j < t_{1j} \mid \alpha, \beta, \sigma\ ) \cdot$$

$$\prod_{j=1}^{n_2} P(\ Y_j > t_{2j} \mid \alpha, \beta, \sigma\ ) \cdot \prod_{j=1}^{n_3} P(\ t_{aj} < Y_j < t_{bj} \mid \alpha, \beta, \sigma\ ) \ ,$$

and the log-likelihood function is

$$\ln L\ (\ y_0, t_1, t_2, t_3 \mid \alpha, \beta, \sigma\ ) = -\frac{n_0}{2} \ln(2\pi\sigma^2) - \frac{1}{2\sigma^2} \sum_{j=1}^{n_0} (y_{0j} - \alpha - \beta\, x_{0j})^2 +$$

$$\sum_{j=1}^{n_1} \ln \Phi(z_{1j}) + \sum_{j=1}^{n_2} \ln \Phi(-z_{2j}) + \sum_{j=1}^{n_3} \ln\ [\Phi(z_{bj}) - \Phi(z_{aj})] \ ,$$

where $z_i \equiv [y_i - \alpha - \beta t_i]/\sigma$; y_0, t_1, t_2, and t_3 are the vectors of the four data types.

Solving $\frac{\partial \ln L}{\partial \sigma} \equiv 0$ implies immediately that the $\hat{\sigma}$, the optimal estimate of σ, must satisfy the following necessary condition:

$$\sigma^2 = \frac{\sum_{j=1}^{n_0}(y_{0j} - \alpha - \beta x_{0j})^2}{n_0 + \sum_{j=1}^{n_1}\frac{\phi(z_{1j})}{\Phi(z_{1j})}z_{1j} - \sum_{j=1}^{n_2}\frac{\phi(z_{2j})}{\Phi(-z_{2j})}z_{2j} + \sum_{j=1}^{n_3}\frac{\phi(z_{bj})z_{bj} - \phi(z_{aj})z_{aj}}{\Phi(z_{bj}) - \Phi(z_{aj})}} \quad .$$

Solving $\frac{\partial \ln L}{\partial \alpha} = 0$ implies that the sum of the "refined residuals" should be zero. Solving $\frac{\partial \ln L}{\partial \beta} = 0$ implies that the vector of refined residuals should be orthogonal to the vectors of means. It follows that the optimal estimate of α and β can be obtained by the "standard least squares" inversion with the censored data all replaced by their conditional expectations, *i.e.*, the "refined observations." Thus σ can be solved iteratively with [6] along with α and β using the EM algorithm. In the non-censored case, this *"domle2"* code gives results identical to those derived by the standard least squares.

APPENDIX C: EMILS EVENT MAGNITUDES

Table C. EMILS Event Magnitudes[1]

Event	Site	P_{max}	P_b	P_a	P_n	L_g	M_S
US651029	Alaska	5.90±0.06	5.54±0.06	5.20±0.07	±___	±___	5.80±0.13
US691002	Alaska	6.55±0.06	6.27±0.06	6.04±0.06	±___	±___	5.57±0.05
US711106	Alaska	6.86±0.09	6.61±0.07	6.40±0.08	±___	±___	6.17±0.05
US631026	Other	5.32±0.21	5.13±0.45	5.29±0.53	4.24±0.53	4.83±0.00	4.30±0.03
US641022	Other	4.62±0.00	4.34±0.00	4.30±0.00	4.06±0.26	±___	4.60±0.00
US671210	Other	5.09±0.07	4.42±0.22	4.02±0.41	±___	±___	±___
US690910	Other	4.78±0.00	4.13±0.00	4.47±0.00	±___	±___	±___
US730517	Other	5.13±0.14	4.92±0.15	4.47±0.20	±___	±___	4.35±0.12
NZ730927	SNZ	5.83±0.06	5.61±0.06	5.41±0.07	5.77±0.17	5.82±0.09	5.70±0.19
NZ731027	SNZ	7.14±0.10	6.97±0.12	6.77±0.14	±___	6.87±0.06	6.00±0.06
NZ741102	SNZ	6.81±0.10	6.64±0.12	6.55±0.14	±___	6.96±0.06	5.60±0.05
NZ751018	SNZ	6.76±0.08	6.53±0.08	6.23±0.10	±___	6.74±0.03	5.44±0.06
PN660930	PNE	5.01±0.09	4.83±0.09	4.72±0.12	±___	4.40±0.00	3.39±0.34
PN671006	PNE	4.74±0.11	4.26±0.16	3.79±0.25	±___	±___	±___
PN680521	PNE	5.36±0.07	5.16±0.09	5.04±0.10	±___	±___	4.63±0.75
PN690902	PNE	4.87±0.09	4.49±0.10	4.14±0.11	4.90±0.19	±___	±___
PN690908	PNE	4.94±0.19	4.20±0.10	4.04±0.03	4.99±0.18	±___	±___
PN690926	PNE	5.62±0.09	5.31±0.09	4.97±0.14	5.86±0.00	±___	3.84±0.26
PN691206	PNE	±___	±___	±___	±___	±___	±___
PN700625	PNE	4.87±0.17	4.58±0.18	4.61±0.21	5.76±0.47	4.76±0.11	±___
PN701212	PNE	6.09±0.11	5.78±0.09	5.49±0.08	±___	±___	4.45±0.17
PN701223	PNE	6.26±0.10	5.94±0.10	5.56±0.10	±___	±___	4.47±0.15
PN710323	PNE	5.72±0.10	5.54±0.08	5.31±0.09	6.33±0.00	6.25±0.24	4.14±0.14
PN710702	PNE	4.51±0.34	4.27±0.30	4.22±0.42	4.74±0.11	±___	±___
PN710710	PNE	5.11±0.12	4.75±0.12	4.32±0.14	5.22±0.28	4.95±0.15	±___
PN710919	PNE	4.40±0.14	4.20±0.13	4.04±0.11	4.89±0.16	4.17±0.10	±___
PN711004	PNE	4.55±0.10	4.22±0.11	4.31±0.10	5.60±0.26	5.44±1.15	±___
PN711022	PNE	5.37±0.11	4.99±0.09	4.92±0.12	5.98±0.00	5.22±0.01	±___
PN720411	PNE	4.79±0.11	4.57±0.10	4.43±0.12	±___	4.46±0.00	±___
PN720709	PNE	4.48±0.15	4.38±0.18	4.35±0.30	4.54±0.49	4.53±0.07	3.43±0.10
PN720820	PNE	5.67±0.08	5.30±0.07	5.05±0.08	5.50±0.00	5.85±0.10	3.56±0.12
PN720904	PNE	5.10±0.00	4.99±0.00	4.80±0.00	4.77±0.00	4.84±0.00	±___
PN720921	PNE	4.96±0.09	4.44±0.10	4.49±0.08	4.43±0.00	4.94±0.08	±___
PN721003	PNE	5.65±0.09	5.24±0.09	4.88±0.13	5.26±0.00	5.92±0.09	±___
PN721124a	PNE	4.74±0.13	4.15±0.23	4.52±0.17	4.67±0.15	±___	±___
PN721124b	PNE	5.11±0.08	4.78±0.10	4.62±0.13	4.44±0.00	5.32±0.14	±___
PN730815	PNE	5.30±0.08	5.06±0.06	4.74±0.11	±___	4.83±0.17	3.30±0.35
PN730828	PNE	5.09±0.09	4.85±0.07	4.53±0.23	±___	±___	±___

1) from Baumstark and Wagner (1994).

Table C. EMILS Event Magnitudes[1] (Cont)							
Event	Site	P_{max}	P_b	P_a	P_n	L_g	M_S
PN730919	PNE	4.97±0.11	4.69±0.10	4.47±0.10	5.63±0.00	4.95±0.48	2.59±0.00
PN730930	PNE	5.31±0.08	4.99±0.09	4.70±0.13	5.71±0.00	5.15±0.04	3.54±0.31
PN731026	PNE	4.81±0.18	4.51±0.22	4.38±0.21	5.19±0.00	4.67±0.00	±___
PN740708	PNE	4.66±0.16	3.91±0.44	4.11±0.37	4.75±0.00	4.33±0.00	±___
PN740814	PNE	5.52±0.06	5.16±0.06	4.86±0.09	5.36±0.00	5.04±0.41	±___
PN740829	PNE	4.99±0.08	4.69±0.08	4.58±0.14	5.18±0.31	4.92±0.67	3.76±0.00
PN741002	PNE	4.59±0.21	3.81±0.18	3.91±0.03	___±___	___±___	___±___
PN750812	PNE	4.98±0.11	4.62±0.12	4.18±0.29	___±___	___±___	___±___
PN750929	PNE	5.07±0.11	4.66±0.13	4.45±0.11	___±___	___±___	___±___
PN761105	PNE	5.12±0.06	4.83±0.10	4.42±0.11	___±___	___±___	3.33±0.35
PN770726	PNE	5.08±0.06	4.85±0.06	4.58±0.07	___±___	___±___	3.66±0.09
PN770810	PNE	4.94±0.09	4.69±0.06	4.43±0.12	3.96±0.00	___±___	3.18±0.13
PN770820	PNE	5.05±0.07	4.79±0.09	4.60±0.12	___±___	___±___	3.61±0.22
PN770910	PNE	4.94±0.06	4.66±0.10	4.41±0.13	___±___	___±___	2.96±0.22
PN780809	PNE	5.68±0.07	5.32±0.07	4.96±0.09	___±___	___±___	3.40±0.17
PN780824	PNE	5.28±0.11	4.89±0.10	4.53±0.15	___±___	___±___	3.49±0.13
PN780921	PNE	5.41±0.15	4.98±0.09	4.71±0.08	___±___	___±___	3.40±0.12
PN781007	PNE	5.06±0.11	4.81±0.13	4.48±0.16	___±___	___±___	___±___
PN781017	PNE	5.76±0.09	5.38±0.08	4.95±0.11	___±___	___±___	3.23±0.09
PN790812	PNE	5.00±0.09	4.68±0.08	4.03±0.30	___±___	___±___	3.29±0.13
PN790906	PNE	5.07±0.11	4.80±0.12	4.39±0.12	___±___	___±___	___±___
PN791004	PNE	5.57±0.11	5.33±0.10	4.97±0.15	___±___	5.02±0.01	3.58±0.11
PN791007	PNE	5.01±0.06	4.75±0.10	4.42±0.11	___±___	___±___	3.20±0.05
PN801008	PNE	5.18±0.12	4.83±0.14	4.59±0.14	4.33±0.00	___±___	3.14±0.15
PN801101	PNE	5.11±0.08	4.91±0.10	4.64±0.12	___±___	___±___	___±___
PN801210	PNE	4.67±0.16	4.33±0.21	4.46±0.22	___±___	___±___	3.51±0.11
PN810525	PNE	5.42±0.11	5.16±0.10	4.89±0.12	5.13±0.00	5.42±0.23	4.00±0.07
PN810902	PNE	___±___	___±___	___±___	4.80±0.00	4.06±0.00	___±___
PN810926a	PNE	5.22±0.17	4.77±0.11	4.50±0.12	5.02±0.00	___±___	3.62±0.03
PN810926b	PNE	5.26±0.10	4.85±0.10	4.67±0.11	5.61±0.00	4.87±0.00	3.44±0.06
PN811022	PNE	5.13±0.13	4.64±0.10	4.37±0.13	___±___	___±___	3.66±0.02
PN820730	PNE	4.87±0.11	4.72±0.10	4.46±0.10	___±___	___±___	2.91±0.27
PN820904	PNE	5.16±0.10	4.77±0.10	4.48±0.11	5.80±0.00	___±___	3.20±0.12
PN820925	PNE	5.40±0.15	4.98±0.13	4.58±0.13	___±___	___±___	3.75±0.03
PN821010	PNE	5.12±0.08	4.85±0.08	4.57±0.10	___±___	___±___	___±___
PN821016a	PNE	5.04±0.10	4.68±0.11	4.57±0.08	___±___	___±___	3.03±0.10
PN821016b	PNE	5.08±0.08	4.70±0.13	4.43±0.08	___±___	5.26±0.00	2.93±0.11
PN821016c	PNE	5.16±0.10	4.76±0.10	4.37±0.12	5.97±0.00	5.18±0.00	3.00±0.08
PN821016d	PNE	5.42±0.07	4.94±0.10	4.65±0.09	___±___	5.01±0.00	3.36±0.07
PN830710a	PNE	5.32±0.09	5.06±0.07	4.72±0.09	5.68±0.00	5.26±0.10	3.12±0.07
PN830710b	PNE	5.34±0.07	5.07±0.07	4.72±0.07	___±___	5.14±0.04	3.14±0.05

1) from Baumstark and Wagner (1994).

Table C. EMILS Event Magnitudes[1] (Cont)							
Event	Site	P_{max}	P_b	P_a	P_n	L_g	M_S
PN830710c	PNE	5.21±0.07	4.82±0.07	4.50±0.12	5.39±0.00	4.98±0.14	3.26±0.09
PN830924a	PNE	5.22±0.12	5.00±0.13	4.65±0.10	___±___	___±___	___±___
PN830924b	PNE	4.97±0.20	4.71±0.18	4.30±0.11	___±___	___±___	___±___
PN830924c	PNE	4.96±0.18	4.66±0.14	4 41±0.18	___±___	___±___	___±___
PN830924d	PNE	5.16±0.20	4.95±0.14	4.56±0.18	___±___	___±___	___±___
PN830924e	PNE	5.18±0.22	4.88±0.20	4.62±0.18	___±___	___±___	___±___
PN830924f	PNE	5.27±0.15	4.97±0.12	4.46±0.14	___±___	___±___	___±___
PN840721a	PNE	5.24±0.09	5.01±0.09	4.68±0.10	___±___	5.17±0.00	3.99±0.12
PN840721b	PNE	5.22±0.07	5.01±0.07	4.64±0.13	___±___	5.17±0.00	3.82±0.11
PN840721c	PNE	5.27±0.07	4.94±0.08	4.63±0.10	___±___	5.00±0.00	___±___
PN840811	PNE	5.08±0.14	4.91±0.08	4.36±0.12	6.29±0.00	5.30±0.49	2.31±0.15
PN840825	PNE	5.40±0.08	5.13±0.09	4.80±0.08	5.33±0.00	4.77±0.16	2.42±0.16
PN840827	PNE	4.69±0.09	4.72±0.12	4.36±0.21	5.39±0.00	4.80±0.39	___±___
PN840828a	PNE	4.34±0.23	4.32±0.26	3.75±0.36	4.30±0.00	___±___	___±___
PN840828b	PNE	4.31±0.18	4.30±0.22	4.06±0.14	___±___	___±___	___±___
PN840917	PNE	5.37±0.15	5.09±0.11	4.69±0.12	___±___	___±___	2.63±0.20
PN841027a	PNE	4.90±0.16	4.63±0.13	3.95±0.37	5.02±0.00	___±___	___±___
PN841027b	PNE	4.90±0.18	4.69±0.15	3.81±0.50	4.76±0.00	5.25±0.00	___±___
PN850718	PNE	4.98±0.12	4.67±0.13	4.33±0.13	5.66±0.21	4.67±0.07	2.40±0.18
PN870419a	PNE	4.54±0.30	3.79±0.36	4.04±0.10	___±___	___±___	2.32±0.16
PN870419b	PNE	4.45±0.22	4.29±0.07	3.76±0.20	___±___	___±___	___±___
PN870706	PNE	5.10±0.25	4.89±0.22	4.86±0.26	___±___	___±___	___±___
PN870724	PNE	5.17±0.11	5.00±0.09	4.66±0.16	___±___	___±___	3.39±0.12
PN870812	PNE	4.96±0.15	4.69±0.13	4.56±0.16	___±___	___±___	___±___
PN871003	PNE	5.13±0.13	4.85±0.16	4.59±0.14	___±___	___±___	3.07±0.09
PN880822	PNE	5.30±0.14	4.93±0.14	4.56±0.17	___±___	___±___	3.41±0.08
PN880906	PNE	4.96±0.23	4.54±0.25	4.36±0.21	___±___	___±___	3.30±0.06

1) from Baumstark and Wagner (1994).

APPENDIX D: MAGNITUDE-MAGNITUDE REGRESSIONS WITH ALTERNATIVE SCHEMES

Table D1. Magnitude:magnitude Regression Results							
Uncertain X & Y, Bootstrap Used, Outlier Retained							
Site	X	Y	N	Slope	Intercept	σ(Y)	ρ
NTS	Pmax	Pb	218	1.061±0.022	-0.675±0.121	0.120	0.96
PMA	Pmax	Pb	58	1.015±0.033	-0.375±0.184	0.082	0.97
RNA	Pmax	Pb	18	0.756±0.167	0.877±0.855	0.102	0.86
YFT	Pmax	Pb	142	1.052±0.026	-0.647±0.141	0.131	0.96
KTS	Pmax	Pb	195	0.987±0.011	-0.129±0.061	0.044	0.99
Deg	Pmax	Pb	98	0.961±0.024	0.006±0.129	0.048	0.99
BNE	Pmax	Pb	30	1.051±0.040	-0.513±0.228	0.047	0.99
BTZ	Pmax	Pb	19	0.999±0.049	-0.209±0.288	0.043	0.99
BSW	Pmax	Pb	48	0.990±0.053	-0.140±0.322	0.025	1.00
NNZ	Pmax	Pb	30	1.052±0.018	-0.483±0.101	0.042	1.00
Sahara	Pmax	Pb	7	0.991±0.125	-0.255±0.683	0.113	0.97
NTS	Pmax	Pa	214	0.921±0.021	-0.166±0.116	0.166	0.91
PMA	Pmax	Pa	58	0.994±0.035	-0.538±0.197	0.126	0.92
RNA	Pmax	Pa	15	0.902±0.201	-0.087±1.034	0.185	0.73
YFT	Pmax	Pa	141	0.887±0.027	0.001±0.144	0.177	0.90
KTS	Pmax	Pa	195	0.965±0.010	-0.267±0.056	0.066	0.99
Deg	Pmax	Pa	98	0.992±0.022	-0.405±0.116	0.078	0.96
BNE	Pmax	Pa	30	1.014±0.040	-0.559±0.226	0.058	0.98
BTZ	Pmax	Pa	19	0.977±0.049	-0.359±0.293	0.062	0.97
BSW	Pmax	Pa	48	1.003±0.054	-0.497±0.328	0.036	0.99
NNZ	Pmax	Pa	30	1.029±0.017	-0.574±0.099	0.066	0.99
Sahara	Pmax	Pa	7	0.733±0.108	0.980±0.591	0.066	0.98
NTS	Pmax	Pn	221	0.961±0.033	-0.009±0.173	0.256	0.84
PMA	Pmax	Pn	54	0.962±0.068	0.153±0.371	0.090	0.95
RNA	Pmax	Pn	22	0.638±0.183	1.315±0.930	0.148	0.72
YFT	Pmax	Pn	145	0.839±0.040	0.624±0.209	0.259	0.81
KTS	Pmax	Pn	113	0.937±0.047	0.257±0.265	0.384	0.73
Deg	Pmax	Pn	55	0.797±0.102	0.978±0.538	0.315	0.63
BNE	Pmax	Pn	20	0.685±0.177	1.500±1.012	0.542	0.35
BTZ	Pmax	Pn	6	0.418±0.362	3.493±2.141	0.170	0.67
BSW	Pmax	Pn	32	0.702±0.202	1.782±1.217	0.359	0.37
NNZ	Pmax	Pn	20	0.921±0.086	0.966±0.465	0.248	0.84
NTS	Pmax	Lg	183	0.776±0.031	1.410±0.168	0.242	0.80
PMA	Pmax	Lg	48	0.831±0.072	1.150±0.402	0.135	0.87
RNA	Pmax	Lg	22	0.776±0.183	1.146±0.928	0.153	0.78
YFT	Pmax	Lg	113	0.693±0.038	1.880±0.206	0.259	0.77
KTS	Pmax	Lg	74	0.725±0.066	1.459±0.390	0.113	0.86

Ta	. Magnitude:magnitude Regression Results (Cont)						
Uncertain X & Y, Bootstrap Used, Outlier Retained							
Site	X	Y	N	Slope	Intercept	σ(Y)	ρ
Deg	Pmax	Lg	12	0.826±0.148	0.825±0.846	0.111	0.91
BNE	Pmax	Lg	20	0.647±0.138	1.920±0.806	0.126	0.78
BTZ	Pmax	Lg	15	0.644±0.126	1.951±0.748	0.107	0.88
BSW	Pmax	Lg	27	0.557±0.221	2.486±1.335	0.107	0.63
NNZ	Pmax	Lg	24	0.710±0.051	1.950±0.304	0.109	0.97
NTS	Pmax	LR	140	1.142±0.035	-1.862±0.195	0.220	0.86
PMA	Pmax	LR	53	1.064±0.047	-1.317±0.260	0.192	0.84
YFT	Pmax	LR	84	1]±0.045	-1.598±0.249	0.203	0.88
KTS	Pmax	LR	154	0.[illegible]9±0.017	-1.235±0.098	0.269	0.81
Deg	Pmax	LR	63	[illegible]7±0.043	-2.476±0.233	0.311	0.74
BNE	Pmax	LR	26	1.212±0.069	-2.962±0.399	0.209	0.86
BTZ	Pmax	LR	18	1.252±0.099	-3.202±0.595	0.238	0.83
BSW	Pmax	LR	47	0.857±0.057	-0.812±0.345	0.200	0.74
NNZ	Pmax	LR	29	0.996±0.023	-[illegible].238±0.140	0.189	0.95

Table D2. Magnitude:magnitude Regression Results							
Standard Least Squares, Outlier Rejected							
Site	X	Y	N	Slope	Intercept	σ(Y)	ρ
NTS	Pmax	Pb	155	1.098±0.011	-0.857±0.057	0.047	0.99
PMA	Pmax	Pb	52	1.100±0.025	-0.840±0.136	0.052	0.99
RNA	Pmax	Pb	17	1.066±0.131	-0.691±0.663	0.085	0.90
YFT	Pmax	Pb	107	1.082±0.015	-0.784±0.080	0.057	0.99
KTS	Pmax	Pb	173	0.987±0.006	-0.125±0.033	0.032	1.00
Deg	Pmax	Pb	86	0.987±0.013	-0.118±0.069	0.034	0.99
BNE	Pmax	Pb	26	1.047±0.021	-0.482±0.122	0.030	1.00
BTZ	Pmax	Pb	19	1.011±0.038	-0.274±0.225	0.043	0.99
BSW	Pmax	Pb	48	1.008±0.014	-0.245±0.087	0.025	1.00
NNZ	Pmax	Pb	29	1.052±0.011	-0.481±0.064	0.034	1.00
Sahara	Pmax	Pb	7	1.001±0.113	-0.300±0.595	0.113	0.97
NTS	Pmax	Pa	156	1.033±0.017	-0.763±0.090	0.071	0.98
PMA	Pmax	Pa	50	0.990±0.038	-0.499±0.211	0.074	0.97
RNA	Pmax	Pa	15	1.097±0.281	-1.085±1.440	0.182	0.73
YFT	Pmax	Pa	113	1.077±0.023	-1.021±0.121	0.087	0.98
KTS	Pmax	Pa	168	0.964±0.008	-0.262±0.045	0.042	0.99
Deg	Pmax	Pa	83	1.019±0.018	-0.538±0.097	0.047	0.99
BNE	Pmax	Pa	28	1.047±0.036	-0.754±0.206	0.047	0.98
BTZ	Pmax	Pa	19	0.988±0.055	-0.422±0.327	0.062	0.97
BSW	Pmax	Pa	44	1.043±0.019	-0.744±0.113	0.028	0.99
NNZ	Pmax	Pa	29	1.028±0.019	-0.565±0.108	0.057	1.00
Sahara	Pmax	Pa	7	0.740±0.066	0.946±0.345	0.065	0.98
NTS	Pmax	Pn	193	1.085±0.022	-0.625±0.120	0.123	0.96
PMA	Pmax	Pn	54	0.982±0.043	0.039±0.235	0.090	0.95
RNA	Pmax	Pn	21	1.026±0.161	-0.670±0.818	0.121	0.83
YFT	Pmax	Pn	137	1.018±0.025	-0.303±0.130	0.117	0.96
KTS	Pmax	Pn	90	0.931±0.047	0.287±0.265	0.192	0.90
Deg	Pmax	Pn	46	0.817±0.094	0.885±0.498	0.184	0.79
BNE	Pmax	Pn	20	0.689±0.431	1.467±2.458	0.542	0.35
BTZ	Pmax	Pn	6	0.409±0.229	3.542±1.340	0.169	0.67
BSW	Pmax	Pn	28	0.501±0.178	2.911±1.077	0.176	0.48
NNZ	Pmax	Pn	19	0.892±0.116	1.088±0.643	0.202	0.88
NTS	Pmax	Lg	149	0.859±0.025	1.023±0.133	0.118	0.94
PMA	Pmax	Lg	46	0.791±0.060	1.370±0.328	0.111	0.89
RNA	Pmax	Lg	22	0.971±0.176	0.154±0.891	0.148	0.78
YFT	Pmax	Lg	96	0.840±0.028	1.159±0.150	0.114	0.95
KTS	Pmax	Lg	74	0.734±0.051	1.398±0.300	0.113	0.86

Table D2. Magnitude:magnitude Regression Results (Cont)							
Standard Least Squares, Outlier Rejected							
Site	X	Y	N	Slope	Intercept	σ(Y)	ρ
Deg	Pmax	Lg	12	0.836±0.121	0.762±0.688	0.111	0.91
BNE	Pmax	Lg	20	0.657±0.125	1.856±0.724	0.126	0.78
BTZ	Pmax	Lg	15	0.658±0.099	1.865±0.583	0.107	0.88
BSW	Pmax	Lg	27	0.584±0.146	2.312±0.881	0.106	0.63
NNZ	Pmax	Lg	24	0.711±0.039	1.935±0.232	0.109	0.97
NTS	Pmax	LR	110	1.008±0.042	-1.119±0.232	0.131	0.92
PMA	Pmax	LR	45	1.079±0.075	-1.442±0.414	0.130	0.91
YFT	Pmax	LR	74	1.061±0.051	-1.478±0.278	0.147	0.93
KTS	Pmax	LR	126	0.914±0.040	-1.155±0.230	0.166	0.90
Deg	Pmax	LR	50	1.204±0.084	-2.734±0.455	0.163	0.90
BNE	Pmax	LR	24	1.504±0.119	-4.683±0.686	0.138	0.94
BTZ	Pmax	LR	18	1.267±0.213	-3.292±1.255	0.238	0.83
BSW	Pmax	LR	42	0.487±0.088	1.460±0.533	0.126	0.66
NNZ	Pmax	LR	25	1.077±0.045	-1.704±0.268	0.112	0.98

Table D3. Magnitude:magnitude Regression Results							
Standard Least Squares, Outlier Retained							
Site	X	Y	N	Slope	Intercept	σ(Y)	ρ
NTS	Pmax	Pb	218	1.087±0.021	-0.817±0.112	0.120	0.96
PMA	Pmax	Pb	58	1.040±0.037	-0.510±0.203	0.082	0.97
RNA	Pmax	Pb	18	0.957±0.139	-0.146±0.708	0.096	0.86
YFT	Pmax	Pb	142	1.077±0.027	-0.782±0.141	0.131	0.96
KTS	Pmax	Pb	195	0.996±0.008	-0.179±0.043	0.044	0.99
Deg	Pmax	Pb	98	0.980±0.017	-0.091±0.093	0.048	0.99
BNE	Pmax	Pb	30	1.064±0.031	-0.589±0.176	0.046	0.99
BTZ	Pmax	Pb	19	1.011±0.038	-0.274±0.225	0.043	0.99
BSW	Pmax	Pb	48	1.008±0.014	-0.245±0.087	0.025	1.00
NNZ	Pmax	Pb	30	1.055±0.014	-0.502±0.079	0.042	1.00
Sahara	Pmax	Pb	7	1.001±0.113	-0.300±0.595	0.113	0.97
NTS	Pmax	Pa	214	0.944±0.029	-0.289±0.157	0.165	0.91
PMA	Pmax	Pa	58	1.019±0.056	-0.675±0.311	0.125	0.92
RNA	Pmax	Pa	15	1.097±0.281	-1.085±1.440	0.182	0.73
YFT	Pmax	Pa	141	0.907±0.036	-0.105±0.193	0.177	0.90
KTS	Pmax	Pa	195	0.973±0.012	-0.316±0.066	0.066	0.99
Deg	Pmax	Pa	98	1.011±0.028	-0.507±0.151	0.077	0.96
BNE	Pmax	Pa	30	1.027±0.038	-0.631±0.218	0.057	0.98
BTZ	Pmax	Pa	19	0.988±0.055	-0.422±0.327	0.062	0.97
BSW	Pmax	Pa	48	1.020±0.021	-0.604±0.125	0.036	0.99
NNZ	Pmax	Pa	30	1.032±0.021	-0.593±0.124	0.066	0.99
Sahara	Pmax	Pa	7	0.740±0.066	0.946±0.345	0.065	0.98
NTS	Pmax	Pn	221	0.986±0.044	-0.144±0.232	0.256	0.84
PMA	Pmax	Pn	54	0.982±0.043	0.039±0.235	0.090	0.95
RNA	Pmax	Pn	22	0.801±0.171	0.486±0.868	0.145	0.72
YFT	Pmax	Pn	145	0.857±0.051	0.526±0.269	0.259	0.81
KTS	Pmax	Pn	113	0.944±0.085	0.207±0.478	0.383	0.73
Deg	Pmax	Pn	55	0.814±0.137	0.878±0.727	0.315	0.63
BNE	Pmax	Pn	20	0.689±0.431	1.467±2.458	0.542	0.35
BTZ	Pmax	Pn	6	0.409±0.229	3.542±1.340	0.169	0.67
BSW	Pmax	Pn	32	0.725±0.332	1.635±1.998	0.358	0.37
NNZ	Pmax	Pn	20	0.918±0.142	0.975±0.788	0.248	0.84
NTS	Pmax	Lg	183	0.799±0.045	1.283±0.239	0.242	0.80
PMA	Pmax	Lg	48	0.853±0.070	1.028±0.387	0.135	0.87
RNA	Pmax	Lg	22	0.971±0.176	0.154±0.891	0.148	0.78
YFT	Pmax	Lg	113	0.707±0.056	1.804±0.298	0.259	0.77
KTS	Pmax	Lg	74	0.734±0.051	1.398±0.300	0.113	0.86

Table D3. Magnitude:magnitude Regression Results (Cont)							
Standard Least Squares, Outlier Retained							
Site	X	Y	N	Slope	Intercept	σ(Y)	ρ
Deg	Pmax	Lg	12	0.836±0.121	0.762±0.688	0.111	0.91
BNE	Pmax	Lg	20	0.657±0.125	1.856±0.724	0.126	0.78
BTZ	Pmax	Lg	15	0.658±0.099	1.865±0.583	0.107	0.88
BSW	Pmax	Lg	27	0.584±0.146	2.312±0.881	0.106	0.63
NNZ	Pmax	Lg	24	0.711±0.039	1.935±0.232	0.109	0.97
NTS	Pmax	LR	140	1.167±0.058	-1.998±0.317	0.220	0.86
PMA	Pmax	LR	53	1.093±0.101	-1.478±0.561	0.192	0.84
YFT	Pmax	LR	84	1.105±0.064	-1.718±0.350	0.203	0.88
KTS	Pmax	LR	154	0.939±0.056	-1.289±0.318	0.269	0.81
Deg	Pmax	LR	63	1.185±0.137	-2.535±0.732	0.311	0.74
BNE	Pmax	LR	26	1.234±0.152	-3.085±0.872	0.209	0.86
BTZ	Pmax	LR	18	1.267±0.213	-3.292±1.255	0.238	0.83
BSW	Pmax	LR	47	0.876±0.118	-0.926±0.704	0.200	0.74
NNZ	Pmax	LR	29	0.999±0.066	-1.256±0.386	0.189	0.95

APPENDIX E: SMALLEST EVENTS

The following Table lists those events with the smallest $m_b(P_{max})$ in each source region. All events with $m_b(P_{max})$ (GLM) ≤ 4.80 are also included.

Table E. Smallest GLM Event(s) of Each Test Site

Event	Site	P_{max}	P_b	P_a	P_n	L_g	M_S
US681208	PMA	4.69±0.07	4.28±0.07	3.92±0.08	4.56±0.09	5.16±0.15	±
US731012	RNA	4.80±0.12	±	±	4.15±0.12	4.82±0.11	±
US780913	RNA	4.69±0.17	±	±	4.57±0.14	4.83±0.15	±
US620706	YFT	4.73±0.17	4.42±0.17	3.90±0.17	4.39±0.18	4.86±0.21	4.26±0.09
US640716	YFT	4.50±0.12	4.10±0.12	4.33±0.12	4.25±0.10	4.96±0.15	±
US641009	YFT	4.76±0.07	4.51±0.07	4.52±0.10	4.57±0.10	5.13±0.21	±
US650218	YFT	4.47±0.12	4.27±0.12	4.42±0.12	4.14±0.10	4.95±0.15	±
US650514	YFT	4.73±0.17	3.97±0.17	±	4.44±0.10	4.71±0.15	±
US650521	YFT	4.69±0.08	4.01±0.08	4.11±0.10	4.44±0.09	5.14±0.15	±
US660625	YFT	4.61±0.07	4.07±0.08	3.83±0.10	4.34±0.11	5.04±0.21	±
US670727	YFT	4.78±0.10	4.19±0.10	4.47±0.10	4.36±0.12	4.79±0.15	±
US680119	YFT	4.68±0.17	4.48±0.17	4.40±0.17	4.53±0.18	±	±
US680325	YFT	4.45±0.12	±	±	4.21±0.12	4.73±0.15	±
US680410	YFT	4.78±0.12	3.96±0.12	4.01±0.12	4.37±0.10	±	±
US690716a	YFT	4.40±0.12	±	±	4.29±0.14	±	±
US691121	YFT	4.79±0.08	4.46±0.10	4.42±0.10	4.77±0.12	5.30±0.21	±
US700205	YFT	4.72±0.08	4.33±0.08	4.02±0.10	4.40±0.09	4.98±0.15	±
US720519	YFT	4.65±0.10	±	±	4.44±0.25	5.06±0.15	±
US750424	YFT	4.57±0.10	3.96±0.10	3.69±0.10	4.51±0.10	4.83±0.15	±
US790803	YFT	4.74±0.06	4.40±0.06	4.21±0.08	4.70±0.11	5.23±0.12	±
US790808	YFT	4.76±0.06	4.41±0.07	4.40±0.06	4.59±0.09	5.29±0.11	±
US820729	YFT	4.54±0.10	3.87±0.12	4.03±0.12	4.44±0.07	4.90±0.09	3.32±0.07
US840131	YFT	4.44±0.12	4.08±0.12	4.37±0.17	4.24±0.08	4.93±0.11	±
US840620	YFT	4.74±0.07	4.28±0.07	4.23±0.07	4.38±0.11	±	3.45±0.05
SH890902	BNE	5.01±0.06	4.81±0.06	4.62±0.06	5.67±0.18	±	3.66±0.05
SH760421	BSW	5.13±0.12	4.97±0.12	4.72±0.12	±	±	2.93±0.17
SH710630	BTZ	5.21±0.04	5.00±0.04	4.76±0.05	5.68±0.25	5.35±0.12	3.32±0.12
DM890217	Deg	4.77±0.17	4.63±0.12	4.01±0.10	5.13±0.14	±	±
NZ641025	NNZ	4.67±0.04	4.47±0.04	4.28±0.04	5.19±0.11	5.34±0.11	±
NZ771009	NNZ	4.53±0.03	4.26±0.04	4.04±0.03	5.10±0.12	±	3.82±0.10
FS640214	Sahara	4.42±0.17	±	±	±	±	±
FS641128	Sahara	4.66±0.12	4.43±0.12	4.45±0.12	±	±	±
FS651001	Sahara	4.51±0.17	±	±	±	±	±

DISTRIBUTION LIST FOR UNCLASSIFIED REPORTS
AFTAC-FUNDED PROJECTS
(Last Revised: 09 Jan 1990)

RECIPIENT	NO. OF COPIES
HQ AFTAC/TTR Patrick AFB, FL 32925-3002	3
HQ AFTAC/CA-STINFO Patrick AFB, FL 32925-3002	1
Defense Technical Information Center Cameron Station Alexandria, VA 32925-5000	2
Other (To be determined by the U.S. Government Project Office)	5

(THIS PAGE INTENTIONALLY LEFT BLANK)